Indian J. pure appl. Phys., Vol. 18 No. 8 pp. 549-638
August 1980
CODEN : IJOPAU ISSN: 0019-5596
18 (8) 549-638 (1980)

INDIAN JOURNAL OF PURE & APPLIED PHYSICS

Published by
PUBLICATIONS & INFORMATION DIRECTORATE, CSIR, NEW DELHI
in association with
THE INDIAN NATIONAL SCIENCE ACADEMY, NEW DELHI

"We have put more innovative ideas into our EM 400 to make it the world's finest Transmission Electron Microscope"

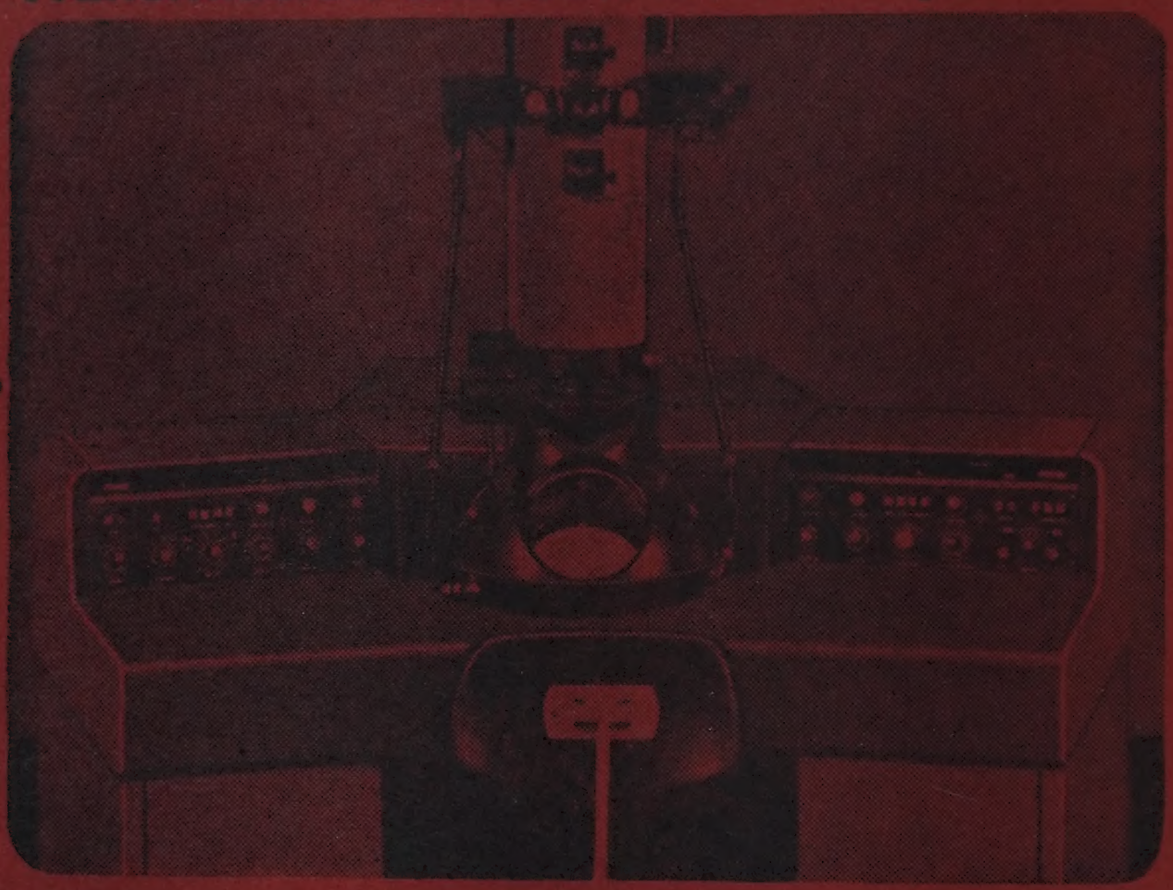

We have given you:

- the cleanest high vacuum
- computer memory controlled image correction
- more accurate magnification and wider range
- automated illumination/exposure
- full display/print-out of operating conditions
- better protection from vibration, stray fields and thermal effects

And more.

WHY?

To give you more information than you have ever had from your specimen.

To provide a solid base for your future electron optical system.

The EM 400 does this better than any other Transmission Electron Microscope.

For details contact:

PHILIPS INDIA LIMITED
Product Division
Science & Industry
Shivsagar Estate, Block 'A'
Worli, Bombay-400 018

PHILIPS

Indian Journal of Pure & Applied Physics

VOLUME 18 No. 8 AUGUST 1980

Published by the Publications & Information Directorate, CSIR, Hillside Road, New Delhi 110 012

Chief Editor : Y R Chadha

The Indian Journal of Pure & Applied Physics is issued monthly. The Directorate assumes no responsibility for the statements and opinions advanced by contributors. The editorial staff in its work of examining papers received for publication is assisted, in an honorary capacity, by a large number of distinguished scientists, working in various parts of India.

Communications regarding contributions for publication in the journal should be addressed to the Editor, Indian Journal of Pure & Applied Physics, Publications & Information Directorate, Hillside Road, New Delhi 110 012.

Correspondence regarding subscriptions and advertisements should be addressed to the Sales & Distribution Officer, Publications & Information Directorate, New Delhi 110 012.

Annual Subscription	**Single Copy**
Rs. 100.00 £ 16.50 $ 42.00	Rs. 10.00 £ 1.80 $ 4.50

50% Discount is admissible to research workers and students and 25 % discount to non-research individuals, on annual subscription. Payments in respect of subscriptions and advertisements may be sent by cheque, bank draft, money order or postal order marked payable *only* to **Publications & Information Directorate, New Delhi 110 012.** Claims for missing numbers of the journal will be allowed only if received within 3 months of the date of issue of the journal plus the time normally required for postal delivery of the journal and the claim.

CSIR SCIENTIFIC PERIODICALS

JOURNAL OF SCIENTIFIC & INDUSTRIAL RESEARCH (monthly)

With a fine record of over 35 years' service to the scientific community, this Journal has grown into India's leading general science periodical. Intended to fulfil the responsibility of helping the research workers to keep themselves abreast of current developments in various fields of science and technology, the Journal carries editorial features highlighting important scientific events in India and abroad; articles on science policy and management of science; review articles on topics of current research interest; technical reports on international and national conferences; reviews of scientific and technical publications; and notes on major advances in various fields.

Annual subscription	**Rs 60.00**	**£ 10.00**	**$ 25.00**
Single copy	6.00	1.00	2.50

INDIAN JOURNAL OF CHEMISTRY (monthly)

This Journal which is running the 18th year of its publication, Consists of the following two sections.

Section A : This section is devoted to papers in Inorganic, Physical, Theoretical and Analytical Chemistry.

Annual subscription	**Rs 70.00**	**£ 12.00**	**$ 30.00**
Single copy	7.00	1.20	3.00

Section B : This section is devoted to papers in Organic Chemistry including Medicinal Chemistry.

Annual subscription	**Rs 70.00**	**£ 12.00**	**$ 30.00**
Single copy	7.00	1.20	3.00

INDIAN JOURNAL OF PURE & APPLIED PHYSICS (monthly)

This Journal, which is running the 18th year of its publication, is devoted to original research communications (full papers and short communications) in all conventional branches of physics (except radio and space physics).

Annual subscription	**Rs 100.00**	**£ 16.50**	**$ 42.00**
Single copy	10.00	1.80	4.50

INDIAN JOURNAL OF RADIO & SPACE PHYSICS (bimonthly)

This Journal serves as a medium for the publication of original rearch work (full papers and communications) in various areas of radio and space physics.

Annual subscription	**Rs 60.00**	**£ 10.00**	**$ 25.00**
Single copy	12.00	2.00	5.00

INDIAN JOURNAL OF TECHNOLOGY (INCLUDING ENGINEERING) (monthly)

This Journal publishes papers reporting results of original research of applied nature pertaining to unit operations, heat and mass transfer, products, processes, instruments, and appliances, etc. The Journal is of special interest to research workers in the departments of applied sciences in universities, institutes of higher technology, commodity research laboratories, industrial cooperative research institutes, and industrial research laboratories.

Annual subscription	**Rs 60.00**	**£ 10.00**	**$ 25.00**
Single copy	6.00	1.00	2.50

INDIAN JOURNAL OF EXPERIMENTAL BIOLOGY (monthly)

This Journal, devoted to the publication of research communications in the fields of experimental botany, zoology, microbiology, pharmacology, endocrinology, nutrition, etc. is the only one in India with such a wide coverage and scope.

Annual subscription	**Rs 120.00**	**£ 20.00**	**$ 50.00**
Single copy	12.00	2.00	5.00

INDIAN JOURNAL OF BIOCHEMISTRY & BIOPHYSICS (bimonthly)

This Journal, published in association with the Society of Biological Chemists (India), Bangalore, is the only research Journal in India devoted exclusively to original research communications in biochemistry and biophysics.

Annual subscription	**Rs 40.00**	**£ 7.00**	**$ 17.00**
Single copy	8.00	1.40	3.50

INDIAN JOURNAL OF MARINE SCIENCES (quarterly)

Commencing publication from June 1972, this Journal is devoted to research communications (full papers and short communications) pertaining to various facets of marine research, viz. biological, physical, geological and chemical oceanography.

Annual subscription	**Rs 40.00**	**£ 7.00**	**$ 17.00**
Single copy	12.00	2.00	5.00

RESEARCH & INDUSTRY (quarterly)

Intended to serve as a link between science and industry, this Journal is addressed primarily to technologists, engineers, executives and others in industry and trade. It publishes informative original articles containing practical details of processes and products developed in India, which show promise of ready utilization, and technical digests on new processes, products, instruments and testing methods which are of interest to industry. Developments in Indian industry are regularly reported.

Annual subscription	**Rs 24.00**	**£ 4.00**	**$ 10.00**
Single copy	7.25	1.30	3.50

INDIAN JOURNAL OF TEXTILE RESEARCH (quarterly)

Commencing publication from March 1976, this Journal is devoted to the publication of papers reporting results of fundamental and applied researches in the field of textiles.

Annual subscription	**Rs 36.00**	**£ 6.00**	**$ 15.00**
Single copy	12.00	2.00	5.00

Please contact

THE SALES & DISTRIBUTION OFFICER
PUBLICATIONS & INFORMATION DIRECTORATE, CSIR
HILLSIDE ROAD, NEW DELHI 110 012

Indian Journal of Pure & Applied Physics

VOLUME 18 No. 8 AUGUST 1980

CONTENTS

CONTENTS

COMMUNICATIONS

NOTES

CONTENTS

NOTES (contd.)

Indian Journal of Pure & Applied Physics
Vol. 18, August 1980, pp. 549-552

Evaluation of Van der Waals Coefficients in Silver & Thallous Halides

A K Kapur
Department of Physics, V S S D College, Kanpur
&
J K Jain
Department of Physics, Agra College, Agra

Received 24 *July* 1978; *accepted* 17 *January* 1980

The van der waals dipole-dipole and dipole-quadrupole interaction coefficients in silver and thallous halides crystals have been estimated using the appropriate values of the crystalline state electronic polarizabilities of the ions evaluated by taking into account the effect of Madelung potential and using the polarizability-radius cube relation. Appropriate values of the effective number of electrons in the ion necessary to account for the actual polarizability of the ion have been used in these calculations.

1. Introduction

The knowledge of the van der waals energy in crystals is of wide use in the study of various physical properties, viz. the cohesive and defect energies, the optical and dielectric behaviour of crystals. However, in calculations of cohesive or binding energies, the magnitudes of van der waals energies are of minor importance (contribute only about 5-10%) but in the estimation of defect energies these are of considerable importance. In predicting the relative stability of different crystal structures, the magnitudes of van der waals energy play the prominent role. It was pointed out by Mayer[1] that the difference in the cohesive energies of a given compound to crystallize in two different structures is quite comparable with the magnitude of van der waals energy. Thus the reliable determination of van der waals energy in ionic crystals is valuable to predict the structure of crystals especially where the phase transformation takes place. An important application of van der waals energy can also be made to study the surface physics of solids, particularly to calculate the surface energies of crystals.

Van der waals dipole-dipole and dipole-quadrupole interaction energies arise from the synchronization of the electronic motions in the ions. The physical origin of the van der waals energy is connected with correlations of electronic motions in different atoms. The instantaneous dipole moment of a closed shell atom induces on a similar atom, a dipole moment. The mutual interaction between these induced dipole moments gives rise to an energy term known as dipole-dipole energy which varies inversely as the sixth power of interatomic separation. In addition, the consideration of the instantaneous higher moments of the charge distribution of the atom yields other attractive terms such as dipole-quadrupole and quadrupole-quadrupole energies, which decay more rapidly with increasing interatomic separation. In typical ionic crystals, the dipole-quadrupole term is only a small fraction of the dipole-dipole term and the quadrupole-quadrupole term can be neglected in the range of observed interionic separations. In the present study, we consider dipole-dipole and dipole-quadrupole interactions only. The choice of silver and thallous halide crystals is made due to the fact that they have a complicated nature of the chemical bonding between the ions. The presence of *d*-electrons in Ag^+ and Tl^+ ions causes the deviations from the purely ionic bonding.

Van der waals energy sensitively depends upon the electronic polarizabilities of the ions and on the effective number of electrons in the ion. The polarizabilities of ions become significantly effective when they enter into the crystalline state from the free state. The electronic polarizabilities of the cation increases and those of an anion decreases, when an ion enters from free state to crystalline state. The changes in the polarizabilities of ions upon entering the crystal are quite significant. In the present study, we have, therefore, used the

essentially crystalline state polarizabilities of the ions evaluated by Jai Shanker *et al.*[2] by taking into account the effect of Madelung potential as suggested by Ruffa[3] and using the polarizability-radius cube relation proposed by Jai Shanker *et al.*[4] These values of electronic polarizabilities present a good agreement with the average values of Tessman *et al.*[5] The effect of the Madelung potential and the polarizability-radius cube relation have also been successfully used by Jain *et al.*[6,7] to evaluate the electronic polarizability of ions in alkaline earth halide crystals and in alkali chalcogenide crystals. The values of electronic polarizability used to evaluate van der waals coefficients are listed in Table 1. It is informative to observe from Table 1 that the electronic polarizability of Ag^+ or Tl^+ ion show a smooth trend of variation from a chloride to the corresponding iodide crystal. This trend of variation is similar to that predicted by Lowndes and Martin[8] for the effective ionic charges in silver and thallous halides. The electronic polarizabilities used in the present study agree with the experimental values and differ from the free-state polarizabilities in a manner suggesting the loosening of cations and tightening of anions in the crystalline state. Thus the values of electronic polarizabilities used in the present study are most appropriate.

Van der waals energy also sensitively depends upon the effective number of electrons (n_i) in the ion necessary to account for the actual polarizability of the ion. Jain *et al.*[9] have taken this effective number (n_i) as equal to the total number of electrons in the ion as used by Ruffa[3] to evaluate the van der waals energy of alkali halide crystals. Mayer[1] and Hajj[10] derived the values of n_i from the optical data of solids, which turns out to be a fraction of the total number of electrons in the ion. However, there is considerable uncertainty in the values of n_i derived from this method due largely to insufficient optical data. It was suggested by Morris[11] that n_i be put equal to the number of outer most electrons in the ion. In fact, any electric field acting on an ion would cause much more displacement in the electrons of the outer most shell than the electrons of the inner shell. The effective n_i should, therefore, be nearer to the number of electrons in the outermost shell than to the total number of electrons in the ion as used by Jain *et al.*[9] In the present study, we have therefore, used the n_i values of halide ions derived by Dick and Overhauser[12] considering the effective value of the charge of the ion. These values of n_i turn out to be a fraction of the total number of electrons in the ion. For silver and thallous ions, we have used n_i as equal to the number of electrons in the outer most orbit of the ion. Thus the values of electronic polarizabilities of the ions and those of n_i used in the present study are most appropriate and promising.

2. Dipole-Dipole Interaction

In the second approximation of perturbation theory, the well known expression for the dipole-dipole interaction energy of the two atoms read as follows

$$W_{dd}(r_{ij}) = -\frac{c_{ij}}{r_{ij}^6} \qquad ...(1)$$

where

$$c_{ij} = 6 \sum_{(a,b)}' \frac{(\mu_{ix}^{0a})^2 (\mu_{jx}^{0b})^2}{E_i^{0a} + E_j^{0b}} \qquad ...(2)$$

Here E_i^{0a} and E_j^{0b} are the energies of the atoms/ions relative to the respective ground states and μ_{ix}^{0a} and μ_{jx}^{0b} are the matrix elements of the x component of the dipole moment of each atom between the ground state and the excited states. The sum is over all the excited states of both the atoms. If one assumes that all the excited states with large matrix elements fall in a narrow energy range and one uses the corresponding one-level formula for the polarizability of the atoms, one obtains the London formula for the coefficient c_{ij} of the dipole-dipole van der waals energy.

$$c_{ij} = \frac{3}{2} \alpha_i \alpha_j \frac{E_i E_j}{E_i + E_j} \qquad ...(3)$$

where E_i and E_j are the appropriate energy parameters and can loosely be referred to as being the average excitation energy. Eq. (3) has been used by various workers, to estimate the dipole-dipole coefficients c_{ij} in alkali halides.

For the van der waals dipole-dipole coefficients C_{++} (for silver-silver and thallous-thallous interactions), $C_{+-}C$ (for silver-halogen and thallous-halogen interactions) and C_{--} (for halogen-halogen interaction), Eq. (3) may be restated in the following forms

$$C_{++} = \frac{3}{4} \alpha_+^2 E_+ \qquad ...(4)$$

$$C_{+-} = \frac{3}{2} \alpha_+ \alpha_- \frac{E_+ E_-}{E_+ + E_-} \qquad ...(5)$$

and

$$C_{--} = \frac{3}{4} \alpha_-^2 E_- \qquad ...(6)$$

Table 1—Electronic Polarizabilities α_i (in Å^3), Effective Number of Electrons (n_i) used in the Present Study and Calculated Values of E_i (in eV)

Crystals	α_+	α_-	n_+	n_-	E_+	E_-
AgCl	2·48	2·87	18	8·7	28·2	18·2
AgBr	2·44	3·69	18	9·9	28·5	17·2
AgI	2·41	3·71	18	11·3	28·6	18·3
TlCl	4·86	2·67	2	8·7	6·72	18 9
TlBr	4·80	3·45	2	9·9	6·76	17·8
TlI	4·73	5·17	2	11·3	6·81	15·5

Table 2—Calculated Van der Waals Dipole-Dipole Interaction Coefficients [c_{ij} in 10^{-60} ergs cm^6] and Dipole-Quadrupole Interaction Coefficients d_{ij} (in 10^{-76} ergs cm^8) for the Iions of Silver Halides and Thallous Halides

Crystal	c_{+-}	c_{++}	c_{--}	d_{+-}	d_{++}	d_{--}
AgCl	189	208	180	293	253	339
AgBr	231	203	280	370	245	416
AgI	239	199	302	368	239	566
TlCl	154	190	161	534	972	293
TlBr	195	187	253	681	948	490
TlI	278	183	497	1010	921	1100

where α_+ and α_- are the electronic polarizabilities and E_+ and E_- are the energy parameters of the cation and anion respectively.

The polarizability α_i and the energy parameter E_i of an ion are not independent of one another but are related through one level formula

$$\alpha_i = \frac{n_i\, e^2\, h^2}{4\,\pi^2\, m\, E_i^2} \qquad ...(7)$$

where n_i is the number of electrons in the atom or ion necessary to account for the actual polarizability; e and m respectively the electronic charge and mass and h the Plank's constant.

3. Dipole-Quadrupole Interaction

The dipole-quadrupole and quadrupole-quadrupole van der Waals interactions of two identical atoms in their spherically symmetric ground state have been treated in the one-level approximation. In the second approximation of perturbation theory, they contribute additional energy terms of the form $-d/r^8$ and $-f/r^{10}$. For most atoms, the dipole-quadrupole term is only a small fraction of the dipole-dipole term and the quadrupole-quadrupole term can be neglected in the range of observed interionic distances. Mayer[1] has given the dipole-quadrupole term in the case of different atoms making additional approximations to express all the intervening matrix elements in terms of polarizabilities. The approximate Mayer formula for the dipole-quadrupole van der waals energy reads as

$$W_{dq}(r_{ij}) = -\frac{d_{ij}}{r_{ij}^8} \qquad ...(8)$$

with

$$d_{ij} = \frac{9}{4}\,\frac{c_{ij}}{e^2}\left[\frac{\alpha_i\, E_i}{n_i} + \frac{\alpha_j\, E_j}{n_j}\right] \qquad ...(9)$$

where n_i and n_j are effective number of electrons in the respective ions necessary to account for the actual polarizabilities.

From Eq. (9), we have for the van der waals dipole-quadrupole coefficients for silver-silver or thallous-thallous, silver-halogen or thallous-halogen, halogen-halogen interactions respectively.

$$d_{++} = \frac{9}{2}\,\frac{c_{++}}{e^2}\left[\frac{\alpha_+\, E_+}{n_+}\right] \qquad ...(10)$$

$$d_{+-} = \frac{9}{4}\,\frac{c_{+-}}{e^2}\left[\frac{\alpha_+\, E_+}{n_+} + \frac{\alpha_-\, E_-}{n_-}\right] \qquad ...(11)$$

$$d_{--} = \frac{9}{2}\,\frac{c_{--}}{e^2}\left[\frac{\alpha_-\, E_-}{n_-}\right] \qquad ...(12)$$

4. Calculations and Results

The values of energy parameter E_i have been calculated using Eq. (7). The values of α_i and n_i used in these calculations are given in Table 1. Using these values of E_i, the van der waals dipole-dipole coefficients c_{++}, c_{+-} and c_{--} have been calculated respectively from Eqs. (4), (5) and (6). These calculated values of c_{++}, c_{+-} and c_{--} are listed in Table 2. Van der waals dipole-quadrupole coefficients d_{++}, d_{+-} and d_{--} in silver halides and thallous halides have been evaluated from Eqs. (10), (11), and (12) respectively. These calculated values of d_{++}, d_{+-} and d_{--} are also given in Table 2. Direct experimental check on the validity of these values is difficult because the cohesive energies of silver halides and thallous halide calculated within the frame work of the Born model do not sensitively depend upon the magnitudes of van der waals energies.[13] The major reason for the preference of our values of van der waals dipole-dipole interaction coefficients and dipole-quadrupole interaction coefficients is because of the more consistent and approximate input parameters (essentially α_i and n_i).

References

1. Mayer J E, *J. chem. Phys.*, **1** (1933), 270.
2. Jai Shanker, Goyal S C & Bakhshi P S, *Indian J. Phys.*, **50** (1976), 918.
3. Ruffa A R, *Phys. Rev.*, **130** (1963), 1412.
4. Jai Shanker, Kumar N & Verma M P, *Indian J. pure appl. Phys.*, **11** (1973), 644.
5. Tessman J R, Kahn A H & Shockley W, *Phys. Rev.*, **92** (1953), 890.
6. Jain J K & Jai Shanker, *Indian J. pure appl. Phys.*, **12** (1974), 803.
7. Jain J K, Jai Shanker & Khandelwal D P, *Phil. Mag.*, **32** (1975), 887.
8. Lowndes R P & Martin D H, *Proc. R. Soc.*, **A308** (1969), 473.
9. Jain J K, Jai Shanker & Khandelwal D P, *Phys. Rev.*, **13** (1976), 2692.
10. Hajj F, *J. chem Phys.*, **44** (1966), 4618.
11. Morris D F C, *Proc. R. Soc.*, **A242** (1957), 116.
12. Dick B G & Overhauser AW, *Phys., Rev.*, **112** (1958), 90.
13. Tosi M P, *Solid St. Phys.*, **16** (1964), 1.

Indian Journal of Pure & Applied Physics
Vol. 18, August 1980, pp. 553-556

Volume Dependence of Poisson's Ratio & the Grüneisen Parameter in Alkali Halides

JAI SHANKER & A P GUPTA*
Physics Department, Agra College, Agra 282 002

Received 22 *June* 1979; *revised received* 9 *November* 1979

An analysis of Grüneisen parameter of 16 alkali halide crystals with NaCl structure has been performed by taking into account the volume dependence of Poisson's ratio. The two Grüneisen parameters related to longitudinal and transverse phonons are calculated using the formulation of D J Pastine [*Phys. Rev.*, **138**C (1965), 767]. The calculations are performed adopting six different potential forms for the repulsive energy. The results for the Grüneisen parameter obtained in the present study compared with other recent investigations, indicates that the present values are closer to corresponding values based on the finite strain theory.

1. Introduction

Studies on the Grüneisen parameter are very useful because of the fact that this parameter is directly related to the dielectric, elastic, thermal and anharmonic properties of solids.[1-6] The usefulness of the Grüneisen parameter has also been extended to understand the geophysical details of the earth's interior.[7,8]

Theories for the Grüneisen parameter have been developed by Slater,[9] and by Dugdale and Mac Donald[10] (DM). It should be emphasized that Slater's theory as well as the formulation of DM are based on the assumption that Poisson's ratio is independent of volume. However, this assumption is not true for real crystals.

In the present paper, we take account of the fact that Poisson's ratio depends on the volume. In addition, we consider two Grüneisen parameters γ_l and γ_t related to longitudinal and transverse phonons, in place of a single parameter. The total energy is supposed to be equally distributed between the pure modes of vibrational frequencies, one mode of longitudinal vibrations and two identical modes of transverse vibrations. Under this assumption, the Grüneisen parameter γ appears as an average given by

$$\gamma = \tfrac{1}{3}(\gamma_l + 2\gamma_t) \qquad \ldots(1)$$

This model gives a more realistic representation of the thermodynamic behaviour of the solid.[11,12]

2. Method of Analysis

The relevant expressions for γ_l and γ_t can be obtained as follows using the theory of elasticity.[9,12]

$$\gamma_l = -\frac{2}{3} - \frac{V}{2}\cdot\frac{d^2P/dV^2}{dP/dV} + \frac{Vd\sigma/dV}{(1-\sigma^2)} \qquad \ldots(2)$$

$$\gamma_t = -\frac{2}{3} - \frac{V}{2}\frac{d^2P/dV^2}{dP/dV} + \frac{3Vd\sigma/dV}{2(1+\sigma)(1-2\sigma)} \qquad \ldots(3)$$

where P is the pressure at volume V and temperature 0K and σ the Poisson's ratio. Eqs. (2) and (3) hold for the acoustic mode and are equally applicable to monoatomic, diatomic and polycrystalline solids.[13] In alkali halide crystals, the expressions for γ_l and γ_t corresponding to optic mode vibrations will be different from Eqs. (2) and (3). In fact, the optic mode γ_l and γ_t are related to the pressure derivatives of dielectric constants.[14] We are concerned here with γ_l and γ_t which are expressed in terms of the pressure derivatives of elastic constants. In fact, these γ_l and γ_t [Eqs. (2) and (3)] correspond to low frequency acoustic modes. The frequency (ω_i) of such a mode is taken to be represented by the formula:

$$\omega_i = v\, k_i$$

where v is the wave velocity appropriate to the mode and k_i is the magnitude of the wave vector of the mode. Such a prescription has been used by previous workers to calculate γ in alkali halides.[15-17]

Following the equation of state,[18] one can write

$$P = -\frac{dW}{dV} \qquad \ldots(4)$$

where W the crystal lattice energy, which, for an ionic solid, is written as follows:

$$W = -\frac{\alpha_M e^2}{r} + B(r) - \frac{C}{r^6} - \frac{D}{r^8}\,. \qquad \ldots(5)$$

* Permanent address : M B Postgraduate College Haldwani 263 139

The first term on the right side of Eq. (5) is the electrostatic potential energy with α_M as the Madelung's constant and r the interionic separation. $B(r)$ is the short range overlap repulsive potential. The last two terms represent the van der Waals potentials with C and D as dipole-dipole and dipole-quadrupole coefficients. With the help of Eq. (5) it is possible to calculate the total potential energy W and its derivatives if one adopts a phenomenological potential form for $B(r)$ showing the functional dependence on interionic separation. Values of dP/dV and d^2P/dV^2 appearing in Eqs. (2) and (3) can be obtained by making use of Eq. (4) which yields (for NaCl structure)

$$\frac{dP}{dV} = -\frac{1}{36r^4}\left(W^{II} - \frac{2}{r}W^{I}\right) \quad ...(6)$$

and

$$\frac{d^2P}{dV^2} = -\frac{1}{216\,r^6}\left(W^{III} - \frac{6}{r}W^{II} + \frac{10W^{I}}{r^2}\right) \quad ...(7)$$

where W^{I}, W^{II} and W^{III} are the first, second and the third order derivatives of the potential energy with respect to interionic separation. Values of Poisson's ratio and its volume dependence can be obtained using the following relations:

$$\sigma = \frac{C_{12}}{C_{11}+C_{12}} \quad ...(8)$$

and

$$V\frac{d\sigma}{dV} = \frac{(C_{11}+2C_{12})}{3(C_{11}+C_{12})^2}\left[C_{12}\frac{dC_{11}}{dP} - C_{11}\frac{dC_{12}}{dP}\right] \quad ...(9)$$

Values of σ and $V\,d\sigma/dV$ have been calculated from Eqs. (8) and (9) using low temperature values of elastic constants recently compiled by Catlow *et al.*[19] The pressure derivatives of elastic constants have been taken from Roberts and Smith[20] and McLean and Smith.[21]

Table 1 - Potential Functions for the Short-range Overlap Repulsive Energy

Potential function	Mathematical representation	Intervening parameters	Ref.
Born-Lande[22]	$A\,r^{-n}$	A and n	22
Born-Mayer[23]	$B\exp(-r/\rho)$	B and ρ	23
Verwey[24]	$\mu\,r^{-12}$	μ	24
Varshni-Shukla[25] Modified	$\lambda_1\exp(-k_1r^2)$	λ_1 and k_1	25
Varshni-Shukla[26-28]	$\lambda_2\exp(-k_2r^{3/2})$	λ_2 and k_2	26,27,28
Logarithmic[29,30]	$a\log(1+br^{-9})$	a and b	29,30

Table 2—Values of the Poisson's Ratio σ, Its Volume Dependence $V\frac{d\sigma}{dV}$ and Grüneisen Parameter Using Different Potentials

Crystal	σ	$V\frac{d\sigma}{dV}$	Borne-Lande			Born-Mayer			Verwey		
			γ_l	γ_t	γ	γ_l	γ_t	γ	γ_l	γ_t	γ
LiF	0·254	0·167	2·31	2·54	2·46	2·07	2·30	2·22	3·66	3·88	3·81
LiCl	0·272	0·243	2·66	3·03	2·91	2·43	2·79	2·67	3·65	4·02	3·89
LiBr	0·252	0·130	2·63	2·80	2·75	2·39	2·56	2·50	3·56	3·73	3·68
LiI	0·311	0·512	3·19	4·17	3·85	2·95	3·93	3·60	3·98	4·96	4·64
NaF	0·174	0·128	2·48	2·60	2·56	2·24	2·36	2·32	3·51	3·63	3·59
NaCl	0·164	0·037	2·59	2·62	2·61	2·34	2·37	2·36	3.43	3·47	3·45
NaBr	0·170	0·071	2·69	2·76	2·73	2·43	2·50	2·47	3·55	3·61	3·59
NaI	0·175	0·052	2·77	2·82	2·80	2·52	2·57	2·55	3·46	3·51	3·49
KF	0·151	0·107	2·65	2·74	2·71	2·40	2·49	2·46	3·52	3·61	3.58
KCl	0·101	−0·090	2·60	2·54	2·56	2·35	2·29	2·31	3·31	3·25	3·27
KBr	0·118	0·023	2·72	2·74	2·73	2·46	2·48	2·47	3·51	3·53	3·52
KI	0·061	−0·217	2·55	2·42	2·46	2·28	2·15	2·19	3·27	3·14	3·18
RbF	0·161	−0·013	2·62	2·61	2·61	2·35	2·34	2·34	3·47	3·46	3·46
RbCl	0·131	0·109	2·88	2·97	2·94	2·63	2·72	2·69	3·49	3·58	3.55
RbBr	0·109	0·034	2·84	2·86	2·85	2·59	2·61	2·60	3·41	3·44	3·43
RbI	0·101	0·044	2·89	2·92	2·91	2·62	2·65	2·64	3·53	3·56	3·55

Table 3—Values of Gruneisen Paramaters Using Different Potentials

Crystal	Varshni-Shukla			ModifiedVarshni-Shukla			Logariathmic			λ	
	γ_l	γ_t	γ	γ_l	γ_t	γ	γ_l	γ_t	γ	(a)	(b)
LiF	1·75	1·99	1·91	1·91	2·15	2·07	1·78	2·01	1·93	—	—
LiCl	2·12	2·50	2·38	2·27	2·65	2·53	2·42	2·79	2·66	—	—
LiBr	2·08	2·76	2·20	2·24	2·42	2·36	2·45	2·63	2·57	2·48	—
LiI	2·60	3·63	3·29	2·75	3·79	3·44	3·14	4·13	3·80	2·38	—
NaF	1·94	2·07	2·02	2·10	2·22	2·18	2·19	2·31	2 27	1·86	—
NaCl	2·04	2·08	2·07	2·20	2·23	2·22	2·48	2·51	2·50	1·69	2·66
NaBr	2·12	2·18	2·16	2·28	2·35	2·32	2·62	2·68	2·66	1·75	2·74
NaI	2·22	2·27	2·26	2·38	2·43	2·41	2.82	2·87	2·85	1·72	2·78
KrF	2·10	2·19	2·16	2·26	2·35	2·32	2·54	2·63	2 60	1·71	—
KCl	2·05	1·99	2·01	2·21	2·14	2·17	2·64	2·58	2·60	1·59	2·52
KBr	2·14	2·16	2·15	2·31	2·33	2·32	2·74	2·75	2·75	1·69	2·50
KI	1·96	1·83	1·87	2·13	1·99	2·04	2·61	2·48	2·52	1·27	2·56
RbF	2·03	2·02	2·02	2·20	2·19	2·19	2·57	2·56	2·56	1·66	—
RbCl	2·33	2·42	2·39	2·49	2·58	2·55	3.01	3·10	3·07	1·45	2·68
RbBr	2·29	2·31	2·31	2·44	2·47	2·46	3 00	3·02	3·01	1·37	2·65
RbI	2·30	2·33	2·32	2·47	2·49	2·49	3·04	3·07	3·06	1·32	2·64

(a) Based on lattice dynamical theory.[35] (b) Based on finite strain theory.[36]

3. Results and Discussion

The evaluation of γ_l and γ_t depends upon the higher order derivatives of the potential energy. To make a comprehensive analysis, we adopt six potential functions for $B(r)$ which have been used by previous investigations.[22-30] These are briefly described in Table 1. The parameters entering these potential forms can be derived from the ultrasonically measured elastic data using the Hildebrand equation of state.[31,32] Values of the van der Waals dipole-dipole and dipole-quadrupole potentials are taken from Hajj[33] and Mayer,[34] respectively. The parameters so derived are used to calculate the derivatives of potential energy and then γ_l, γ_t and average γ using Eqs. (1)-(5). Poisson's ratio and its volume dependence based on Eqs. (8) and (9) are given in Tables 2 and 3. Calculated values of γ_l, γ_t and γ are also presented in Tables 2 and 3.

It is seen from Table 2 and 5 that values of the Grüneisen parameter depend sensitively on the form of the potential energy used in the calculations. Values of γ_l, γ_t and γ based on the Verwey potential are significantly larger than those obtained from other potential forms. Recently there have been several attempts to calculate γ for alkali halides using alternative approaches based on lattice dynamical theory[35] and finite strain theory.[36] The results of these investigations are also included in Table 3 for the sake of comparison. It is found that our calculated values of γ are closer to the corresponding values based on the finite strain theory.

Acknowledgement

We are grateful to the referee for his valuable comments.

References

1. Grüneisen E, *Handbuch der physik*, Vol. 10 (Springer Verlag, Berlin), 1926.
2. Anderson O L, *Phys. Rev.*, 144 (1966), 553.
3. Ruppin R & Roberts R W, *Phys., Rev.*, **B3** (1971), 1406; B4 (1971), 2041.
4. Madan M P, *Physics*, 51 (1971) 526; *J. appl. Phys.*, 44 (1973), 1388.
5. Lowndes R P & Martin D H, *Proc. R. Soc.*, A136 (1970), 351.
6. Fontenella J, Andeen C & Schuele D, *Phys. Rev.*, B6 (1972), 582.
7. Soga N, Schreiber E & Anderson O L, *J. Geophys. Res.*, 71 (1966), 5315.
8. Thomsen L & Anderson O L, *J. Geophys. Res.*, 74 (1969), 981.
9. Slater J C, *Introduction to chemical physics* (McGraw Hill, New York), 1939.
10. Dugdale J S & McDonald D K C, *Phys. Rev.*, 89 (1953), 832.
11. Migault A & Romain J P, *J. Phys. Chem. Solids*, 38 (1977), 555.
12. Pastine D J, *Phys. Rev.*, 138 (1965), 767.

13. Anderson O L, Schreiber E, Liebermann R C & Soga N, *Geophys. Rev.*, 6 (1968), 491.
14. Singh A V, Sharma J C & Shanker J, *Physica*, **94B** (1968), 331.
15. Schuele D E & Smith C S, *J. Phys. Chem. Solids*, **25** (1964), 801.
16. Miller R A & Smith C S, *J. Phys. Chem. Solids*, **25** (1964), 1279.
17. Bartels R A & Schuele D E, *J. Phys., Chem. Solids*, **26** (1965), 537.
18. Tosi M P, *Solid St. Phys.*, 16 (1964), 1.
19. Catlow C R A, Diller K M & Norgett M J, *J. Phys.*, C10 (1977), 1395.
20. Roberts R W & Smith C S, *J. Phys. Chem. Solids*, **31** (1970), 619; 31 (1970), 2397.
21. McLean K O & Smith C S, *J. Phys. Chem. Solids*, **33** (1972), 279.
22. Born M & Lande A, *Verh. Dtsch. Phys. Ges.*, **20** (1918), 210.
23. Born M & Mayer J E, *Z. Phys.*, 75 (1932), 1.
24. Verwey E J W, *Recl. Trav. Chim. Payes Bas.*, 65 (1946), 521.
25. Varshni Y P & Shukla R C, *J. chem. Phys.*, **35** (1961), 582; *Rev. mod. Phys.*, **35** (1963), 130.
26. Patel M N, Gohel V B & Trivedi M D, *Indian J. Phys.*, 41 (1967), 235.
27. Sharma M N & Tripathi S R, *J. Phys. Chem. Solids*, **36** (1975), 45.
28. Sharma M N, Gautam A K & Tripathi S R, *J. phys. Soc. Japan*, **40** (1976), 651.
29. Prakash S & Behari J, *Indian J. pure appl. Phys.*, **7** (1969), 709.
30. Sharma M N & Jain R, *J. phys. Soc. Japan*, 35 (1973), 194.
31. Smith C S & Cain L S, *J. Phys. Chem. Solids*, **36** (1975), 205.
32. Shanker J, Gupta A P & Sharma O P, *Phil. Mag.*, **B37** (1978), 329.
33. Hajj F, *J. chem. Phys.*, **44** (1966), 4618.
34. Mayer J E, *J. chem. Phys.*, **1** (1933), 270.
35. Demarset (Jr) H H, *J. Phys. Chem. Solids*, 35 (1974), 1393.
36. Palciauskas V V, *J. Phys. Chem. Solids*, 36 (1975), 611.

Indian Journal of Pure & Applied Physics
Vol. 18, August 1980, pp. 557-561

Compressibility of Simple Metals on Harrison-Potential

K S Sharma & C M Kachhava
Department of Physics, University of Rajasthan, Jaipur 302 004

Received 5 *April* 1979; *revised received* 24 *August* 1979

An analytical expression for the compressibility of simple metals has been derived for the model potential of Harrison. The potential parameters have been determined from the low wave-vector form-factor data. The formulation tested on seven metals reveals that the calculated values of the binding energy and compressibility show a good accord with the experimental data.

1. Introduction

The problem encountered in the derivation of the compressibility formula mainly arises from the involvement of complicated functions like dielectric screening and interaction potential, which show their appearance in band structure component of the binding energy through energy wavenumber characteristic. The present literature on the subject reveals that results[1-3] of compressibility on the Ashcroft-potential[4] only are available. On the other hand, Harrison's form of potential has shown[5-9] great promise in the appropriate description of a series of metallic properties like phonon dispersion, elastic constants and binding energy. Hence, we consider it worthwhile to study this potential function for the deduction of compressibility of simple metals. It is a common knowledge that most of the band structure contributions for the equilibrium properties (like binding energy and compressibility) originate from form factors below $q = 2k_F$. Thus, the available parameters of the Harrison's potential deduced from properties like phonon-frequencies, which predominantly involve large **q** form factors, are unsuitable for equilibrium properties. This has been demonstrated for the case of Al by Kachhava,[9] who suggested the use of the experimental values of low **q** form factors. We first derive the compressibility formula on the basis of Harrison's potential and then extend this method of parameter calculation for alkali metals and Pb.

2. Theory

We propose a form in the direct space for the electron-ion interaction potential that consists of the Coulomb term and well-known exponential term for the repulsive part, that is predicted quantum mechanically. Thus, we can write the effective model potential as :

$$V(r) = -\frac{z}{r} + a\, e^{-br} \qquad ...(1)$$

where, a and b are the potential parameters; z the valence and r is electron-ion separation distance. Its wavenumber space version is of the form :

$$V(q) = \frac{1}{\Omega_0}\left[-\frac{4\pi z}{q^2} + \frac{ab}{(b^2+q^2)^2} \right] \qquad ...(2)$$

On substituting $a = \beta/r_c^3$ and $b = 1/r_c$ we get the following :

$$V(q) = \frac{1}{\Omega_0}\left[-\frac{4\pi z}{q^2} + \frac{\beta}{(1+q^2 r_c^2)^2} \right] \qquad ...(3)$$

which incidentally is the famous form given by Harrison.[5] Here Ω_0 represents the ionic volume and q is the magnitude of the scattering vector. The screened form-factors are then defined by

$$V_s(q) = V(q)/\epsilon_q \qquad ...(4)$$

where ϵ_q is the dielectric screening function. The corresponding energy-wavenumber characteristic per ion is given by[10]

$$F(q) = -\frac{\Omega_0 q^2}{8\pi}\left[V(q) \right]^2 \left(1 - \frac{1}{\epsilon_q} \right) \qquad ...(5)$$

This allows us to write the binding energy in the following form:[2]

$$U_0 \text{ (Rydberg/atom)} = -\frac{\alpha' z^{5/3}}{r_s} + \frac{2{\cdot}21z}{r_s^2} - \frac{0{\cdot}916z}{r_s}$$
$$- (0{\cdot}115 - 0{\cdot}031 \ln r_s)\, z + \frac{2\beta z}{\Omega_0} + 2 \sum_{\mathbf{h}}{}' F(\mathbf{h}) \qquad ...(6)$$

where $\alpha' = 1{\cdot}79186$ for bcc and $1{\cdot}79175$ for fcc cry-s tals, **h** is the reciprocal lattice vector, and various terms on the right of Eq. (6) represent respectively

*On leave from : Maharani Shri Jaya College Bharatpur 321 001

Table 1—Form Factor Data and Potential Parameters for Simple Metals

	Li	Na	K	Rb	Cs	Al	Pb
q/k_F	2·26	1·96	1·86	1·88	1·78	1·56	1·38
$V_s(q)$ (Rydberg)	0·0000*	0·0000*	0·0000*	0·0000*	−0·0013†	0·0179*	−0·084*
q/k_F	1·26	1·50	1·57	1·57	1·57	1·76	1·42
$V_s(q)$ (Rydberg)	−0·0468†	−0·0232†	−0·0101†	−0·0102†	−0·0071†	−0·0562*	−0·077†
a (Rydberg)	427·4	353·7	221·4	202·4	183·6	1860·8	969·5
b (au^{-1})	2·688	2·058	1·441	1·342	1·208	3·185	2·427
β (Rydberg au^3)	22·0	40·6	74·0	83·7	104·2	57·6	67·8
r_c (au)	0·372	0·486	0·694	0·745	0·828	0·314	0·412

* Experimental point, Ref. 11 † from Heine-Abarenkov model potential from factor curves, Ref. 11

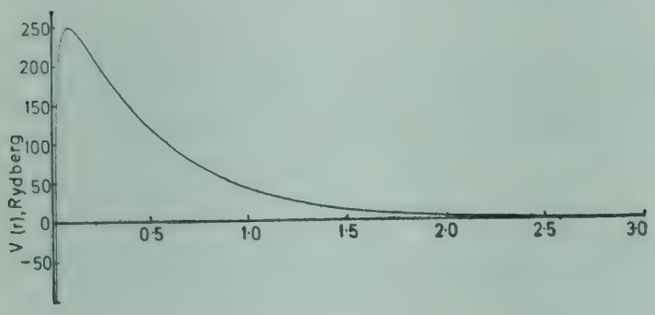

Fig. 1—A typical curve for Harrison's potential in r-space

the electrostatic, kinetic, exchange, correlation, Hartree and band-structure contributions. The prime over sigma excludes $\mathbf{h} = 0$ from the summation.

We are now set for the calculation of the static compressibility, $(1/K)$, which is given by

$$\Omega_0 K = \frac{1}{9}\left[r_s^2 \frac{\partial^2 U_0}{\partial r_s^2} - 2r_s \frac{\partial U_0}{\partial r_s} \right] \quad ...(7)$$

The evaluation of Eq. (7) using Eq. (6) is straightforward, except for the band-structure part, and is given by

$$\Omega_0 K \text{ (Rydberg/atom)} = -\frac{4}{9}\frac{\alpha' z^{5/3}}{r_s} + \frac{22{\cdot}1z}{9r_s^2} - \frac{3{\cdot}664z}{9r_s} - 0{\cdot}0103z + \frac{4\beta z}{\Omega_0} + 2\Omega_0 K_b \quad ...(8)$$

where the terms have been arranged in the same sequence as in Eq. (6). The derivation of $\Omega_0 K_b$ creates problems as $F(\mathbf{h})$ is not a direct function of the electron density parameter r_s.

Observing that $F \equiv F(\Omega_0, h, k_F)$ and that Ω_0 is directly proportional to the cube of r_s, while h ($\equiv |\mathbf{h}|$) and the Fermi-radius, k_F, both vary inversely with r_s, we write

$$r_s \frac{\partial F}{\partial r_s} = 3\Omega_0 \frac{\partial F}{\partial \Omega_0} - h \frac{\partial F}{\partial h} - k_F \frac{\partial F}{\partial k_F} \quad ...(9)$$

We proceed carrying out the above differentiations by employing Hartree type of dielectric screening function given by

$$\epsilon_q = 1 + \frac{2k_F}{\pi q^2}\left[1 + \frac{4k_F^2 - q^2}{4k_F q} \ln \left| \frac{2k_F + q}{2k_F - q} \right| \right] \quad ...(10)$$

and obtain

$$r_s \frac{\partial F}{\partial r_s} = F\left[\frac{1}{\epsilon_h} - 5 - \frac{4P}{\Omega_0 V} \right] \quad ...(11)$$

A further differentiation of Eq. (11) yields

$$r_s^2 \frac{\partial^2 F}{\partial r_s^2} = F\left[18 + 2\left(1 - \frac{1}{\epsilon_h}\right)\left(5 - \frac{1}{\epsilon_h}\right) + \frac{4P}{\Omega_0 V}\left(11 - \frac{2}{\epsilon_h}\right) - \frac{16Q}{\Omega_0 V} + 2\left(1 + \frac{2P}{\Omega_0 V}\right)^2 \right] \quad ...(12)$$

where $V \equiv V(\mathbf{h})$, $F \equiv F(\mathbf{h})$ and we have assumed that

$$P = \frac{4\pi z}{h^2} - \frac{2\beta h^2 r_c^2}{(1 + h^2 r_c^2)^3},$$

and

$$Q = \frac{4\pi z}{h^2} - \frac{3\beta h^4 r_c^4}{(1 + h^2 r_c^2)^4}$$

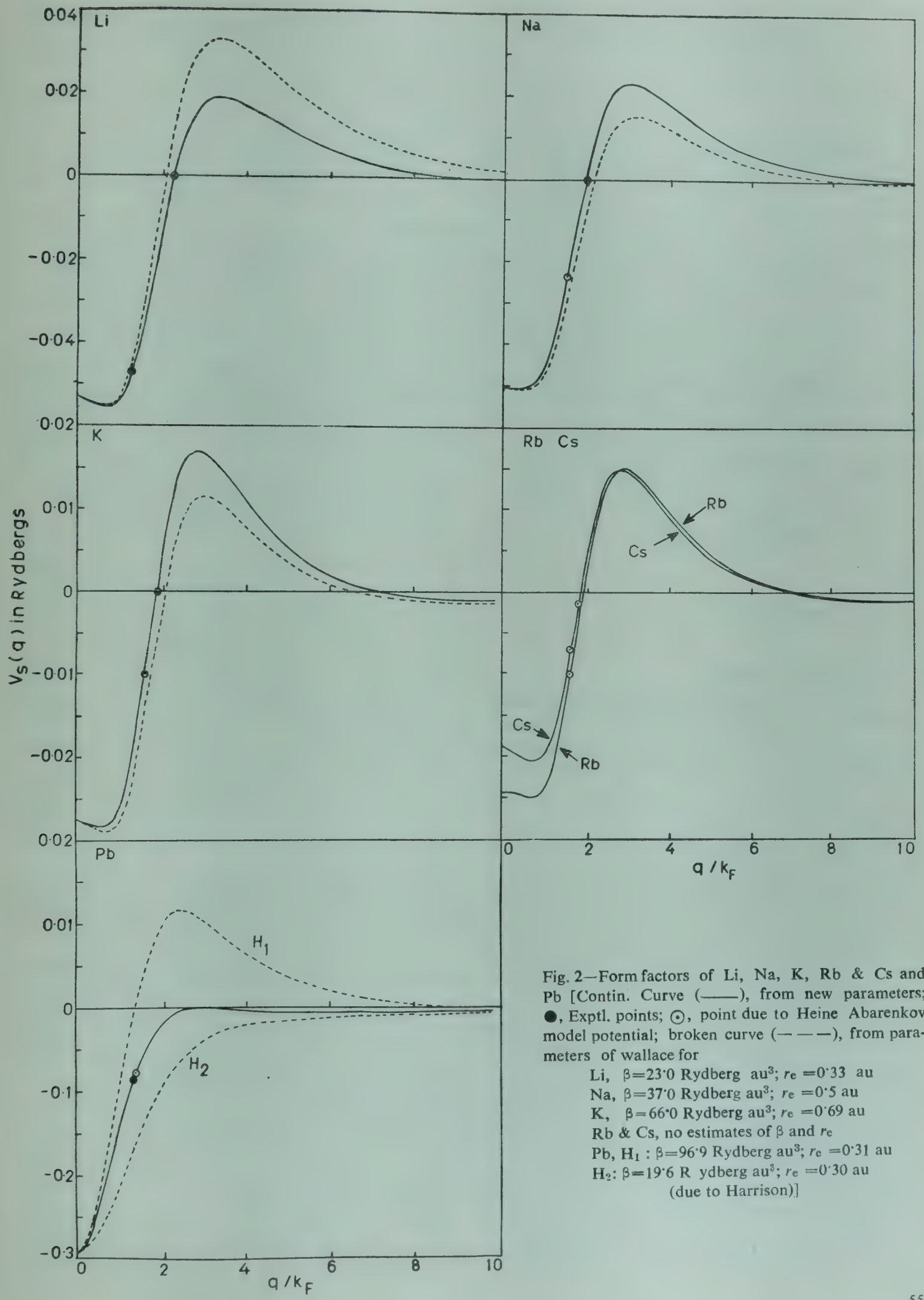

Fig. 2—Form factors of Li, Na, K, Rb & Cs and Pb [Contin. Curve (——), from new parameters; ●, Exptl. points; ⊙, point due to Heine Abarenkov model potential; broken curve (— — —), from parameters of wallace for

Li, $\beta=23{\cdot}0$ Rydberg au^3; $r_e=0{\cdot}33$ au
Na, $\beta=37{\cdot}0$ Rydberg au^3; $r_e=0{\cdot}5$ au
K, $\beta=66{\cdot}0$ Rydberg au^3; $r_e=0{\cdot}69$ au
Rb & Cs, no estimates of β and r_e
Pb, H_1 : $\beta=96{\cdot}9$ Rydberg au^3; $r_e=0{\cdot}31$ au
H_2: $\beta=19{\cdot}6$ R ydberg au^3; $r_e=0{\cdot}30$ au
(due to Harrison)]

Table 2—Binding Energy ($-U_0$) and Inverse Compressibility ($\Omega_0 K$) of a Number of Metals

	Li	Na	K	Rb	Cs	Al	Pb
			Rydberg/atom				
			Binding energy				
Present calculations	0·553	0·467	0·382	0·366	0·339	4·18	7·30
Kachhava	0·539	0·463	0·384	0·362	0·337	4·31	6·01
Exptl.	0·511	0·460	0·390	0·366	0·345	4·16	7·16
			Inverse compressibility				
Present calculations	0·125	0·122	0·129	0·112	0·112	0·507	0·596
Kachhava	0·126	0·126	0·114	0·112	0·105	0·703	0·885
Exptl.	0·123	0·129	0·123	0·116	0·116	0·546	0·595

Eq. (7) could now be exploited to yield the band structure contribution to the compressibility in the following form :

$$\Omega_0 K_b = \frac{2}{9} \sum_h' F \left[20 + \frac{1-7\,\epsilon_h}{\epsilon_h^2} - \frac{4P}{\epsilon_h \Omega_0 V} + \left(\frac{2P}{\Omega_0 V}\right)^2 + \frac{2R}{\Omega_0 V} \right] \quad .. (13)$$

where

$$R = 15\,P + 4\,Q$$

3. Results and Discussion

The potential parameters for Al were determined by Kachhava[9] from the experimental form factors;[11] however, it has been observed that the available experimental data[11] are not sufficient for Cs, whereas for Li, Rb and also for Cs, these seem to be partially unreliable for the purpose of calculating the parameters. For the sake of uniformity, we therefore, use one of the experimental points and a suitably chosen point on the form factor curves,[11] obtained from the Heine-Abarenkov model potential, for calculating the potential parameters. The selected sets of form factors and the calculated parameters are collected in Table 1. The experimental data for Cs being unreliable, we use both the points of the form factors obtained from Heine-Abarenkov model potential for this metal. The typical curve for the Harrison's potential in the direct space is reproduced in a graphical form in Fig. 1, which can be modified for a particular metal choosing appropriate values of a and b (Table 1). The form factors obtained from the new parameters have been compared with the relevant curves obtained on the basis of the parameters of Wallace[6,7] for Li, Na and K in Fig. 2, where we also show the points employed presently by us for the calculation of parameters. It may be observed from these graphs that the convergence of form factors according to the new parameters is faster compared to the parameters obtained from phonon frequencies. In Fig. 2, we also display the form factors of Rb and Cs. Further, a better convergence for the form factors of Pb also can be observed for the new parameters as compared to the two sets of Harrison[5] from Fig. 2. The calculated values of the binding energy and compressibility on the basis of the self-consistent screening of Singwi *et al.*,[12] which takes into account the exchange and correlation effects are presented in Table 2. It may be remarked that in the above formulation, where we replace ϵ_h in the final results by the self-consistent screening to qualitatively include the exchange and correlation effects, the corrections to these effects are of the first order. For the sake of comparison we have included the theoretical results from the Ashcroft-potential presented by Kachhava,[2,3] and Sharma and Kachhava,[13] who claimed improvement on the work of Ashcroft and Langreth[14] for the same potential. We find that in most of the cases our results, both for binding-energy and compressibility, are better than Kachhava's values. The present results are also better than those of Price *et al.*[1] on Na for the compressibility. The same statement holds good in connection with the comparison with the calculations performed by Saxena *et al.*[15] However, our results for Na and K are slightly inferior to the values of Brovman *et al.*,[16] who made calculations on a different potential and struck nearly a perfect agreement with the experimental data for Na and K. Not withstanding the above discussion, we would like to bring home the important point that the motivation of the present work was to report the direct space form of the highly well established Harrison's potential and to determine its parameters in the best possible way and consequently report the corresponding results for binding energy

and compressibility for a number of metals. This obviously completes the sequence of results for the various metallic properties on the basis of Harrison's pseudopotential in a successful way. The closeness between our theoretical results and the experimental data[17] not only lends support to the second order perturbation theory but also justifies the motivation behind the present investigation.

Acknowledgement

The authors express their deep sense of gratitude to Prof. T Toya of Hokkaido University, Japan, for continued encouragement and are thankful to Dr M P Saksena for providing the necessary departmental facilities. One of the authors (KSS) is also thankful to Dr M L Gupta for his keen interest in the work and to the University Grants Commission, New Delhi, for financial assistance.

References

1. Price D L, Singwi K S & Tosi M P, *Phys. Rev.*, B2 (1970), 2983.
2. Kachhava C M, *Phys. Status Solidi*, (b) 52 (1972), 547.
3. Kachhava C M, *J. Phys.*, *F* 3 (1972), 24.
4. Ashcroft N W, *Phys. Lett.*, **23** (1966), 48.
5. Harrison W A, *Phys. Rev.*, 139 (1965), 179.
6. Wallace D C, *Phys. Rev.*, 176 (1968), 832.
7. Wallace D C, *Phys. Rev.*, 178 (1969), 900.
8. Wallace D C, *Phys. Rev.*, 187 (1969), 991.
9. Kachhava C M, *Solid. St. Commun.*, **11** (1972), 473.
10. Harrison W A, *Pseudopotentials in the theory of metals*, (Benjamin, New York) 1966.
11. Ehrenreich H, Seitz F & Turnbull D, *Solid St. Phys.*, 24 (Academic Press, New York), 1970, 183.
12. Singwi K S, Sjölander A, Tosi M P & Land R H, *Phys. Rev.*, **B1** (1970), 1044.
13. Sharma K S & Kachhava C M, *Indian J. pure appl. Phys.*, (1980), In Press.
14. Ashcroft N W & Langreth D C, *Phys. Rev.*, 155 (1967), 682.
15. Saxena V K, Kapoor Q S & Bhattacharya D L, *Phys. Status. Solidi*, 34 (1969), 147.
16. Brovman E G, Kagan Yu & Kholas A, *Soviet Phys. Solid St.*, 12 (1970), 786.
17. Kachhava C M, *Physics Lett.*, 39A (1972), 265.

Indian Journal of Pure & Applied Physics
Vol. 18, August 1980, pp. 562-567

X-Ray Induced Thermoluminescence in $CaSO_4$: Sm Phosphors

S G Sabnis & S H Pawar

Materials Research Laboratory, Department of Physics, Shivaji University, Kolhapur 416 004

Received 14 *May* 1979; *revised received* 29 *February* 1980

The thermoluminescence (TL) of X-ray irradiated $CaSO_4$: Sm phosphors, prepared in the laboratory with and without the addition of Na_2SO_4, has been studied in the temperature range of 300-600 K for a warming rate of 50 K min^{-1}. $CaSO_4$: Sm phosphors without charge compensator (Na_2SO_4) give two main glow peaks at 383 K and 503 K together with two unresolved shoulders at 410 K and 478 K. The general features of the glow curves are discussed. The addition of charge compensator (Na_2SO_4) in $CaSO_4$: Sm phosphors is found to influence the general features of glow curves. The conclusions are drawn regarding the possible role of charge compensator in thermoluminescence behaviour of $CaSO_4$: Sm phosphors. The values of activation energies have been estimated by various methods. An attempt has been made to find the type of kinetics involved in TL process of $CaSO_4$: Sm (Na_2SO_4) phosphors.

1. Introduction

There is a revival of interest in the rare earth (RE) activated $CaSO_4$ phosphors due to their applications in the field of radiation dosimetry. The gamma irradiation-induced thermoluminescence (TL) in $CaSO_4$: RE phosphors has been studied extensively by Nambi *et al.*[1] and Nambi and Bapat[2] and has revealed the mechanism of TL in these phosphors. Recently, the use of these phosphors in diagnostic X-ray analysis has been suggested.[3,4] However, not much details are available on X-ray irradiation-induced TL in these phosphors, as far as the authors are aware. In the present paper, a report is made on X-ray irradiation-induced TL in $CaSO_4$: Sm phosphors. The concentration of Sm has been varied systematically in these phosphors upto 0·375 wt% of Sm, and its role on TL output has been investigated.

Many workers[1-6] have doped $CaSO_4$ with RE^{3+} at the place of Ca^{2+}, by creating a vacancy of Ca^{2+} for the charge compensation to occur. This will, however, restrict the entry of RE^{3+} in the host lattice. In the present investigation, Sm^{3+} has been used as a dopant along with Na^+ ion as the charge compensator. The role of charge compensator on the TL of $CaSO_4$:Sm phosphors has been revealed. Without charge compensator, many overlapping glow peaks have been observed above room temperature while with the charge compensator only a single, sharp and intense glow peak has been recorded. The activation energies and the type of kinetics involved in the TL process of $CaSO_4$:Sm phosphors both with and without charge compensator have been estimated.

2. Experimental Details

2.1 Sample Preparation

Calcium sulphate phophors doped with Sm as an activator were prepared from an Indian mineral, gypsum, following closely the method of Nambi *et al.*[1] The details have been reported earlier.[7] In brief, 10 g of purified gypsum, 1 g of Na_2SO_4 and appropriate quantity of Sm_2O_3 were dissolved in concentrated H_2SO_4 of A R grade and the mixture was heated to 300°C for about 8 hr. The heat-treated residue was washed repeatedly with hot distilled water to remove the excess unused traces of Na_2SO_4 and then dried at 60°C. Final heat treatment for 2 hr at 600°C was given to the phosphor which was then quenched to room temperature. The concentration of Sm was varied from 0 to 0·375 wt%. Some phosphors were prepared without addition of Na_2SO_4.

2.2 X-ray irradiation

X-ray irradiation was done using a Philips sealed tube (molybdenum target) which was operated at 30 kV and 11 mA. The samples were exposed to X-rays for 1 hr at room temperature. To study the dosage dependence of TL of $CaSO_4$:Sm phosphors, irradiation time was varied from 0 to almost 180 min.

2.3 Measurements of TL Glow Curves

TL glow curves were recorded above room temperature (300 K) up to about 600 K at a linear heating rate of 50 K min^{-1} using IP 21 photomultiplier tube (typical operating voltage 1000 V) and Ominscribe

strip chart recorder. A fixed quantity of X-ray irradiated sample was spread uniformly over a circular depression of a metal strip to which chromel-alumel thermocouple was spot-welded for measuring the instantaneous temperature at the phosphor. A water filter which cuts of the undesirable heat radiation was interposed between the sample and photomultiplier housing assembly.

3. Experimental Results

3.1 TL Glow Curves and Activator Concentration Effects

Thermoluminescence of $CaSO_4$: Sm phosphors prepared with and without added Na_2SO_4 were studied. The nature of glow curves for Na_2SO_4 added $CaSO_4$: Sm phosphors is altogether different from that of phosphors without Na_2SO_4. Fig. 1 shows the typical glow curves for these samples. The curves are obtained after normalizing the maximum glow peak intensity to a value of 100 and shifting the ordinates suitably to avoid overlapping and to render the comparison easier. The curve (a) of Fig. 1 which represents the glow curve of $CaSO_4$ phosphor without activator is four-fold magnified as it gives weak and diffused glow peaks. The curves (b) to (e) of Fig. 1 are the glow curves for $CaSO_4$:Sm phosphors with increase in concentration of Sm. These curves consist of 4 glow peaks lying at about 383, 410, 478 and 503 K and they are referred to respectively as Ist, IInd, IIIrd and IVth glow peaks in the further discussion.

From Fig. 1, it is noted that though the nature of the glow curves remains unaltered intensities of the glow peaks are changed markedly especially for Ist and IVth glow peaks. This variation in the intensities of I and IV peaks with samarium concentration in $CaSO_4$: Sm phosphors, is depicted in Fig. 2. The nature of the curves is of complex type. On examining the glow curves of Fig. 1, it is observed further that the temperatures of the glow peaks are slightly shifted to lower values with increase in concentration of Sm in $CaSO_4$:Sm phosphors.

Fig. 3 gives a single, sharp and intense glow peak lying at about 390 K for typical Na_2SO_4 added $CaSO_4$:Sm phosphor (PS 27). In order to understand the effect of Sm concentration on the glow curves of Na_2SO_4 added $CaSO_4$: Sm phosphors, a series of 11 phosphors were prepared varying the concentration of Sm from 0 to 0·375 wt% and glow curves were investigated. It is worthnoting that the appearance of the single and sharp glow peak (Fig. 3) did not alter with increase in concentration of Sm but its intensity changed remarkably. As the area under the glow curve gives the total TL

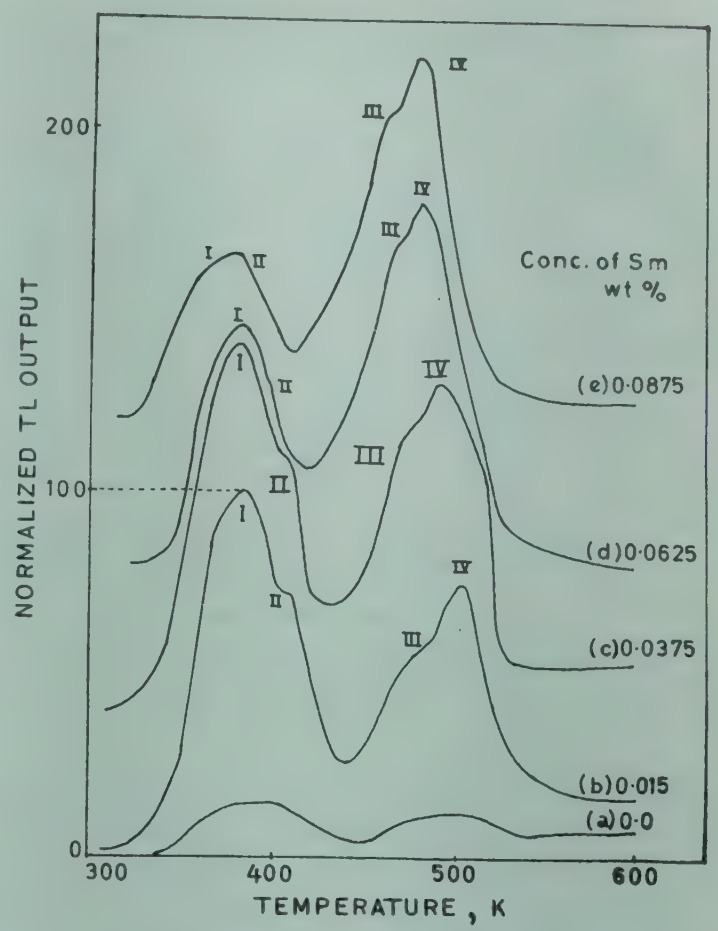

Fig. 1—TL glow curves of typical $CaSO_4$:Sm phosphors (without Na_2SO_4) [Curves a-e correspond to different concentrations of Sm e.g. (a), 0, (b), 0·015, (c), 0·0375, (d), 0·0625 and (e), 0·0875 wt% in $CaSO_4$ phosphors]

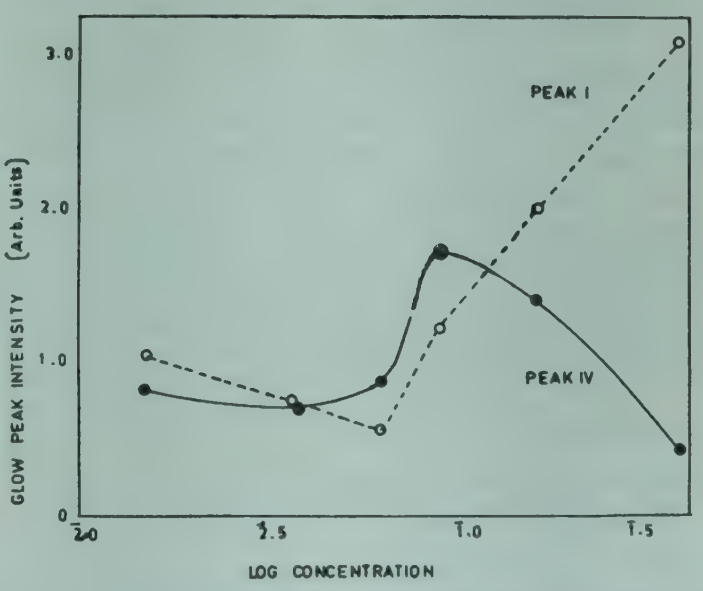

Fig. 2—Variation of intensities of glow peaks I and IV versus log of concentration of Sm in $CaSO_4$: Sm phosphors without Na_2SO_4

output, the variation of TL output with Sm concentration is shown in Fig. 4. The TL output exhibits a sharp increase during initial addition of dopant concentration reaching a maximum at an optimum concentration level of 0·0875% by wt of Sm, after

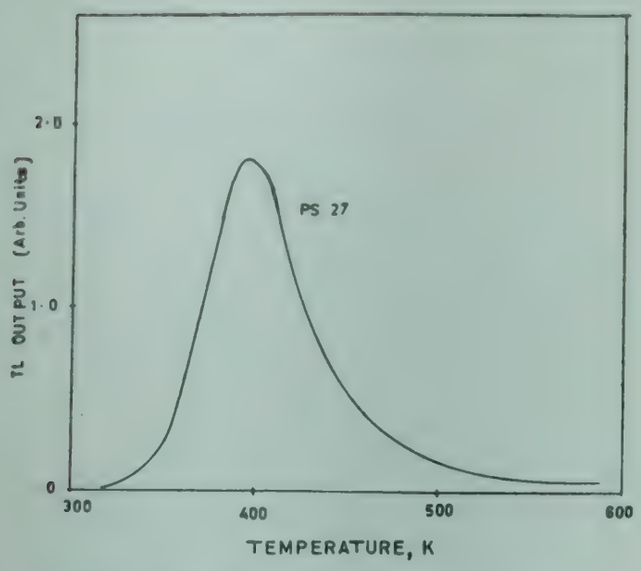

Fig. 3—Typical glow curve of $CaSO_4$:Sm (Na_2SO_4) phosphor

which the TL output gradually falls off with further increase in the concentration of dopant. This is called concentration quenching. The curve is normalized assuming the maximum intensity at optimum concentration to be 100. The theoretical fit for concentration quenching is also illustrated in Fig. 4. A similar behaviour is observed for a series of $CaSO_4$:Sm phosphors without Na_2SO_4 and is shown in Fig. 4.

3.2 Effect of X-ray Irradiation Time on Glow Peak Intensity

From the concentration quenching data, the phosphors with (PS28) and without (PS24) Na_2SO_4 giving the optimum TL output were selected for this study and exposed to different X-ray irradiation times. The nature of the glow curves was not affected but the intensities of glow peaks increased with increase in X-ray irradiation time. This variation of intensities with X-ray irradiation time both for PS28 and PS24 phosphors, is shown in Fig. 5.

4. Discussion

4.1 Glow Peak Activation Energies and Type of Kinetics Involved in TL Process

In X-ray irradiated $CaSO_4$:Sm phosphors, glow peaks observed (Fig. 1) lie at about 383, 410, 478 and 503 K. The values of activation energies were obtained by using the relation[1]

$$E = (3{\cdot}12 \times 10^{-3}\, T_g - 0{\cdot}23)\ \text{eV} \qquad \ldots(1)$$

where T_g is the glow peak temperature, and E the activation energy. The estimated values of activation energies of the respective glow peaks are 0·97, 1·05, 1·25 and 1·34 eV. This is in good agreement with the results reported earlier.[1]

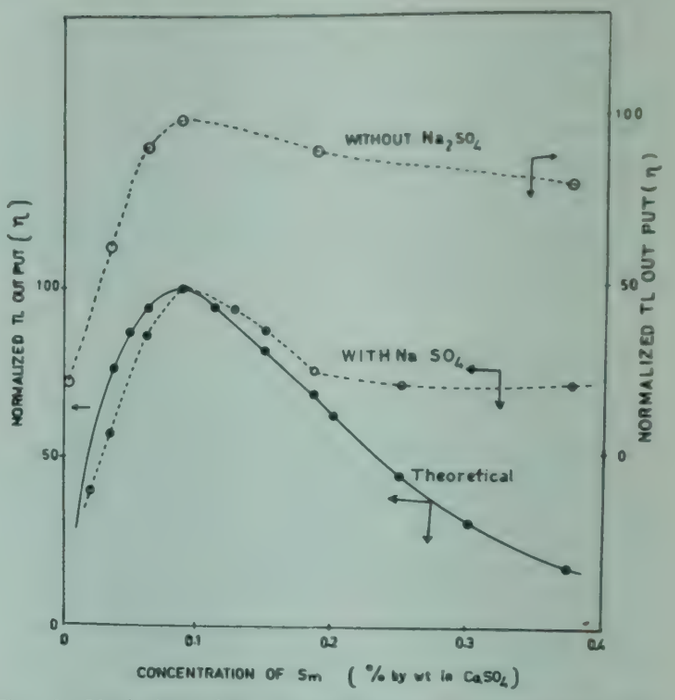

Fig. 4—Variation of TL output with Sm concentration con-[tin. curve (——), theoretical, and broken curve (– – –), experimental]

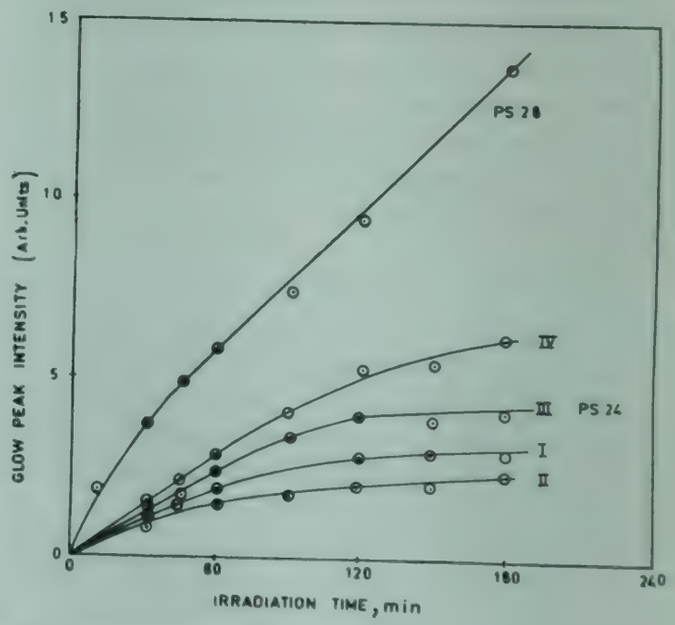

Fig. 5—Variation of the intensities of glow peaks with X-ray irradiation time for PS28 and PS24 phosphors with Sm 0·0875 wt%

As there are no data available in the literature regarding TL and the type of kinetics involved in $CaSO_4$:Sm (Na_2SO_4) phosphors, the results obtained are discussed at length here. Since $CaSO_4$:Sm phosphors with Na_2SO_4 exhibit a single, sharp and intense glow peak, the analysis of the glow curves becomes relatively simple. Activation energies associated with TL glow peaks can be estimated in several ways.[8] In the present investigation, only 4 methods were tried.

Table 1—Estimated Values of Activation Energies (eV) by Different Methods and Determination of the Order of Kinetics of $CaSO_4$: Sm (Na_2SO_4) Phosphors

Sample No	Wt% of Sm	Initial rise method, Ref. 9	Halperin & Braner Method, Refs. 10, 11		Chen's Method, Ref. 12		Nambi, Ref. 1	$g=\delta/w$	e^{-1} $(1+\Delta)$
			for first order kinetics	for second order kinetics	for first order kinetics	for second order kinetics			
PS25	0·015	0·87	0·77	0·86	0·74	0·88	1·00	0·53	0·39
PS26	0·0375	0·89	0·72	0·80	0·69	0·81	1·00	0·54	0·40
PS27	0 0625	0·93	0·77	0·86	0·73	0·87	0·99	0·60	0·39
PS28	0·0875	0·95	0·78	0·88	0·77	0·84	1·01	0·55	0·40

The first method used is the initial rise method[9] where the intensity of thermoluminescence in the initial part of the glow curve is expressed in the form

$$I = F \exp\left(\frac{-E}{kT}\right) \qquad \ldots(2)$$

where, F is the function of number of filled traps, k the Boltzmann's constant and I the TL intensity at absolute temperature T. A plot of ln I against T^{-1} is linear with a slope E/k.

The values of activation energies obtained by using the initial rise method, Halperin and Braner equation,[10,11] Chen's equation[12] and Nambi[1] are given in Table 1 for $CaSO_4$:Sm phosphors with charge compensator. It can be noted from Table 1 that the values of activation energies obtained with initial rise method, which is insensitive to the order of kinetics, are close to the values for second order kinetics. This indicates that the addition of Na_2SO_4 for charge compensation in $CaSO_4$:Sm phosphors, does not alter their second order kinetics in TL process.

Halperin and Braner[11] have suggested a simple method of determining the order of kinetics from the shape of the glow peak. The method defines a parameter called symmetry factor $g = \delta/w$, where δ is the half-width towards the fall-off of the glow peak and w the full width of the glow peak at half peak intensity. The values of $g \leqslant e^{-1}\ (1 + \Delta)$ correspond to the first order kinetics while larger values of g to the second order kinetics, where $\Delta = 2k\ T_g/E$. In the present investigation, the values of g and $e^{-1}\ (1 + \Delta)$ are estimated from the shape of the glow peak for $CaSO_4$: Sm (Na_2SO_4) phosphors and are summarized in Table 1. The values of $g > e^{-1}\ (1 + \Delta)$ can be noted from Table 1 supporting the second order kinetics in TL process of $CaSO_4$: Sm (Na_2SO_4) phosphors.

4.2 Dosage Dependence of Thermoluminescence

Thermoluminescence glow curves presented in Figs. 1 and 3 are obtained with the irradiation time 1 hr which is within the linear range of Fig. 5. These dosages are so chosen as to produce the minimum amount of damage to the crystal. The low dosage assures that only a small percentage of the trapping centres is filled. The origin of TL in RE doped $CaSO_4$ phosphors has been attributed to the reduction of RE^{3+} to RE^{2+} by the capture of an electron in the irradiation process and its conversion back to RE^{3+} in the heating process of thermoluminescence.[1,6,13] It is evident from Fig. 5 that the concentration of Sm^{2+} produced by irradiation exhibits saturation with dosage. The dosage saturation of TL of $CaSO_4$: Sm phosphors without charge compensator can be explained by assuming that only a limited number of trivalent Sm ions is available for the reduction of charge.

4.3 Concentration Quenching

The falling off in the TL output after optimum concentration (Fig. 4) is thought of in terms of concentration quenching effect. The theoretical curve for the concentration quenching is plotted by using modified equation of Ewles and Lee.[14]

$$\eta = \frac{K}{1 + \alpha\, c^{-1} \exp n\, c} \qquad \ldots(3)$$

where, K is the normalizing constant; α, constant involving the absorption coefficient of activator and structure; n, number of lattice ions associated with radiative centres; c the concentration in wt% and η the normalized output.

Although the theoretical curve for concentration quenching gives the nearest fit to our experimental points, at very low and very high concentrations the points are deviating from the theoretical curve. The reason for this complexity arising at high and

low doping is not understood. The quenching in Sm^{3+} is due to energy transfer from one ion to a lower lying level of another ion by transitions that are matched in energy at optimum concentration of 0·0875% wt of Sm.

4.4 Glow Peak Temperatures

The observed decrease in glow peak temperature (T_g) with increase in dopant concentration (Fig. 1) is evident by relation:[15]

$$T_g = \frac{E_g}{k \ln\left(\frac{S T_g}{\beta}\right)} \left[1 + f(S, \beta, E_g)\right]^{-1} \quad \ldots(4)$$

where, S is the escape frequency factor; β the heating rate and

$$f(S, \beta, E_g) = \frac{\ln\left[\frac{k T_g}{E_g}\right]}{\ln\left[\frac{S T_g}{\beta}\right]}$$

when there is no retrapping and monomolecular recombination
and

$$f(S, \beta, E_g) = \frac{\ln\left\{\frac{2 n_0}{N} \frac{k T_g}{E_g}\left[1 + \frac{n_0}{N}\int_0^{T_g} \frac{S}{\beta} \exp(E_g/kT)\, dT\right]^{-1}\right\}}{\ln\left[\frac{S T_g}{\beta}\right]}$$

when retrapping equals the recombinations (second order kinetics).

The values of $f(S, \beta, E_g)$ in second order kinetics depend on n_0/N which is not the case in first order kinetics. The value of n_0/N can be altered either by increasing concentration of dopant in the phosphor or by increasing the irradiation dosage. The increase in the value of n_0/N will increase $f(S, \beta, E_g)$ and decrease T_g. This explains the decrease in T_g with the increase in concentration of Sm in $CaSO_4$ phosphors. The slight change in T_g with increase in concentration, as shown in Fig. 1, can be noted in support of second order kinetics. Similarly the decrease of T_g with dosage in $CaSO_4$:Sm phosphors as reported earlier by the authors gives an additional evidence.[16]

4.5 Effect of Na_2SO_4 on TL Behaviour of $CaSO_4$: Sm Phosphors

Comparing Figs. 1 and 3 which represent the glow curves of $CaSO_4$: Sm phosphors of without and with Na_2SO_4 respectively, it is seen that the addition of Na_2SO_4 wipes out the levels corresponding to II, III and IV peaks. In addition, the TL output is increased remarkably. These observations are understood on the basis of charge compensation theory of Kroger and Helligmann.[17] In the absence of Na_2SO_4, two Sm^{3+} ions may be incorporated by removing three Ca^{++} ions giving rise to Ca^{++} vacancy in $CaSO_4$. In presence of Na_2SO_4, Sm^{3+} and Na^+ ions will be incorporated at the places of two Ca^{++} ions and there will be no predominant defects.

As predicated above, the lattice defects are Ca^{++} vacancies in these phosphors, and these defects might be responsible for TL glow peaks. In heat-treated $CaSO_4$, Ca^{++} vacancies are likely to occur, as it is heated in the atmosphere of H_2SO_4. This has been confirmed by thermoelectric power measurements, where the phosphor is found to be of *p*-type.[18] However, the addition of Na_2SO_4 prevents Ca^{++} vacancies, as Na^+ ions go into the lattice both interstitially and substitutionally. A similar mechanism has been suggested to explain the magnetic behaviour of these phosphors.[7]

5. Conclusions

1 The Na_2SO_4 added $CaSO_4$: Sm phosphors give a single glow peak, while $CaSO_4$:Sm phosphor without Na_2SO_4 give 4 glow peaks.

2 The second order kinetics has been observed in both phosphors.

3 The TL output increases with increase in X-ray irradiation time for both phosphors.

4 Concentration quenching effect has been observed with the optimum TL output at 0·0875 wt% of Sm.

Acknowledgement

The authors are grateful to Mr R M Raverkar, Principal, Science College, Karad, for his constant encouragement and to Mr M R Mulla for his help in experimental arrangement.

References

1. Nambi K S V, Bapat V N & Ganguly A K, *J. Phys.*, C 7 (1974), 4403.
2. Nambi K S V & Bapat V N, *Indo-Soviet Conf. on Solid State Materials*, Indian Institute of Science, Bangalore, 1972.
3. Viswanathan P S, Ayappan P & Sasane J B, *Proc. Nat. Symp. on Thermoluminescence and its Application, RRC Kalpakam*, Madras, 1975, (Department of Atomic Energy, Govt. of India, Bombay), 1 1975, 414.
4. Yamashita T, Nada N, Onishi H & Kitmura S, *USAEC Report Conf.* 680920, (1968), 4.
5. Yamashita T *et al.*, *Health Phys.*, 21 (1972), 295.
6. Bapat V N, *J. Phys.*, C10 (1977), 465.
7. Sabnis S G & Pawar S H, *Indian J. pure appl. Phys.*, 15 (1977), 817.

8. Shalgaonkar C S & Narlikar A V, *J. material Sci.*, 7 (1972), 1465.
9. Lehmann W, *J. Luminescence*, 5 (1972), 87.
10. Halperin A, Braner A A, Ben-Zvi A & Kristianpoller N, *Phys. Rev.*, 117 (1960), 416.
11. Halperin A & Braner A A, *Phys. Rev.*, **117** (1960), 408.
12. Chen R, *J. appl. Phys.*, 40 (1969), 570.
13. Merz J L & Pershan P S, *Phys. Rev.*, **162** (1967), 217.
14. Ewles J & Lee N, *J. electrochem. Soc.*, **100** (1953), 392.
15. Merz J L, *Technical Report No.* 514, (Harvard University, Cambridge, Massachusetts), 1966, 4.6.
16. Sabnis S G & Pawar S H, *Symposium on Luminescence and Allied Phenomena*, Indian Institute of Technology, Kharagpur, December, 1978.
17. Kroger F A & Hellingmann J E, *J. electrochem. Soc.*, 95 (1949), 68.
18. Pawar S H, *Indian J. pure appl. Phys.*, 16 (1978), 1034.

Indian Journal of Pure & Applied Physics
Vol. 18, August 1980, pp. 568-572

Electrical Conductivity & Thermoelectric Power in As_2S_3 Glasses

M Datta, P N Banerjee & D L Bhattacharya
Physics Department, Calcutta University, Calcutta 700 009
and
S S Prasad & K P Srivastava
Central Glass & Ceramic Research Institute, Calcutta 700 032

Received 30 *July* 1979; *revised received* 17 *December* 1979

The dc electrical conductivity (σ) and the thermoelectric power (S) for bulk As_2S_3 samples prepared in different melting schedules were measured at different temperatures (T) below the glass transition temperature ($T_g \sim 480$ K). The log σ versus $1/T$ curves for all these samples were, in general, linear but deviated from linearity at temperatures lower than 393 K. The thermoelectric data show that the samples are of p-type. An approximate linear fit indicates that the activation energies obtained from the thermo-emf data and those from the dc electrical conductivity differ. The experimental results indicate a mixed conduction process involving non-localized states and hopping between localized states. The conduction mechanism in these glasses is very much dependent on the production conditions.

1. Introduction

The electrical properties of amorphous As_2S_3 glass have been investigated by many workers.[1-7] Most of these studies have been confined to the properties of the glasses of different compositions but prepared by the same technique. The present paper reports on the dc electrical conductivity and Seebeck effect in bulk samples of As_2S_3 prepared in two somewhat different melting schedules, at temperatures below the glass transition temperature.

2. Experimental Details

2.1 Sample Preparation and Characterization

As_2S_3 glasses were prepared by the distillation method employing a silica apparatus consisting of a distillation tube, condenser arm and accumulator. As and S in stoichiometric ratio of 2 and 3 with some excess sulphur (0·25%) were first reacted in the distillation tube at approximately 800 K and then distilled at about 950 K into the accumulator. The glasses were then stirred to homogenize them and collected in a mould, kept at 500 K, and then annealed at 475 K. The entire operation was carried out in dry N_2 atmosphere.

Samples A and B refer to two sets of different melting schedules of which A_1, A_2, A_3 correspond to three pieces taken from different regions of the A sample and B_1, B_2 are two pieces taken similarly from the B sample.

Compositional analysis for these materials show that in A sample the As and S contents are 39 and 61 at. % whereas in B sample, it is 38·5 and 61·5 at. % respectively.

X-ray diffraction patterns show that the samples A and B are both non-crystalline. The radial distribution functions of these glasses were determined (Nandi A K, Pal S and Mukherjee B, personal communication) from an independent X-ray powder diffraction experiment. The results obtained can be interpreted according to a chain crossing model (CCM) in which a sulphur chain structure is formed and the As atoms do not form bonds with other As atoms. A theoretical value of the coordination number $\eta = 2{\cdot}22$ was obtained. From the area under the first peak in the radial distribution function, the coordination number found experimentally is 2·26 for the A sample and 2·49 for the B sample. From a random covalent model calculation, η is found to be 2·95. The structures in A and B samples may thus be regarded as maintaining predominantly a chain-like structure of sulphur atoms.

The glass transition temperatures (T_g) were measured by electrical conductivity (σ) experiments at different temperatures (T). Plots of log σ against $1/T$ show a distinct change in slope at a high temperature, which corresponds to T_g (about 480 K for both A and B samples). Values of T_g for A and B samples are (484 ± 6) K and (483 ± 8) K respectively, which is slightly greater than that reported in the literature.[6]

2.2 Electrical Properties

Three pieces A_1, A_2, A_3 of sample A and two pieces B_1, B_2 of sample B in the form of rectangular parallelopipeds of dimensions 2·5 cm × 0·8 cm × 0·6 cm were used. A high-impedance power-supply and

an Electrometer Amplifier (ECIL, model EA 815), calibrated in the range of resistance from $10^6\ \Omega$ to $10^{14}\ \Omega$, were connected in series with the sample using shielded wires. Electrical contacts between the sample and suitably designed brass clamps were made using colloidal graphite paint and applying only a small pressure. There was no difference in the measured conductivity when the area-thickness ratio of the samples was changed, or when the contact pressures were changed. This showed that the effect of contact resistance is negligible in our experiments. The current-voltage (I-V) characteristics were measured at different temperatures ranging from 350 to 460 K (below the transition temperature, $T_g \sim 480$ K) using applied voltages up to 200V. For each voltage, sufficient time was allowed for the current to reach a steady value. The temperatures of the enclosure in which a sample was kept were measured with a previously calibrated chromel-alumel thermocouple located very near to the specimen.

A schematic diagram for measuring the Seebeck effect is shown in Fig. 1, which is more or less similar to that of Kolomiets.[8] The samples were in the form of parallelopipeds of dimensions 0·6 cm × 0·8 cm × 1 cm and were clamped between two brass plates. Copper wires soldered to the brass plates were connected to the Electrometer Amplifier. Two chromel-alumel junctions were attached to two brass plates for measuring the temperatures of the two ends, electrical insulation being provided by thin mica sheets. On one side of the sample, a small heater coil was attached and was insulated from the sample with an asbestos sheet (thickness ~ 7 mm). This sheet also serves to produce a small temperature gradient in the sample. The maximum temperature gradient developed in our experiment was 8 K/mm. All electrical leads were shielded and maintained at a constant temperature. The temperature of the oven was measured with an independent chromel-alumel thermocouple.

The thermo-emfs generated in As_2S_3 glass for different temperature-gradients at a constant average temperature were measured. The Seebeck emf was noted after maintaining a constant temperature difference across the sample for a period of 1-1½ hr. The experiment was repeated by changing the constant average temperature in order to measure the Seebeck coefficients at different average temperatures.

During the measurements of the dc electrical conductivities and also thermoelectric powers, the

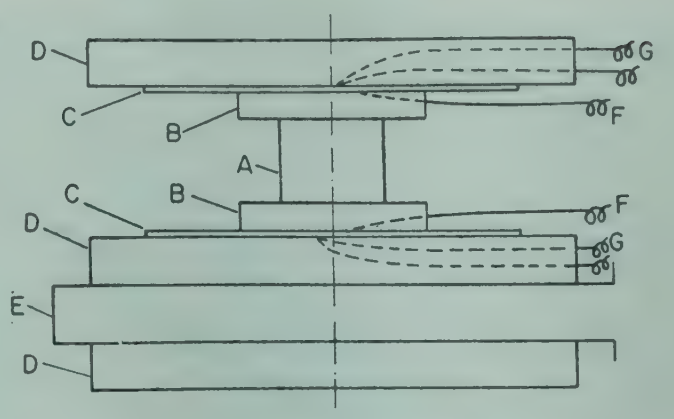

Fig. 1—Schematic diagram of the set-up for measuring Seebeck emf

temperatures were always kept steady for at least 4 hr before readings were taken.

3. Experimental Results

3.1 dc Electrical Conductivity

The I-V characteristics were plotted at different temperatures (below 480 K, which is the glass transition temperature) for each sample. The behaviour was found to be ohmic in general, excepting for the B sample which showed non-ohmic behaviour above an applied voltage of 140 V (Fig. 2). The value of σ, the dc electrical conductivity at each temperature, was calculated and a curve showing $\log \sigma$ against $1/T$ was drawn for each sample and a straight line was fitted to the data, excepting those at low temperatures by the least squares method for the samples A_2, A_3, B_1 and B_2, which show slight deviations from linearity (Fig. 3) in each sample.

The dc electrical conductivities of most of these glasses obey the relation.

$$\sigma = C \exp [-E_c/kT] \qquad (1)$$

where C and E_c are called the pre-exponential factor and the activation energy for conductivity respectively.[8,9] The values of E_c and C obtained for the different samples investigated are listed in Table 1.

3.2 Thermoelectric Power

For Seebeck coefficient measurements, the values of thermo-emf (e) and the corresponding values of temperature differences across the junctions were recorded for each (average) temperature. Because of high resistance of the samples, Seebeck data could be obtained over only a very limited range of temperatures. Temperature differences introduced were

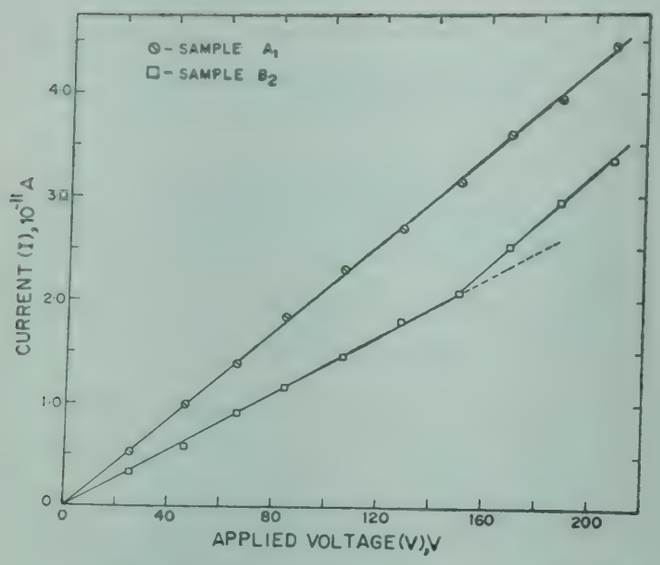

Fig. 2—Typical plots of I-V characteristics for two samples A_1 and B_2 of As_2S_3 showing ohmic behaviour for A sample and non-ohmic behaviour for B sample above 140V

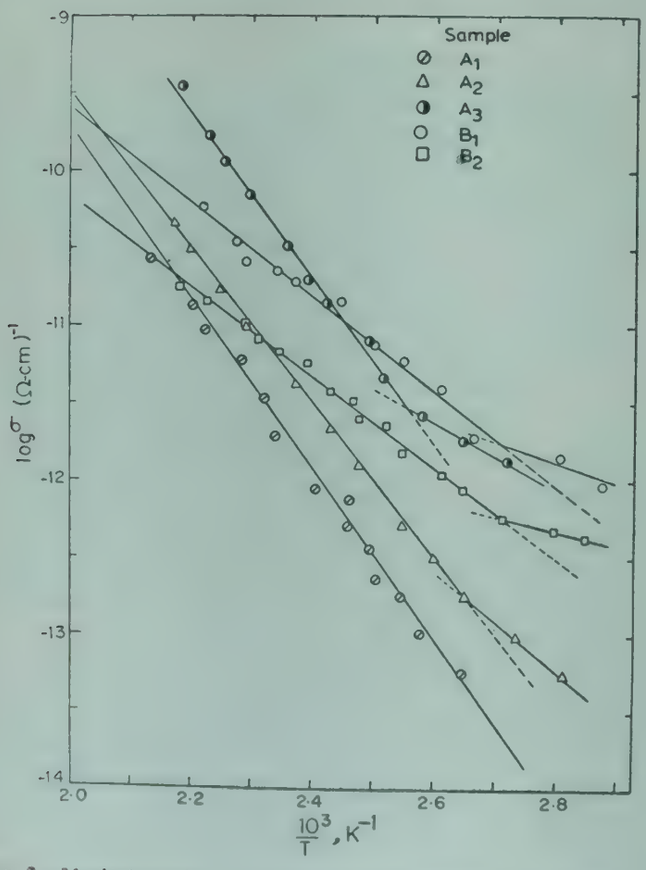

Fig. 3—Variation of dc conductivity with temperature, plotted as log σ against $10^3/T$ for five samples of As_2S_3

from 0 to 48 K in steps of 5-6 K and the e-t graphs were found to be straight lines for each average temperature, when the temperature difference was greater than 15 K. No thermo-emf could be observed across the junctions below this temperature difference.

Table 1—Values of Conductivity Activation Energy (E_c) and Pre-exponent C for As_2S_3 Glasses

Sample	E_c eV	Mean E_c eV	E_c (eV) (below ~393 K)	Mean E_c (eV) (below ~393 K)	C Ω^{-1}-cm^{-1}
A_1	1·09				16·71
A_2	0·96	1·04±0·05	0·647	0·62±0·02	1·16
A_3	1·07		0·60		155·2
B_1	0·61	0·60± 02	0·33	0·34±0·01	$3·1\times10^{-4}$
B_2	0·58		0·35		$4·5\times10^{-5}$

The thermoelectric power S of each sample was determined from the slope of the e-t lines and the different values of S were plotted against $1/T$ as shown in Fig. 4. Using the standard one-carrier formula[9]

$$S = [k/e]\,[\{E_s/(k\,T)\} + A] \qquad ...(2)$$

the values for the activation energies E_s and the intercepts A were obtained from Fig. 4 and found to be 0·333 eV (−8·43) for sample A and 0·256 eV (−6·24) for sample B respectively.

Both the A and B samples were found to be of p-type. This is in agreement with the observations of Seager and Quinn[6] but the magnitudes of S found by us are considerably lower.

4. Discussion

According to Mott's model,[9] the mechanism of electrical conduction in As_2S_3 can be explained as follows.

(a) If conduction occurs due to holes excited into the normalized valence band (E_v), then

$$\sigma = \sigma_0 \exp\,[-(E_F - E_V)/k\,T] \qquad ...(3)$$

where E_F is the Fermi energy. The ln σ versus $1/T$ plot should be a straight line if E_F-E_V is a linear function of T (Ref. 10). So Eq. (3) may be written in a modified form, as

$$\sigma = \sigma_0 \exp\,[\gamma/k] \exp\,[-E\,(0)/k\,T]$$
$$C = \exp\,[-E\,(0)/k\,T] \qquad .. (4)$$

where γ is the temperature coefficient of activation energy and $E\,(0)$ is the activation energy at $T = 0$. C usually should have values between 10^1 and 10^3 Ω^{-1}-cm^{-1}.

(b) If hole conduction occurs due to thermally assisted tunnelling in the localized gap states near the mobility edge E_A, then a hopping energy term Δw_1 in addition to the activation energy $(E_A - E_F)$ is required to raise a hole to the appropriate localized state near E_A. The expression for conductivity is then

$$\sigma = \sigma_1 \exp\,[-(E_t - E_A + \Delta w_1)/kT] \qquad ...(5)$$

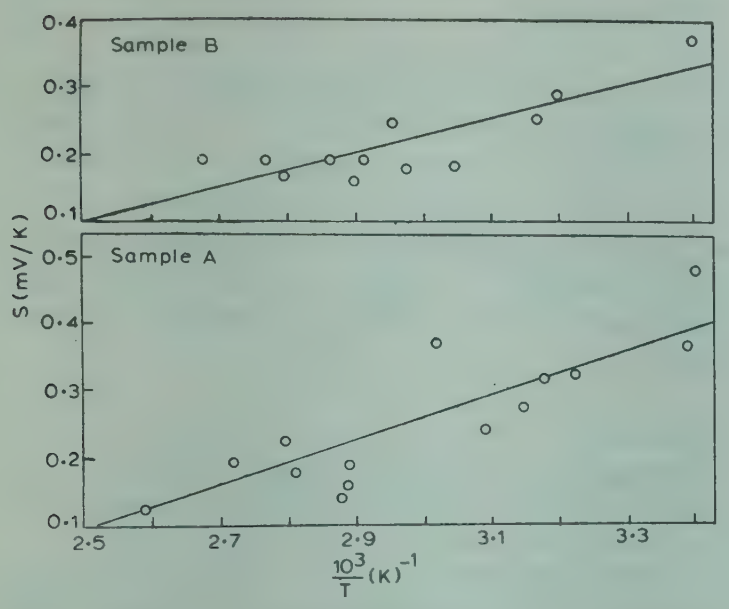

Fig. 4 —Variation of thermoelectric power (S) with reciprocal of temperature ($1/T$) for two samples of As_2S_3

Since the mobility drops sharply above E_V, we would have $\sigma_1 \ll \sigma_0$. So, the conductivity curve should have a lower activation energy at relatively lower temperature with respect to that at higher temperature, because the tunnelling probability decreases more rapidly as we go towards the gap centre.

(c) If conduction is due to carriers hopping between localized states E_F, then

$$\sigma = \sigma_2 \exp [-\Delta w_2/k\,T] \quad ...(6)$$

Δw_2 being the hopping energy that has the same physical meaning as Δw_1. Since the density of states near E_F is smaller than that near the band edge, $\sigma_2 \ll \sigma_1$.

From the values of C and E as given in Table 1, we conclude that at high temperature, conduction in sample A is primarily due to mechanism (a), whereas for B samples, conduction is due to the hopping of carriers into localized states near E_F for all temperatures under investigation.

In our experiment, the slope of the log σ versus $1/T$ curve decreases suddenly at temperature below about 393 K, consistent with previous observations.[4,11,12] The average activation energies for conduction in samples A and B are 1·04 and 0·59 eV, dropping to 0·62 and 0·34 eV respectively at relatively low temperatures. Reported values of E_c in As_2S_3 glasses in the literature lie between 1·025 and 1·2 eV (Ref. 1, 2, 4, 6, 7). The activation energy in our A sample agrees quite well with the published values of others, whereas for the B sample there is a considerable difference. Thus the preparation conditions of the amorphous glasses play an important role in their electrical properties and in the B samples, it is quite possible that the structural inhomogeneities are much greater than those in sample A, because the coordination numbers in samples A and B are different.

If conduction takes place in only one energy band then the plots of log σ versus $1/T$ and thermoelectric power S versus $1/T$ should yield the same slope. But in our experiments those two values are quite different which is in agreement with that observed by other workers.[6,13-15] It has been suggested that the reason for the occurrence of the phenomenon is due to thermally activated hopping of carriers at the band edge. We find that our values for the thermopower activation energy is not even of the same order as that obtained from the conductivity experiments at relatively low temperatures. Moreover, the absolute value of S is also small compared to that obtained by other workers.[6] These differences allow us to conclude that an ambipolar conduction mechanism is applicable in our samples. In ambipolar conduction, that is, for conduction of both types of carriers, the absolute value of S may very well become lowered. In this case, an additional exponential term describing the conduction of electrons must be added to the conductivity expression in p-type material. Depending on the relative magnitudes of the pre-factors and the activation energies, it is then possible that the conductivity curve should have two slopes with one type of carrier dominating at lower temperatures and the other at relatively higher temperatures. Then the expression for the electrical conductivity can be written in the form[6]

$$\ln \sigma = C_1 - [(E_p - E_F)/k\,T] + C_2\,T^{-(n+1)/4} \quad ...(7)$$

where E_p is the effective conduction level near the bottom of the localized states, and n the power law dependence of the density of localized states. The value of n in Eq. (7) is found to be equal to 3 from our experiments. Introducing a new parameter T_0, our experimental data for the conductivity for the A and B samples can be expressed as

$$\ln \sigma = C_1 - [(E_p - E_F)/k\,T] - C_2\,(T^{-1} - T_0^{-1}) \quad ...(8)$$

T_0 is thus a temperature at which the trapped carriers become released, i.e. it is the temperature below which the conduction mechanism takes place via the localized states at the band edge. Values of C_2 and T_0 are listed in Table 2. We note that Eq. (8) is valid at temperatures below 393 K approximately, around which there is a change in the slope of the log σ versus $1/T$ curve.

5 Conclusions

1. For bulk samples of As_2S_3, prepared by different melting schedules, the dc electrical conductivity and the thermoelectric power measurements below the glass transition temperature (T_g) show that

Table 2—Values of the Constant C_1 and Parameters T_0 for Different A and B Samples

Sample	$C_2 \times 10_{-3}$	T_0 (K)
A_1	—	—
A_2	1·73	377
A_3	3·20	392
B_1	1·67	369
B_2	1·89	369

the activation energies are very much dependent on the melting schedule.

2. Two types of conduction mechanisms, viz. conduction via extended states and hopping between localized states are expected to be operative in any sample in different temperature ranges. The variation of the values of the conductivity pre-exponents C for different samples indicate that hopping conduction process takes place at temperatures lower than about 393 K for all the samples. Thus it appears that there exists a transition temperature below which hopping conduction taking place through localized states at the valence band edges, becomes prominent for any sample prepared in any manner.

3. The activation energies calculated from the thermoelectric power and the dc conductivity values were found to be different. This shows that a process of mixed conduction occurs below the transition temperature in the samples prepared under any melting schedule. In such a case, one may introduce a parameter T_0 which is a constant for a given melting schedule.

Acknowledgement

The authors are grateful to the Director, Central Glass and Ceramic Research Institute, Calcutta, for providing experimental facilities for the preparation of the samples. Thanks are due to Dr N R Pan and Mr S K Das for their kind cooperation and for help in computer programming. One of the authors (M D) wishes to thank the University Grants Commission, New Delhi, for providing financial assistance.

References

1. Edmond J. T, *J. Non-cryst. Solids*, 1 (1968), 39.
2. Kolomiets B T, Mazets T F & Efendier Sh M, *J. Non-cryst. Solids*, 4 (1970), 45.
3. South R B & Owen A E, *Proc 5th Int. Conf. on Amorphous and Liquid Semiconductors, Garmisch-Partenkirchen, West Germany*, Vol 1 (Taylor & Francis, London), 1974, 305.
4. Bobb L C, Kramer K & Byer H H, *J. Non-cryst. Solids*. 21 (1976), 441.
5. Moribe H & Saji M, *Japan J. appl. Phys.*, 13 (1974), 284.
6. Seager C H & Quinn Rod K, *J. Non-cryst. Solids*, 17 (1975), 386.
7. Owen A E & Robertson J M, *J. Non-cryst. Solids*, 2 (1970), 40.
8. Kolomiets B T, *Soviet Phys. Semicond.*, 5 (1972), 1346.
9. Mott N F & Davis E A, *Electronic processes in non-crystalline Materials* (Clarendon Press, Oxford), 1971.
10. Edmond J T, *Brit. J. appl. Phys.*, 17 (1966), 979.
11. Seager C H, Emin D & Quinn Rod K, *Phys. Rev.*, B8 (1973), 4746.
12. Croitoru N, Vescan L, Popescu C & Lazarescu M, *J. Non-cryst. Solids*, 4 (1970), 493.
13. Nagels P, Callaerts R, Denayer M & Coninck R De, *J. Non-cryst. Solids*, 4 (1970), 295.
14. Nagels P, Callaerts R & Denayer M, *Proc. 5th international Conference on amorphous and liquid semiconductors, Garmisch-Partenkirchen, West Germany* (Taylor & Francis, London, 1 (1974), 867.
15. Strunk R, *J. Non-cryst. Solids*, 12 (1973), 168.

Indian Journal of Pure & Applied Physics
Vol. 18, August 1980, pp. 573-576

Calculation of Transverse & Longitudinal Electrical Susceptibilities in ADP-type Crystals

B K Chaudhuri, S Ganguli & D Nath

Department of Magnetism, Indian Association for the Cultivation of Science, Calcutta 700 032

Received 9 *February* 1979

Using temperature dependent Green's function method, electrical susceptibilities in $NH_4H_2PO_4$ (ADP) and its deuterated form (DADP) have been calculated with modified transverse Ising model. The parameters of the model used have also been calculated from the fitting of experimental values of the susceptibilities. It is observed that the long range anti-ferroelectric interaction is sufficient to explain the transverse susceptibilities in these crystals. Longitudinal susceptibilities, however, depend both on the short range proton-proton interaction like KH_2PO_4 (KDP) and long range dipole-dipole interaction constants.

1. Introduction

Ammonium dihydrogen phosphate (ADP) having the chemical formula $NH_4H_2PO_4$ is one of the isomorphs of KH_2PO_4 undergoing first order transition[1] at 148 K. The crystal of $ND_4D_2PO_4$ (DADP), obtained by the substitution of H by D shows a transition at 242 K. The changes in the dielectric constants of these crystals at the phase transitions are shown in Fig. 1. The space group of ADP at room temperature is $I\bar{4}2d$ as in KH_2PO_4 and below the phase transition point group becomes $P2_12_12_1$ in the orthorhombic system.[2] However, in contrast to the case of KH_2PO_4, the orthorhomic system of ADP has the *a* and *b* axes parallel to the *a* and *b* axes respectively of the body-centred lattice at room temperature. Assuming that sideways-$(H_2PO_4)^-$ has energy lower by ϵ_0 than for up or down $(H_2PO_4)^-$, Nagamiya[3] quantitatively explained the phase transition in ADP. Nagamiya also predicted that at low temperature all the $(H_2PO_4)^-$ are oriented sideways [Fig. 2(a)]. The dipole arrangement corresponding to this structure is shown in Fig. 2(a), where the total polarization of the crystal vanishes as the dipole moments cancel indicating anti-ferroelectric behaviour of ADP. Keeling and Pepinsky[2] also proposed a dipole arrangement similar to Fig. 2(a) from their elaborate X-ray structural analysis.

Very recently, Ishibashi *et al.*[4] have presented a theory for the anti-ferroelectric phase transition in ADP considering dipolar arrangement shown in Fig. 2(a). This theory does not adequately explain the dielectric properties along the transverse (*a*) and longitudinal (*c*) directions. Havlin *et al.*[5] again extended the model of Ishibashi *et al.*[4] and calculated transverse and longitudinal susceptibilities semiclassically. Their model is based on the four-sublattice pseudo-spin model of Slater[6] first proposed for the KH_2PO_4 crystal. They also modified their calculations by introducing Slater-Takagi parameters similar to the case of KH_2PO_4 But the introduction of such parameters though successfully explains dielectric constants of ADP-type crystals, brings out unnecessary complication in the theoretical expressions introducing one more unknown parameter.

In the present article it has been shown that the four-sublattice cluster model [Fig. 2(b)] can be directly treated with thermodynamic Green's functions without any modification. In this sense, our calculations are more exact and very good fitting with the transverse and longitudinal susceptibilities and indicates the validity of our calculations. Our purpose is also to apply the Green's function technique to describe phase transitions in these anti-ferroelectric crystals and compare with the calculations of Ishibashi *et al.*[4] and Havlin *et al.*[5] who used semiclassical method in their calculations.

2. Theory

The four-sublattice model of ADP is shown in Fig. 2(b). Following Havlin *et al.*[5] the hydrogen bonds along each transverse direction are divided into sublattices, designated by 1 and 2. The bond is labelled plus or minus when the displacement of its proton towards its spin-up position contributes positively or negatively to the polarization along *a* and *b* axes which are defined by

$$P_a \equiv \sum_i S_{iz}^{+a} - \sum_i S_{iz}^{-a}$$

$$\text{and } P_b \equiv \sum_i S_{iz}^{+b} - \sum_i S_{iz}^{-b}, \text{ respectively.}$$

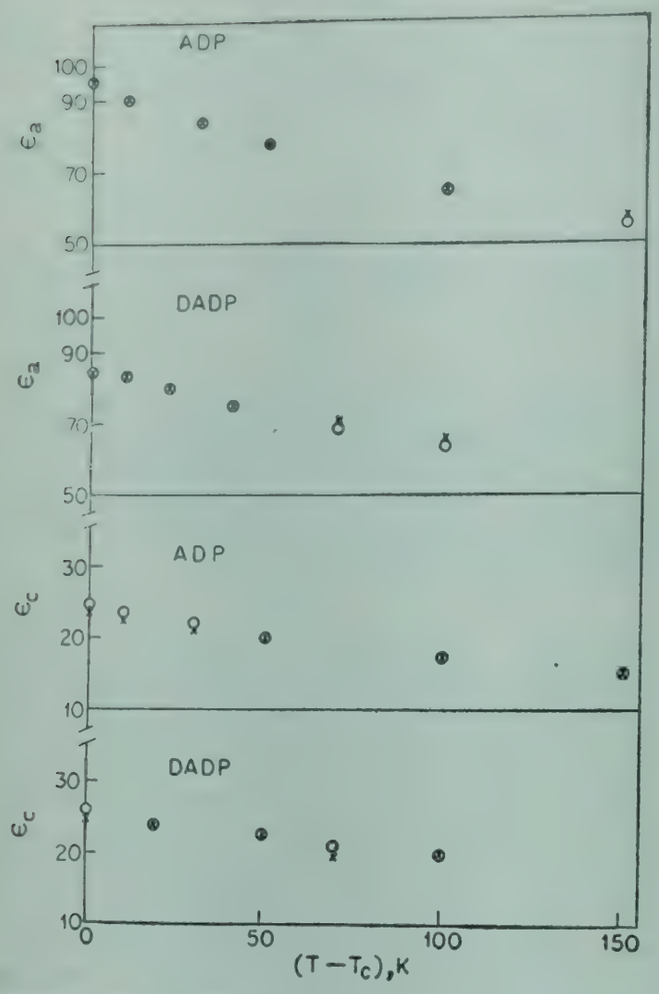

Fig. 1—Thermal variations of transverse (ϵ_a) and longitudinal (ϵ_c) dielectric constants of ADP and deuterated ADP (DADP) [×, experimental (Ref. 10-13); o, theoretical]

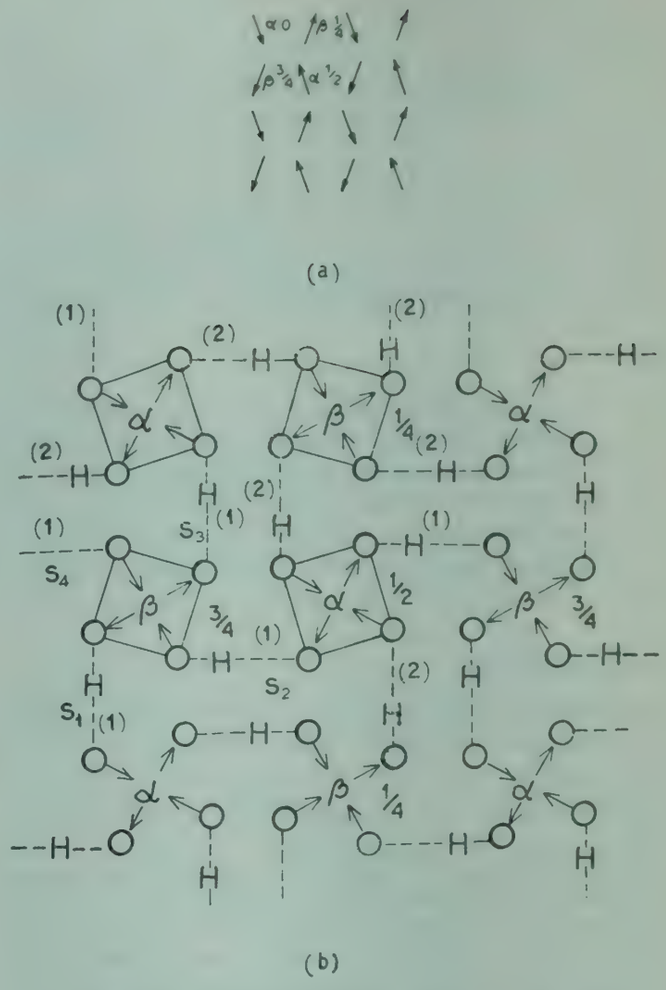

Fig. 2—(a) Dipole moments induced in PO_4 groups[3]; (b) four sub-lattice model of ADP shown by squares [α and β denote phosphorus atoms and the numbers near them indicate the heights along the *c*-axis. O denotes oxygen atom (Ref. 3).]

S_z are the usual pseudospin operators applied previously in KH_2PO_4 and its isomorphs.[7] Considering Fig. 2(b), the required Hamiltonian[5] containing anti-ferroelectric interaction between the transverse dipoles of the two different sublattices in each direction can be wrjtten as

$$\mathcal{H} = -\frac{1}{2}\sum_{i,j} J_{ij}\, S_{iz}\, S_{jz} - \left(\mu_e\, E_c + r\left\langle z \right\rangle\right)\sum_i S_{iz}$$

$$-\sum_{\alpha=a,b}\left[\mu_a\, E_\alpha - \frac{1}{2}\lambda\left\langle S_z^{+\alpha}(2) - S_z^{-\alpha}(2)\right\rangle\right]$$

$$\left(\sum_i S_{iz}^{+\alpha}(1) - \sum_i S_{iz}^{-\alpha}(1)\right)$$

$$-\sum_{\alpha=a,b}\left[\mu_a\, E_\alpha - \frac{1}{2}\lambda\left\langle S_z^{+\alpha}(1) - S_z^{-\alpha}(1)\right\rangle\right]$$

$$\left(\sum_i S_{iz}^{+\alpha}(2) - \sum_i S_{iz}^{-\alpha}(2)\right) \qquad \ldots(1)$$

The first term represents the effective short range proton-proton interaction. The second term represents the interaction of the spins with an external electric field along the *c* direction and their interaction with the average longitudinal polarization $\left\langle Z \right\rangle$ via the long-range dipole-dipole interaction constant γ.

Here $\left\langle Z \right\rangle$ is defined by

$$\left\langle Z \right\rangle = \frac{1}{2N}\left\langle \sum_{i=1}^{2N} S_{iz} \right\rangle$$

where N is the number of PO_4 groups. The last terms represent the interaction of the transverse polarization of the four sublattices with an external transverse field and also the long-range transverse dipole-dipole anti-ferroelectric interaction between transverse dipole moments of different sublattices aligned in the same transverse direction. The quantity λ is the long-range anti-ferroelectric interaction constant, and the symbols $S_z^{\pm\alpha}(1)$ and $S_z^{\pm\alpha}(2)$ stand for pseudospins in sublattices (1) and (2) respectively.

associated with the direction α ($\alpha = a$ or b); μ_e and μ_a are the dipole moments along the longitudinal and transverse directions respectively.

Following Zubarev,[8] the Green's functions for our calculations can be written as (in units of $\hbar = 1$)

$$G_{ij}^{mn}(t-t') = \left\langle\!\left\langle S_i^n(t) \,\middle|\, S_j^n(t') \right\rangle\!\right\rangle \quad \ldots(2)$$

The Fourier transform of Eq. (2) has the form

$$E\left\langle\!\left\langle S_i^m \,\middle|\, S_j^n \right\rangle\!\right\rangle = (2\pi)^{-1}\left\langle \left[S_i^m, S_j^n \right] \right\rangle + \left\langle\!\left\langle \left[S_i^m, H \right] \,\middle|\, S_j^m \right\rangle\!\right\rangle \quad \ldots(2a)$$

where $\langle \ldots\ldots \rangle$ denotes the statistical average of the enclosed operators. The correlation functions of the two operators are calculated using the spectral theorem,[8] viz.

$$\left\langle S_j^n S_i^m \right\rangle = \lim_{\epsilon \to 0} \int_{-\infty}^{\infty} \frac{P}{Q} - \mathrm{R}\, dE \quad \ldots 2(b)$$

where $P = \left\langle S_i^m \,\middle|\, S_j^n \right\rangle_{E+i\epsilon} - \left\langle S_i^m \,\middle|\, S_j^n \right\rangle_{E-i\epsilon}$

$Q = e^{\beta E} - 1$ and $R = e^{-iE(t-t')}$

where $m, n = x, y$ or z. For different values of m and n, Eq. (2a) gives nine-coupled equations. To linearize the complex Green's function like $\left\langle\!\left\langle S_i^m S_j^n \,\middle|\, S_k \right\rangle\!\right\rangle$, we used the procedure of Bogolyubov and Tyablikov.[9]

The complete set of equations of motion can be written for sublattice (1) in $+a$ direction as

$$G_a \Phi_a = \psi_a \quad \ldots(3)$$

where G_a is a (9×9) matrix given by

$$G_a = m_a' \begin{bmatrix} 1 & 0 & 0 \\ 0 & 1 & 0 \\ 0 & 0 & 1 \end{bmatrix}$$

$$m_a' = \begin{bmatrix} E & (i\lambda' - i\mu_a E_a) & 0 \\ -(i\lambda' - i\mu_a E_a) & E & 0 \\ 0 & 0 & E \end{bmatrix}$$

$$\Phi_a = \begin{vmatrix} G_{+a}^{xx}(1) \\ G_{+a}^{yx}(1) \\ G_{+a}^{zx}(1) \\ G_{+a}^{xy}(1) \\ G_{+a}^{yy}(1) \\ G_{+a}^{zy}(1) \\ G_{+a}^{xz}(1) \\ G_{+a}^{yz}(1) \\ G_{+a}^{zz}(1) \end{vmatrix} \qquad \psi_a = \frac{i}{2\pi} \begin{vmatrix} 0 \\ -\langle S_z^{+a}(1) \rangle \\ \langle S_y^{+a}(1) \rangle \\ \langle S_x^{+a}(1) \rangle \\ 0 \\ -\langle S_x^{+a}(1) \rangle \\ -\langle S_y^{+a}(1) \rangle \\ \langle S_x^{+a}(1) \rangle \\ 0 \end{vmatrix}$$

where $\lambda' = \lambda\left(\left\langle S_z^{+a}(2) \right\rangle - \left\langle S_z^{-a}(2) \right\rangle \right)$

Solving Eq. (3) the individual Green's functions are obtained and the correlation functions calculated using Eq. (2b).

Now since the correlation functions are finite and obey the identity

$$\left\langle S_x^2 \right\rangle + \left\langle S_y^2 \right\rangle + \left\langle S_z^2 \right\rangle = S(S+1) \quad \ldots(4)$$

we get

$$\left\langle S_z^{+a}(1) \right\rangle = -S(S+1) \tanh \frac{\beta(\lambda' - \mu_a E_a)}{2} \quad \ldots(5)$$

Similarly for sublattice (1) in $-a$ direction and for sublattice (2) in $+a$ and $-a$ directions we have

$$\left\langle S_z^{-a}(1) \right\rangle = S(S+1) \tanh \frac{\beta(\lambda' - \mu_a E_a)}{2} \quad \ldots(6)$$

$$\left\langle S_z^{+a}(2) \right\rangle = -S(S+1) \tanh \frac{\beta(\lambda'' - \mu_a E_a)}{2} \quad \ldots(7)$$

$$\left\langle S_z^{-a}(2) \right\rangle = S(S+1) \tanh \frac{\beta(\lambda'' - \mu_a E_a)}{2} \quad \ldots(8)$$

where

$$\lambda'' = \lambda\left(\left\langle S_z^{+a}(1) \right\rangle - \left\langle S_z^{-a}(1) \right\rangle \right)$$

Thus the total polarization in transverse direction is given by

$$P_a = \left\langle S_z^{+a}(1) \right\rangle + \left\langle S_z^{+a}(2) \right\rangle - \left\langle S_z^{-a}(1) \right\rangle - \left\langle S_z^{-a}(2) \right\rangle$$

$$= -2S(S+1) \left[\tanh \frac{\beta(\lambda' - \mu_a E_a)}{2} + \tanh \frac{\beta(\lambda'' - \mu_a E_a)}{2} \right] \quad \ldots(9)$$

Transverse susceptibility is obtained from

$$\chi_a = \left(\frac{\partial P_a}{\partial E_a} \right)_{Ea=0} N_a \mu_a = \frac{S(S+1) N_a \mu_a^2}{k_B T} \left[2 - \left(\tanh^2 \frac{\lambda'}{2 k_B T} + \tanh^2 \frac{\lambda''}{2 k_B T} \right) \right] \quad \ldots(10)$$

Now putting $\left[\left\langle S_z^{+\alpha}(1) - S_z^{-\alpha}(1) \right\rangle = \left\langle S_z^{+\alpha}(2) - S_z^{-\alpha}(2) \right\rangle = 2 \right]$ for anti-ferroelectric phase, we get

$$\chi_a = \frac{2S(S+1)}{k_B T} N_a \mu_a^2 \left[1 - \tanh^2 \frac{\lambda}{k_B T} \right] \quad \ldots(11)$$

Similarly considering the Green's functions in the longitudinal direction, we get total polarization as

$$P_c = \langle S_z \rangle = S(S+1) \times \tanh \frac{(J'+\gamma)\langle S^z \rangle + \mu_c E_c}{2 k_B T} \quad \ldots(12)$$

The corresponding susceptibility obtained by putting $\langle S^z \rangle = 1$ for ferroelectric phase is calculated from

$$\chi_c = \frac{S(S+1) N_c \mu_c^2}{2 k_B T} \left[1 - \tanh^2 \frac{J'+\gamma}{2 k_B T} \right] \quad \ldots(13)$$

3. Results and Discussion

Eqs. (11) and (13) are used to fit the experimental results[10-13] of transverse and longitudinal susceptibilities of ADP and DADP. The experimental and the theoretically calculated points are shown in Fig. 1. The corresponding values of the model parameters, viz. the transverse and longitudinal dipole moments μ_a and μ_c, long-range dipole-dipole interaction constant γ, long-range anti-ferroelectric interaction constant λ and short-range proton-proton interaction J' are shown in Table 1 both for ADP and DADP. The exact fitting of experimental data with the theory (as shown in Fig. 1) for a single set of the above parameters definitely indicates the validity of the above Green's function theory and the RPA-type decoupling used to linearize the complex Green's functions. Expressions (11) and (13) do not, however, directly contain the Slater-Takagi parameter as observed in the expressions derived by Havlin *et al.*[5] It is, therefore, not clear whether anti-ferroelectric (AFE) transition in ADP is permissible for both positive and negative values of ϵ_0 associated with the Slater-Tagaki parameter. It is also observed from our calculations that the longitudinal susceptibility data can be well fitted with the theory even in the absence of long-range interaction, as in the case of KDP-type crystals. The AFE transition associated with χ_a is also independent of γ as is shown by Eq. (11). This indicates less importance of γ in AFE transition. This was also pointed out by Havlin *et al.*[5]

The present Hamiltonian does not contain the tunnelling energy term which is, of course, most important for phase transition in KDP family. It has been observed by us (to be published) that the susceptibility expressions derived by considering tunnelling term in the Hamiltonian also fits the experimental data well. Further, proton-lattice interaction term has also been not taken into account in the present calculation. A detailed calculation considering all these terms is expected to elucidate more interesting features in ADP family. Theoretical work in this direction using thermodynamic Green's function is in progress.

Table 1—Pseudospin Model Parameters for ADP and DADP Crystals

Crystal	T_c K	N_a/k_B $\times 10^{-36}$ cm K	λ/k_B K	N_c/k_B $\times 10^{-36}$ cm K	$J'+\gamma$ k_B K	$10^{18}\,\mu_a$ cgs units	$10^{18}\,\mu_c$ cgs units
(ADP)	148	78·331	70	31·255	140	2·95	4·7
(DADP)	242	73·046	73	22·5908	140	3·5	6·8

References

1. Mason W P, *Piezoelectric crystals and their application to ultrasonics* (Academic Press, New York), 1956.
2. Keeling R O & Pepinsky R, *Z. Krist.*, 106 (1955), 236.
3. Nagamiya T, *Prog. theor. Phys.*, 7 (1952), 275.
4. Ishibashi Y, Ohya S & Takagi Y, *J. phys. Soc. Japan*, **33** (1972), 1545; **37** (1974), 1035.
5. Havlin S, Litov E & Sompolinsky H, *Phys. Rev.*, **B14** (1976), 1297.
6. Slater J C, *J. chem. Phys.*, 9 (1941), 16.
7. Blinc R & Zeks B, *Adv. Phys.*, 21 (1972), 693.
8. Zubarev D N, *Soviet Phys. Usp.*, **3** (1960), 320.
9. Bogolyubov N N & Tyablikov S V, *Soviet Phys. Dokl.*, 4 (1959), 604.
10. Mason W P, *Phys. Rev.*, 69 (1946), 173.
11. Mason W P & Matthias B T, *Phys. Rev.*, 88 (1952), 477.
12. Busch G, *Helv. phys. acta*, 11 (1938), 269.
13. Eisnen I Ya, *Bull. Acad. Sci. SSSR, Phys. Ser.*, **24** (1960), 1327.

Indian Journal of Pure & Applied Physics
Vol. 18, August 1980, pp. 577-582

Entropy Contributions in Determining the Relative Stabilities of Polytypes

M A Wahab & G C Trigunayat
Department of Physics & Astrophysics, University of Delhi, Delhi 110 007

Received 21 *April* 1979

A quantitative estimation has been made of the role played by the entropy part in determining the relative stabilities of the various possible polytypes of a given substance. Employing the large amount of experimental data now available for three richly polytypic substances, viz. CdI_2, ZnS and SiC, the entropy contribution per atom has been calculated as a function of the average fault order degree of the polytypes. This value has been compared with the stacking fault-energy (SFE), evaluated by using Born's formula, to obtain a quantitative estimate of the specific surface free-energy of the polytypes. The SFE values are nearly 12 orders of magnitude higher than the entropy contributions. The implications of this observation are pointed out.

1. Introduction

During the last decade, several attempts have been made to explain the phenomenon of polytypism in materials such as CdI_2, SiC, ZnS and PbI_2. Among the various aspects, a vital one concerns with the influence of stacking faults on the growth and transformation of polytypes,[1-5] and its relevance in the stabilization of polytypes.[6-8] However, in this connection, the contribution of fault entropy to the specific surface free-energy of the faults has been neglected by the earlier workers because of uncertainty in the calculations.

In order to understand completely the influence of stacking faults and the role played by the fault entropy, it is necessary to estimate quantitatively the stacking fault-energy (to be denoted as SFE in the following) and the entropy contribution for the parent and the faulted structures, respectively. Based on the hard-ball central-force model, Hirth *et al.*[9] and subsequently Tiwari *et al.*[7,8] have attempted a qualitative estimation of the relative SFE's of close-packed structures in terms of distortional energies. The model proposed by Tiwari *et al.*[7,8] is an extension of the Hirth and Lothe's procedure[9] and is a generalization for all polytypic materials and for metallic and alloy phases. However, these models do not provide a definite idea of the energy differences as also of any justification for the non-consideration of the fault entropy part.

In the last two decades, a vast amount of experimental data has become available on three richly polytypic compounds, viz. CdI_2, SiC and ZnS. So far nearly 240, 130 and 155 polytypes, respectively, of these compounds have been discovered, of which complete crystal structures of 69, 38 and 136 polytypes respectively, have been determined.[10,11] The crystal structure data provide a good statistical average of the number of layers in the unit cell and of the state of the order of a crystal with reference to a given ideal structure. These values, coupled with the knowledge of the temperature of growth of the compounds, have been used by us to estimate quantitatively the SFE's and the entropy contributions, and hence the specific surface free-energies of the faults, on CdI_2, SiC and ZnS. The conclusions drawn therefrom are reported in the present paper.

2. Calculation of Fault Order Degree (α)

The state of order of a given faulted structure with respect to a standard reference structure can be specified by the quantity, the fault order degree (α). The procedure for determining α is as follows. In the case of CdI_2, all polytypes have been found to grow at the room temperature, hence the standard reference structure is chosen as the most common polytype 4H. In the cases of SiC and ZnS, polytypes have been found to form only in the high temperature ranges, hence the reference structure has been taken as the low temperature modification 3C. For estimating α for a given structure, the various nearest-neighbour sequences in the unit cell of the structure are written down in the classical ABC-notation. The first nearest-neighbour relationships are not considered since they remain same for all close-packed structures and thus do not contribute to the stacking fault energies. In the second, third, etc. nearest-neighbour sequences, a layer sandwiched between two layers of the same orientation (e.g.

ABA, BCB, CAC, etc.) is denoted by e ('equal' neighbours; hexagonal orientation) and a layer sandwiched between two layers of different orientations (e.g. ABC, BCA, CAB, etc.) is denoted by u ('unequal' neighbours; cubic orientation).

The nearest-neighbour relationships for the parent structure 4H (ABCB————) and for an eight-layered faulted structure, viz. $8H_3$ (ABACABCB——) of CdI_2, are listed in Table 1. Similar relationships for the parent structure 3C and the faulted structure 8H of SiC and ZnS are given in Table 2.

In the case of CdI_2, the fault order degree α for a given structure is given by the ratio of the number of pair sequences in ee and uu orientations to the total number of layers in the unit cell. In the case of SiC and ZnS, it is simply specified by the ratio of the number of layers in the hexagonal orientation e to the total number of layers in the unit cell. Thus, α for the CdI_2 structure $8H_3$ will be given by,

$$\alpha_{8H_3} = \frac{N_{ee} + N_{uu}}{N} = \frac{1 + 1}{8} = \frac{1}{4}$$

and for the SiC and ZnS structure 8H by,

$$\alpha_{8H} = \frac{N_e}{N} = \frac{2}{8} = \frac{1}{4} .$$

The values of α have been calculated for all the known structures[10,11] of CdI_2, SiC and Zns. These are listed in Table 3. It is seen that more than one structure can have the same value of α.

Table 1—Second Nearest-Neighbour Relationships for the Parent Structure 4H (ABCB— — — —) and for the Faulted Eight-layered Structure $8H_3$ (ABACABCB) of CdI_2

Second neighbour sequence	Layer orientation	Pair sequence
Structure 4H (ABCB — — — —)		
ABC	u	ue
BCB	e	eu
CBA	u	ue
BAB	e	eu
Structure $8H_3$ (ABACABCB)		
ABA	e	eu
BAC	u	ue
ACA	e	eu
CAB	u	uu→
ABC	u	ue
BCB	e	eu
CBA	u	ue
BAB	e	ee→

Table 2—Second Nearest-Neighbour Relationships for the Parent Structure 3C (ABC — — — —) and for the Faulted Eight-layered Structure 8H (ABCABACB — — — —) of SiC and ZnS

Second neighbour sequence	Layer orientation
Structure 3C (ABC — — — —)	
ABC	u
BCA	u
CAB	u
Structure 8H (ABCABACB — — — —)	
ABC	u
BCA	u
CAB	u
ABA	e→
BAC	u
ACB	u
CBA	u
BAB	e→

3. Calculation of S_k (α) for Different Polytypic Crystals

After knowing the value of the fault order degree (α), the configurational entropy S_k (α) can be calculated by using the well known formula:[12]

$$S_k(\alpha) = k \log W = -kN[\alpha \log \alpha + (1-\alpha)\log(1-\alpha)] \quad \ldots(1)$$

where k is the Boltzmann's constant and W represents the relative probability for finding the system in the state of order α. We shall use Eq. (1) to estimate S_k (α) for the three structures, CdI_2, SiC and ZnS.

CdI_2

By using Eq. (1), we have

$$S_k(\alpha) = -1{\cdot}38 \times 10^{-23} \times 20\,[0{\cdot}34 \log 0{\cdot}34 + 0{\cdot}66 \log 0{\cdot}66]\ \text{JK}^{-1} \simeq 7{\cdot}728 \times 10^{-23}\ \text{JK}^{-1}$$

The CdI_2 crystals grow around 300 K. Therefore,

$$T.S_k(\alpha) \simeq 300 \times 7{\cdot}728 \times 10^{-23} \simeq 0{\cdot}55 \times 10^{-23}\ \text{kcal}.$$

This is the value of S_k (α) for N (= 20) layers. Therefore, for one layer,

$$T.S_k(\alpha) \simeq 0{\cdot}027 \times 10^{-23}\ \text{kcal/layer}$$

The laboratory grown crystals of CdI_2, SiC and ZnS have typically basal plane size about 1 mm^2, so that one layer contains nearly $1\text{mm}^2/(a)^2$ atoms. Hence the contribution per atom will be

[for CdI_2, SiC and ZnS, $1\text{mm}^2/(a)^2 \sim 10^{12}$],

$$T.S_k(\alpha) \simeq 27{\cdot}00 \times 10^{-26} \times 10^{-12}\ \text{kcal/atom} \simeq 27 \times 10^{-38}\ \text{kcal/atom}$$

SiC

$$S_k(\alpha) = -1{\cdot}38 \times 10^{-23} \times 35\,[0{\cdot}35 \log 0{\cdot}35 + 0{\cdot}65 \log 0{\cdot}65]\ \text{JK}^{-1} \simeq 13{\cdot}52 \times 10^{-23}\ \text{JK}^{-1}$$

The SiC polytypes grow around 2300 K. Therefore,

$$T.S_k(\alpha) \simeq 2300 \times 13{\cdot}52 \times 10^{-23}\text{J} \simeq 7{\cdot}43 \times 10^{-23}\ \text{kcal}$$

Table 3—Values of α for the CdI_2, ZnS and SiC Polytypes with Known Crystal Structures

α	Polytypes	α	Polytypes
	CdI_2 Polytypes*		
0 0000	4H	0·2858	$14H_3$
0·0666	$30H_3$	0·3000	$26H_3$
0·0679	$26H_2$	0·3333	$6H_1$, $6H_2$, $12H_2$, $12H_3$, $12H_4$, $12H_6$, $18H_4$, $30H_1$, 36H, $36R_1$, $36R_2$
0·0833	$24H_2$, 72R	0·4000	$20H_2$
0·1000	40H, $60R_1$	0·4285	$14H_2$, $14H_4$
0·1111	$18H_1$, $18H_5$	0·5000	2H*, $8H_2$, $12H_5$, 12R, $16H_2$
0·1250	$16H_5$, $16H_7$, $32H_1$	0·5714	$28H_4$
0·1428	$14H_1$, $28H_1$, $28H_2$, $28H_2$, 42R, $84R_1$, $84R_2$	0·6000	$10H_2$, $10H_4$
0·1666	$12H_1$, $24H_1$	0·6363	$22H_1$
0·1764	$34H_1$	0·6666	$12H_7$, $12H_8$
0·2000	$10H_1$, $10H_2$, $20H_1$, $20H_5$, $20H_6$, $30H_2$, $30H_4$, 30R	0·6923 0·7777	$26H_1$ $18H_2$
0·2222	$18H_3$	0·8000	$20H_3$, $20H_4$
0·2500	$8H_3$, $16H_1$, $16H_2$, $16H_4$, $16H_6$, 24R		
	Average N = 20; Average α = 0·3351 ≃ 0·34		
	SiC Polytypes*		
0·0000	3C	0·3529	$51R_1$
0·1052	57R	0·3571	84R
0·2500	8H, $24R_1$	0·3589	39H
0·2558	174R	0·3704	27H, 39R, 99R
0·2857	21R	0·3704	27H
0·3055	36H	0·3750	16H
0·3076	39R	0·3928	168R
0·3243	111R	0·4000	10H, 15R, 75R, 90R, 270R
0·3333	6H	0·4285	14H
0·3358	393R	0·4444	18H, 27H
0·3404	141R	0·4500	120R
0·3428	105R	0·4705	$51R_2$
0·3448	87R	0·5000	4H
0·3478	$69R_1$, $69R_2$	1·0000	2H
	Average N = 35; Average α = 0·35		

α	Polytypes	α	Polytypes
	ZnS Polytypes*		
0·0000	3C	0·2307 0·2500	$78H_3$, $78R_4$ 8H, $16H_2$, $24H_{10}$, $24R_1$, $24R_2$, $48R_2$, $48R_6$, $48R_8$, $72R_3$, $72R_4$, $72R_7$, $72R_8$, $72R_{13}$, $72R_{14}$
0·0714	$28H_2$, $84R_1$	0·2727	$66R_1$, $66R_4$
0·0833	$24H_6$, $24H_9$, $72H_{12}$, $72H_{16}$	0·2857	$14H_1$, $14H_3$, $42H_5$, $42H_6$, $84R_3$
0·0909	$22H_1$, $22H_2$, $44H_1$, $66H_5$	0·3000	$20H_2$, $20H_4$, $20H_5$, $60R_1$, $60R_6$, $60R_7$, $60R_8$, $60R_9$
0·1000	$20H_3$, $20H_6$, $60R_2$, $60R_4$, $60R_5$, $60R_{13}$	0·3333	6H, $12H_3$, $24H_2$, $24H_5$, $24H_{11}$, $30R_1$, $36R_3$, $36R_4$
0·1052	$114R_1$, $114R_3$	0·3571	$28R_3$
0·1111	$54R_1$	0·3750	$16H_3$, $48R_3$
0·1250	$16H_1$, $16H_4$, $48R_1$, $48R_4$, $48R_5$, $48R_7$, $96R_1$	0·4000	$10H_3$, 15R, $30R_3$
0·1428	$14H_2$, $28H_1$, $28H_3$, $42R_1$, $42R_2$, $42R_3$, $42R_4$, $84R_2$	0·4117	34H
0·1500	$120R_1$, $120R_2$	0·4545	$44H_2$
0·1538	$26H_1$, $78H_1$, $78R_2$	0·5000	4H, 12R
0·1666	$12H_1$, $12H_2$, $24H_1$, $24H_3$, $24H_4$, $24H_7$, $24H_8$, $36R_2$, $36R_5$, $36R_6$, $72R_1$, $72R_2$, $72R_5$, $72R_6$, $72R_9$, $72R_{10}$, $72R_{11}$, $72R_{15}$,	0·5263	$114R_4$
0·1818	$66R_2$, $66R_3$	0·5714	21R
0·2000	$10H_1$, $10H_2$, $20H_1$, $20H_7$, $20H_8$, $30R_1$, $30R_2$, $60R_3$, $60R_{10}$, $60R_{11}$, $60R_{12}$, $60R_{14}$, $60R_{15}$	0·5882	102R
0·2105	$114R_2$	0·6666	18R
0·2222	9R, $18H_1$, $18H_2$, $18H_3$, $54R_2$, $54R_3$, $54R_4$	1·0000	2H
	Average N = 18; Average α = 0·2920 ≃ 0·29		

*Since 2H (AB — — — —) has all its layer orientations as e, no pair sequence need to be considered for the evaluation of α for the CdI_2 structure. Like the case of SiC and ZnS, here α is determined by the ratio of the number of layers in the u orientation to the total number of layers in the unit cell.

This is the value of $S_k(\alpha)$ for N (= 35) layers. Therefore, for one layer,

$$T.S_k(\alpha) \simeq 0{\cdot}22 \times 10^{-23} \text{ kcal/layer}$$

As before, the contribution per atom is,

$$T.S_k(\alpha) \simeq 22 \times 10^{-25} \times 10^{-12} \text{ kcal/atom}$$
$$\simeq 22 \times 10^{-37} \text{ kcal/atom.}$$

ZnS

$$S_k(\alpha) = -1{\cdot}38 \times 10^{-23} \times 18\,[0{\cdot}29 \log 0{\cdot}28 + 0{\cdot}71 \log 0{\cdot}71]\ \text{JK}^{-1}$$
$$\simeq 6{\cdot}45 \times 10^{-23}\ \text{JK}^{-1}$$

The ZnS polytypes grow around 1300 K. Therefore,

$$T.S_k(\alpha) \simeq 1300 \times 6{\cdot}45 \times 10^{-23} \text{ J}$$
$$\simeq 2{\cdot}00 \text{ kcal.}$$

This is the value of $S_k(\alpha)$ for N (=18) layers. Therefore,

$$T.S_k(\alpha) \simeq 0{\cdot}11 \times 10^{-23} \text{ kcal/layer}$$

Finally, we have the contribution per atom as,

$$T.S_k(\alpha) \simeq 11{\cdot}00 \times 10^{-25} \times 10^{-12} \text{ kcal/atom}$$
$$\simeq 11{\cdot}00 \times 10^{-37} \text{ kcal/atom}$$

The total entropy S consists of the configurational part $S_k(\alpha)$ and the vibrational part $S_v(\alpha)$. A quantitative estimation of $S_v(\alpha)$ has not been possible so far as it involves the stupendous task of evaluation of all the eigen vibrations of the lattice. For a compound consisting of two kinds of atoms, Jagodzinski[13] has made a qualitative estimate according to which initially the value of $S_v(\alpha)$ falls steeply with the increase of α from zero to nearly 10%, after which the fall becomes gradual. Thus, it can be inferred that $S_v(\alpha)$ is more or less constant as a function of α. Hence, variations in the total entropy S may be taken as having been caused by the changes in $S_k(\alpha)$.

4. Quantitative Estimation of the Stacking Fault-Energy

Strictly speaking, the SFE for a given fault can be quantitatively estimated by calculating energy of interaction between neighbouring layers. This is an extremely difficult task as it involves interaction of all the atoms in one layer with all those in the other layer. An approximate estimate can be obtained by evaluating the energy of interaction of a reference atom in one layer with respect to a large number of neighbouring atoms in the adjoining layer. We have adopted this approach in our evaluations of SFE.

We assume that the charge distribution throughout the unit cell is spherically symmetric and the energy of interaction for the various atoms in one layer depends only on their distances from the reference atom in the other layer and is independent of the direction. The second and the third layer interactions have been calculated for two different typical layer sequences, viz.

(i) Second layer interaction: Sequences ABA and ABC

(ii) Third layer interaction: Sequences ABCA and ABCB

The various bond lengths with respect to the reference atom and the corresponding number of bonds having the same length have been determined for 54 atoms in each case, following the procedure employed earlier by Hirth *et al.*[9] and Tiwari *et al.*[7,8] The bond lengths for the farthest atoms are nearly four times the value of the a dimension of the unit cell, at which distance the Coulomb forces become appreciably weak. The values for the respective cases are listed in Table 4. Using these data, the Coulomb energies of all the above-mentioned sequences are obtained by the well-known Born's formula[14]

$$E_c = e^2 \sum_j \frac{n_j}{\gamma_j} \qquad \ldots(2)$$

where n_j is the number of iodine atoms (or number of bonds) at a distance r_j and γ_j the distance of iodine atoms w.r.t. a reference iodine atom (i.e. the bond length in a, the minimum distance between iodine atoms). Since in the present case, we are dealing with structures consisting of the same kind of ions, all the terms in the summation have the same sign.

It is a difficult matter to decide the relative proportions of ionic and covalent bonds in a compound. However, in a general way it may be said that greater is the difference between the electro-negativities of the constituent elements, the more ionic is the character of the bond. Various formulae for approximate quantitative estimations of the content of the ionic bonding in compounds have also been proposed.[14] Applying this criterion, the relative contents of ionic bonding are not found to be widely different in the three polytypic compounds, CdI_2, ZnS and SiC although the absolute magnitude of the content decreases in that order. In the following evaluation, aimed to achieve at best an order of magnitude accuracy, the three compounds have been regarded as sufficiently ionic in character to justify the use of the Born's formula [Eq. (2)].

Sequence ABA

$$E_c(\text{ABA}) = \frac{e^2}{a}\left(\frac{1}{\sqrt{8/3}} + \frac{6}{\sqrt{11/3}} + \frac{6}{\sqrt{17/3}} + \frac{6}{\sqrt{20/3}} + \frac{12}{\sqrt{29/3}} + \frac{6}{\sqrt{35/3}} + \frac{6}{\sqrt{44/3}} + \frac{11}{\sqrt{47/3}}\right) \times \frac{1}{54}$$

Table 4—Bond Lengths for the Different Sequences

Bonds γ_j →	Magnitude (in units of a)	Number of bonds having the same length
Sequence ABA; Plane of Termination A		
γ_1	$\sqrt{8/3}$	1
γ_2	$\sqrt{11/3}$	6
γ_3	$\sqrt{17/3}$	6
γ_4	$\sqrt{20/3}$	6
γ_5	$\sqrt{29/3}$	12
γ_6	$\sqrt{35/3}$	6
γ_7	$\sqrt{44/3}$	6
γ_8	$\sqrt{47/3}$	12 (limited to 11 in the calculations)
Sequence ABC; Plane of Termination C		
γ_1	$\sqrt{3}$	3
γ_2	$\sqrt{4}$	3
γ_3	$\sqrt{5}$	6
γ_4	$\sqrt{7}$	6
γ_5	$\sqrt{8}$	3
γ_6	$\sqrt{9}$	6
γ_7	$\sqrt{11}$	3
γ_8	$\sqrt{12}$	6
γ_9	$\sqrt{13}$	6
γ_{10}	$\sqrt{15}$	6
γ_{11}	$\sqrt{17}$	6
Sequence ABCA; Plane of Termination A		
γ_1	$\sqrt{6}$	1
γ_2	$\sqrt{7}$	6
γ_3	$\sqrt{9}$	6
γ_4	$\sqrt{10}$	6
γ_5	$\sqrt{13}$	12
γ_6	$\sqrt{15}$	6
γ_7	$\sqrt{18}$	6
γ_8	$\sqrt{19}$	12 (limited to 11 in the calculations)
Sequence ABCB; Plane of Termination B		
γ_1	$\sqrt{19/3}$	3
γ_2	$\sqrt{22/3}$	3
γ_3	$\sqrt{25/3}$	6
γ_4	$\sqrt{31/3}$	6
γ_5	$\sqrt{34/3}$	3
γ_6	$\sqrt{37/3}$	6
γ_7	$\sqrt{43/3}$	3
γ_8	$\sqrt{46/3}$	6
γ_9	$\sqrt{49/3}$	6
γ_{10}	$\sqrt{56/3}$	6
γ_{11}	$\sqrt{61/3}$	6

Substituting the value of $e = 4{\cdot}80298 \times 10^{-10}$ esu and $a = 4{\cdot}24$ Å, one gets

E_c (ABA) $= 0{\cdot}0448583 \times 10^{-23}$ kcal/atom.

Sequences ABC, ABCA and ABCB

Proceeding in the same manner as before, one gets

E_c (ABC) $= 0{\cdot}0448507 \times 10^{-23}$ kcal/atom

E_c (ABCA) $= 0{\cdot}0372091 \times 10^{-23}$ kcal/atom

E_c (ABCB) $= 0{\cdot}0372091 \times 10^{-23}$ kcal/atom

We find that the difference between the energies of the structures ABA and ABC is,

E_c (ABA) $- E_c$ (ABC) $= 0{\cdot}0000076 \times 10^{-23}$ kcal/atom

$$= 7{\cdot}6 \times 10^{-29} \text{ kcal/atom} \quad \ldots (3)$$

and between the energies of the structures ABCB, and ABCA is,

E_c (ABCA) $- E_c$ (ABCB) $= 0{\cdot}0000071 \times 10^{-23}$ kcal/atom

$$= 7{\cdot}1 \times 10^{-29} \text{ kcal/atom} \quad \ldots (4)$$

The comparison of the SFE values obtained from Eqs. (3) and (4) with the entropy contributions, found earlier to be of the order 10^{-37}-10^{-38} kcal/atom, shows a vast difference of nearly 9 orders of magnitude. Hence in the estimation of specific surface free-energy values, the entropy contributions can be safely neglected in comparison to the SFE values which alone should determine the relative stabilities of the different possible polytypic structures. Thus, a prominent uncertainty involved in the theoretical evaluation of the specific surface free-energy by Hirth *et al.*[9] and others[4,5,7,8] is resolved.

It has been pointed out that another source of uncertainty can arise from the neglect of the possible existence of non-central forces[9] since the preceding calculations have assumed a hard-ball central-force model. The calculations of contributions on this account are at an embryonic stage, nevertheless it may be said that their effect can be only marginal and the hard-ball central-force model may be regarded as sufficiently good for order of magnitude estimates.

For the quantitative estimation of SFE, the earlier workers[5,7-9] have assumed that the second nearest-neighbour faults contribute to the major part of the fault-energy and the contribution from the third and higher nearest-neighbour sequences are negligible in comparison to the former. But Eqs. (3) and (4) show that the quantitative values for the second and third nearest-neighbour sequences are very close to each other, although their magnitudes

are quite small. This fact should be taken into consideration in any future quantitative evaluations of the stacking fault-energy.

References

1. Jagodzinski H, *Acta Crystallogr.*, 7 (1954), 17.
2. Jagodzinski H, *Kristallographia*, 16 (1971), 1235.
3. Alexander E, Mardix S & Steinberger I T, *Phil. Mag.*, 21 (1970), 174.
4. Prasad R & Srivastava O N, *J. appl. Cryst.*, 4 (1971), 516.
5. Pandey D & Krishna P, *Phil. Mag.*, 31 (1975), 1113.
6. Agrawal V K, *Acta Crystallogr.*, 28 (1972), 93.
7. Tiwari R S, Rai A K & Srivastava O N, *Phys. Rev.*, 9 (1974), 5155.
8. Tiwari R S, Rai A K & Srivastava O N, *Phys. Status Solidi*, 31 (1975), 941.
9. Hirth J P & Lathe J, *Theory of dislocation* (McGraw-Hill, New York), 1968, 293, 348.
10. Trigunayat G C & Verma A R, *Physics and chemistry of materials with layered structure*, (Reidel, Amsterdam), Vol. 2, 1976.
11. Jain P C, *Refinements in the method of structure analysis of polytypes and determination of crystal structures of 21 new* CdI_2 *polytypes*, Ph D thesis, Delhi University, Delhi, 1976.
12. Verma A R & Krishna P, *Polymorphism and polytypism in crystals* (Wiley, New York), 1976, 264.
13. Jagodzinski H, *Neues Jahrb Minen. Mh.*, 3 (1954), 49.
14. Pauling L, *Nature of Chemical bond and the structure of molecules and crystals* (Oxford Publishing Co., Oxford), 1960, 507.

Indian Journal of Pure & Applied Physics
Vol. 18, August 1980, pp. 583-587

Dielectric Studies on the Liquid & Solid Phases of Chlorobenzene *cis*-Decalin Mixtures

ABHAI MANSINGH, C B AGARWAL* & RAMADHAR SINGH
Department of Physics & Astrophysics, University of Delhi, Delhi 110 007

Received 7 *August* 1979; *revised received* 4 *October* 1979

The dielectric constant (ϵ') and loss tangent (tan δ) at five concentrations (12·98, 18·05, 20·80, 21·99 and 25·01 mole %) of chlorobenzene in *cis*-decalin have been measured in the frequency region 0·1-100 kHz and in the temperature region 77-300 K. The variation of ϵ' and tan δ with temperature shows that below about 160 K, the dielectric behaviour is consistent with the earlier reported α and β relaxations. The value of ϵ' continuously increases with decreasing temperature up to about 135 K after which there is a rapid fall to a low value which further decreases slowly with further fall in temperature. The dielectric behaviour in the heating run is similar to that in the cooling run up to about 160 K after which the sample crystallizes and the dielectric constant falls to a low value. The dielectric constant in the crystalline phase is lower than that of glassy phase below the glass transition temperature (T_g) indicating that below T_g there is restricted rotation of dipoles while in the crystalline phase the dipole rotational freedom is completely stopped. The crystallization temperature does not show any systematic change with concentration.

1. Introduction

Substances in the glassy state retain some degree of molecular rotational freedom which can be detected by dielectric, or mechanical, or NMR studies.[1] The presence of such rotational freedom giving rise to the dielectric relaxation has generally been associated with the motion of a side group in polymers and long chain alcohols.[1] Certain rigid nearly spherical polar molecules show rotational freedom for some region in the solid phase on freezing and the rotational freedom is stopped at a temperature below the freezing point.[2-4] However, most of the simple rigid molecules do not have the rotational freedom in the solid phase. Johari and Goldstein[5] have studied the solid phases of a large number of solutions of simple rigid polar molecules in the rigid non-polar molecule *cis*-decalin which forms the glassy phase in the pure state. They have observed dielectric relaxation at low temperatures in the solid phase above and below a glass transition temperature T_g and termed the relaxation above T_g as α-relaxation and that below T_g as the β-relaxation.

Several studies have been made to understand the character of α- and β-relaxations in the solid phase of the solutions of rigid polar molecules in *cis*-decalin and some other glass-forming solvents.[6-8] However, the detailed dielectric studies have been made only in the narrow temperature range near T_g. The effect of the concentration of the solute molecules on the α- and β-relaxations has also not been investigated in detail.[7] Hence it was considered interesting to study the dielectric behaviour of solutions of chlorobenzene in *cis*-decalin at different concentrations over a wide temperature range to cover both solid and liquid phases. Five concentrations of chlorobenzene in *cis*-decalin were taken and measurements of ϵ' and tan δ were made in the frequency region 0·1-100 kHz and the temperature region 77-300 K. The results of these measurements are presented in this paper.

2. Experimental Procedure

A General Radio 716 CS bridge was used with a Hewlett-Packard 209A oscillator and GR 1232 tuned amplifier/null detector to measure the capacitance and tan δ in the frequency range 0·1-100 kHz. A gold-plated cylindrical cell was used for two-terminal measurements. The cell capacitance was measured at room temperature by using standard pure liquids (benzene, carbon tetrachloride and cyclohexane). The capacitance of the empty cell was measured from 77 to 300 K and the variation in the capacitance was less than 0·05 pF in this temperature range, hence the cell constant (30·98 pF) determined at room temperature was used to evaluate ϵ' and tan δ of solutions at different temperatures.[9] The cell was placed in a large aluminium block on which a heater coil was wrapped. The

*Permanent address : Department of Physics, D S College Aligarh 202 001

whole assembly was placed in a thermocole (insulator) bucket. The space between the aluminium block and the bucket was filled with glass wool insulation. A copper-constantan thermocouple was placed in a hole drilled in the sample cell so that the thermocouple was close to the sample. The variation of ϵ' with temperature was measured both in cooling and heating runs. The whole assembly was cooled down to 77 K with liquid nitrogen and the cooling rate was kept at about 1·5°C/min. The heating rate was kept at about 0·5°C/min for accurate measurements at different frequencies. At least three runs were taken for each solution and the reproducibility of results in the heating runs were better than 0·5 % in dielectric constant and 1 % in tan δ.

AnalaR grade *cis*-decalin was procured from M/s BDH Chemicals, England, and chlorobenzene from M/s BDH Chemicals, India. The chemicals were further purified by fractional distillation; the boiling points of both the chemicals were in good agreement with the literature values. The dielectric constants of pure *cis*-decalin and chlorobenzene at room temperature were also found in good agreement with the reported values. Five concentrations (12·98, 18·05, 20·80, 21·99 and 25·01 mole %) of chlorobenzene in *cis*-decalin were used to make five samples for ϵ' and tan δ measurements in the temperature range 77-300 K.

3. Results and Discussion

The measured loss tangent (tan δ) as a function of temperature in the range 77-165 K and for different frequencies is given in Fig. 1, for 12·98 mole % solution in a heating run. Similar results were obtained for other concentration solutions and these are consistent with those reported by Johari and Goldstein.[5] It may be noticed in this figure that clear peaks in tan δ corresponding to α-relaxation are observed above 135 K. The measuring frequency f may be taken equal to the relaxation frequency f_0 ($f_0 = 1/2\pi\tau$, where τ is the relaxation time) at the temperature where peak in tan δ appears. The relaxation frequency f_0 increases with increasing temperature and the activation energy ΔW, assuming $f_0 \propto \exp(-\Delta W/kT)$, comes out to be ~35 kcal/mole. It is apparent from Fig. 2, that the magnitude of α-relaxation peak increases with increasing concentration but there is a negligible change in the temperature of the peak with change in concentration. The activation energy also does not show any systematic increase with concentration. At temperatures below 135 K, peaks (or shoulder) in measured tan δ, corresponding to the β-relaxation, were observed at 0·1 kHz and 1 kHz (Fig. 1). The magnitude of the β-relaxation peak is considerably smaller than that of the α-relaxation peak, in agreement with the reported results of Johari and Goldstein.[5] The tan δ peaks for the β-relaxation become more pronounced for higher concentration solutions (Fig. 2) but there is hardly any change in the temperature of the peak with concentration. The fact that α- and β-relaxation peaks in tan δ for different concentrations occur almost at the same temperature at a given frequency, suggests that the relaxation frequency is determined mainly by the viscosity of the glassy phase of *cis*-decalin and the dipole-dipole interactions of the solute molecules (chlorobenzene) have negligible effect on the relaxation frequency.

The variation of ϵ' with temperature at 1 kHz for one concentration is given in Fig. 3 for both heating and cooling runs. It may be noticed that in

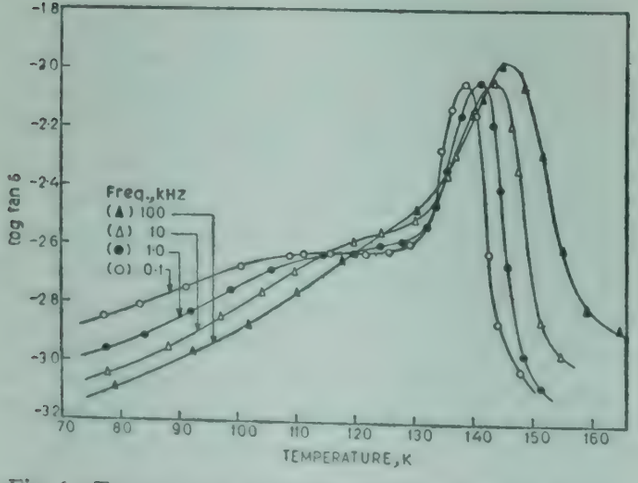

Fig. 1—Temperature dependence of dielectric loss factor (log tan δ) for 12·98 mole % chlorobenzene/*cis*-decalin solution

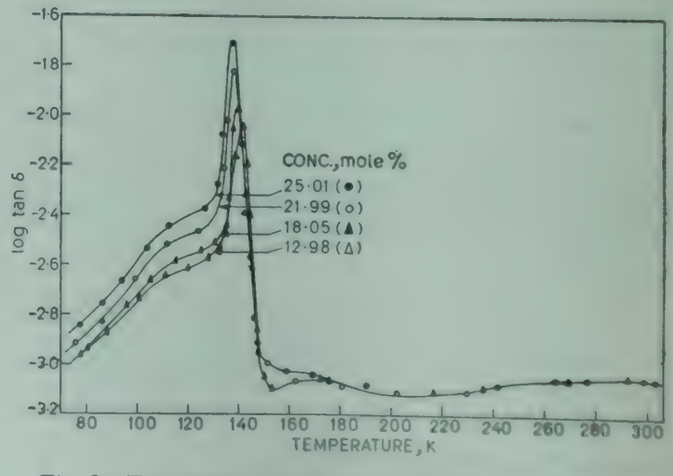

Fig. 2—Temperature dependence of dielectric loss factor (log tan δ) at 1·0 kHz for four concentrations of chlorobenzene/*cis*-decalin solution

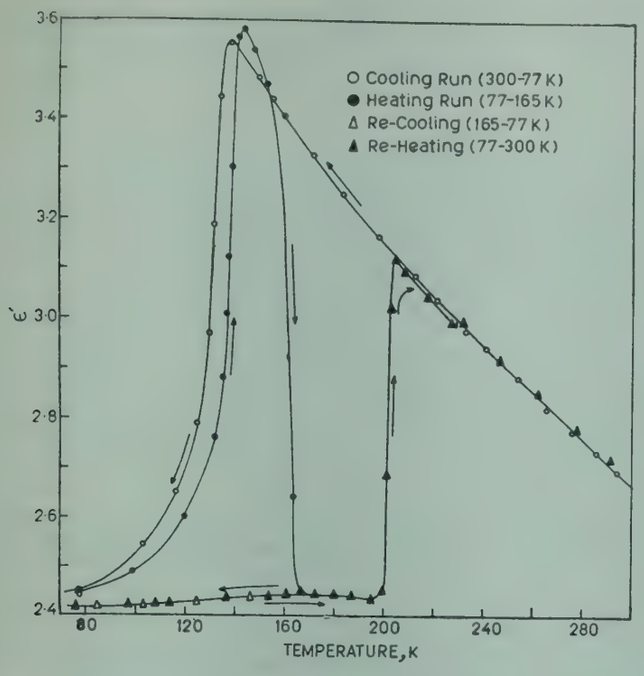

Fig. 3—Temperature dependence of dielectric constant (ϵ') for 25·01 mole % chlorobenzene/*cis*-decalin in cooling and heating runs

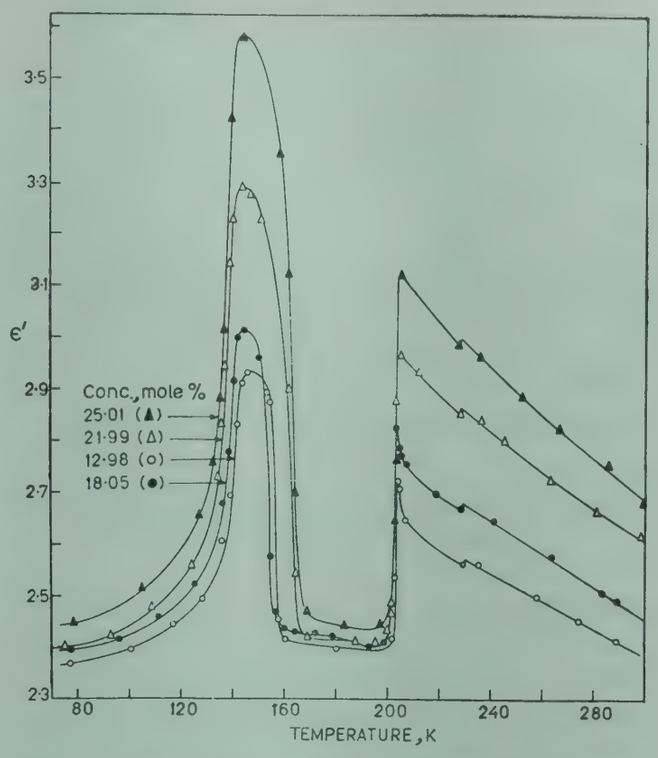

Fig. 4 – Temperature dependence of dielectric constant (ϵ') at 1 kHz for four concentrations of chlorobenzene/*cis*-decalin

the cooling run the dielectric constant keeps on increasing with decreasing temperature down to about 135 K. This is consistent with the expected behaviour of a liquid going into the glassy phase and the fall in the value of ϵ' at about 135 K indicates a phase transition. In the heating run, the dielectric constant suddenly increases to a high value at about 135 K and then shows a small decrease with increasing temperature but the value suddenly drops to a low value at about a 160 K. On further heating, the dielectric constant again increases to high liquid value at about 200 K and a small but sudden break is observed at about 230 K. If the temperature in the heating run is not allowed to increase above 200 K, and the sample is cooled again after ϵ' has dropped to a low value at about 160 K (Fig. 3), then the value remains low upto 77 K and is lower than the value of ϵ' in the first cooling run. On re-heating the sample, ϵ' remains low upto 200 K.

Such a behaviour of the variation of ϵ' with temperature has not been reported earlier. However, it can be explained in the following way. On cooling the sample, the liquid phase goes to an amorphous glassy phase-I with complete dipole rotational freedom, this phase changes at a glass transition temperature T_g (135 K) to a brittle glassy phase-II of restricted dipole rotation. On heating, glassy phase-II changes to glassy phase-I at T_g Amorphous or glassy phase is a metastable state and the lifetime of this metastable state depends on the temperature. At a critical temperature T_c at which the viscosity becomes low enough to permit rapid crystallization, the amorphous phase changes to the crystalline phase. The crystalline phase cannot be converted to the amorphous phase by cooling. The sudden drop in ϵ' at 160 K on heating suggests that the glassy phase-I changes to a crystalline phase.

A similar behaviour in heating and cooling runs of other concentration solutions was observed. The heating run for four concentrations is given in Fig. 4. The crystallization temperature T_c for different concentrations of solute molecules was between 155 K and 165 K, but there was no systematic shift in T_c with increasing concentration. Such an irregular shift in T_c may be due to slight differences in the heating rates.

The variation ϵ' with temperature (heating run) at four frequencies and for one concentration is given in Fig. 5. The overall behaviour at different frequencies is similar to that shown in Fig. 4. The additional features noted are as follows.

(1) No dispersion is observed in the liquid phase above 200 K as well as in the crystalline phase between 160 and 200 K, while clear dielectric dispersion is observed in the temperature region below about 155 K. (2) The sudden drop in ϵ' (at 160 K) and rise at 200 K is observed at the same temperature at all frequencies indicating that the crystallization temperature and melting temperature are well characterized by ϵ'. (3) In the phase above 135 K,

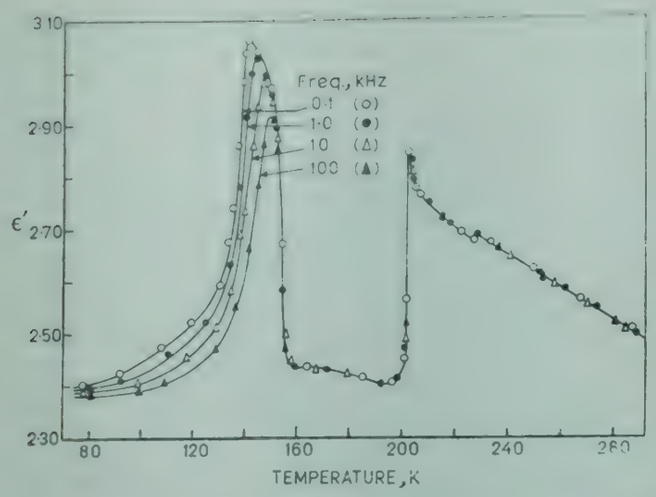

Fig. 5—Temperature dependence of dielectric constant (ϵ') for 18·05 mole % chlorobenzene/*cis*-decalin

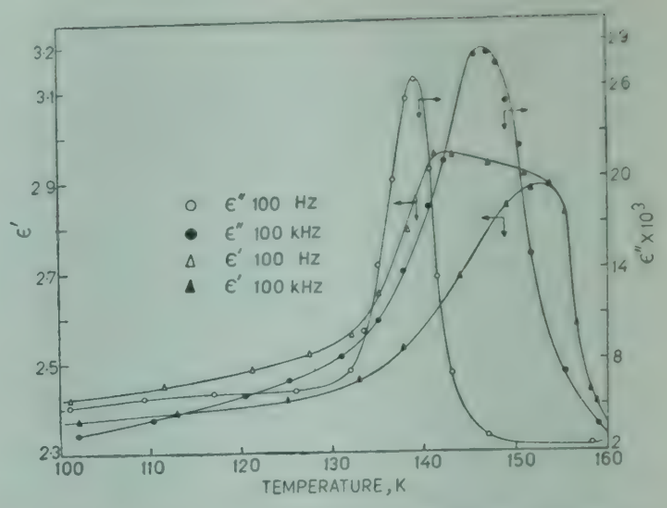

Fig. 6—Temperature dependence of dielectric constant (ϵ') and dielectric loss (ϵ'') for 12·98 mole % chlorobenzene/*cis*-decalin mixture

the temperature at which peak in ϵ' appears, depends on frequency of measurement. Hence the peaks in ϵ' cannot be taken as indicating the glass transition temperature T_g because T_g depends on the frequency.

The peaks in ϵ' at different frequencies and their shift with temperature (in the region 135-155 K) can be explained by the following Debye equation

$$\epsilon' - \epsilon_\infty = \frac{\epsilon_0 - \epsilon_\infty}{1 + (f/f_0)^2}, \quad \epsilon'' = \frac{(\epsilon_0 - \epsilon_\infty)\ (f/f_0)}{1 + (f/f_0)^2} \qquad \ldots(1)$$

where ϵ_0 is the static value of ϵ, ϵ_∞ the high frequency limiting value, and ϵ' the value at the measuring frequency f. If $f \gg f_0$ then ϵ' will be equal to ϵ_∞. As f approaches f_0, ϵ' increases and attains the static value ϵ_0 for $f \ll f_0$.

If we assume that at T_g, $f_0 \ll f$ then ϵ' will be closer to ϵ_∞ and will have a low value, hence no sudden increase in ϵ' indicating a free dipole rotation at T_g will be observed even when the rotational freedom of the dipoles has been attained. This phenomenon yielding a very low relaxation frequency f_0 (much lower than 100 Hz) at the transition temperature, prohibits the determination of the exact glass transition temperature (T_g) from observation of abrupt changes in ϵ'. It may be noticed in Fig. 4 that a rapid increase in ϵ' starts at around 130 K and thus one may guess that the transition temperature at which the dipole rotational freedom starts is between 130 and 135 K. Above the transition temperature, f_0 increases with increasing temperature and so f becomes closer to f_0 and ϵ' increases with temperature. At temperatures where $f \ll f_0$, ϵ' becomes the static dielectric constant. A peak in ϵ' clearly indicates that the static value has been reached and the static dielectric constant decreases with increasing temperature. It is obvious that the temperature at which the frequency of 100 kHz will be smaller than f_0 will be higher than the temperature at which 100 Hz will be smaller than f_0. This will cause a shift in the peak of ϵ' to a higher temperature for higher frequencies. In Fig. 6, ϵ' and ϵ'' are plotted against temperature (130-160 K) on an expanded scale. The values of only two frequencies are plotted for the sake of clarity. At a given frequency, peak in ϵ'' appears at a lower temperature than the peak in ϵ'. This is expected because the peak in ϵ'' occurs when $f = f_0$ and in ϵ' when $f \ll f_0$.

It may be pointed out that Eq. (1) is valid for Debye-type (relaxation) dispersion for a single relaxation time. However, the basic character of dispersion is not changed even in the presence of distribution of relaxation times, and the explanation for the appearance of peak in ϵ' at different temperatures for different frequencies will be valid even in the presence of distribution of relaxation times. It is worth investigating whether the present data of ϵ' and ϵ'' conform to a single relaxation time or a distribution of relaxation times. If we assume that $\epsilon_\infty = 2{\cdot}356$ (the value at 77 K for 100 kHz), then the peak value of ϵ''_{max} at 100 Hz in Fig. 6 should have been equal to 0·3 from Eq. (1). However, the measured value of ϵ''_{max} is considerably lower indicating a distribution of relaxation times. The static dielectric constant decreases with temperature and one would expect that the peak value of ϵ''_{max} at 100 kHz should have been lower than ϵ''_{max} at 100 Hz. However, the measured value of ϵ''_{max} at 100 kHz is higher than that at 100 Hz. This suggests that the distribution parameter decreases with increasing temperature, which will cause an increase in ϵ''_{max} and compensate for the decrease in ϵ_0

The higher value of tan δ_{max} at 100 kHz as compared to that at 1 kHz has also been reported by Johari and Goldstein.[5]

4. Conclusions

1. The variation of ϵ' and tan δ with temperature in heating runs shows that below 160 K, the dielectric behaviour of chlorobenzene in *cis*-decalin is consistent with the reported α- and β-relaxations. 2. The relaxation frequency is mainly controlled by the glassy matrix and the dipolar interactions have negligible effect. 3. The dielectric constant measurements show that the liquid mixture goes to an amorphous or glassy phase-I on cooling which changes to a brittle glassy phase-II at about 135 K. 4. On heating, the glassy phase-II of restricted rotation changes to glassy phase-I of free dipole rotation at T_g ($\sim$135 K). 5. Glassy phase-I goes to a crystalline phase at 160 K in which the dipole rotational freedom is completely stopped. 6. The exact glass transition temperature cannot be determined by the present measurements as the relaxation frequency at T_g appears to be much lower than the lowest measuring frequency of 100 Hz.

Acknowledgement

The authors acknowledge the useful suggestions from Prof. Graham Williams. They are thankful to the University Grants Commission, New Delhi, for financial support.

References

1. McCrum N G, Read B E & Williams G, *Anelastic and dielectric effects in polymeric solids* (John Wiley, New York), 1967.
2. Krishnaji & Mansingh A, *J. chem. Phys.*, 44 (1966), 1590.
3. Clemett C & Davies M, *J. Physique (Geneva)*, (1960), 77.
4. Hill N E, Vaughan E, Price A H & Davies M, *Dielectric properties and molecular behaviour* (van Nostrand-Reinhold, London), 1969.
5. Johari G P & Goldstein M, *J. chem. Phys.*, 53 (1970) 2372.
6. Goldstein M, *J. chem. Phys.*, 51 (1969), 3728.
7. Johari G P & Smyth C P, *J. chem. Phys.*, 56 (1972), 4411.
8. Johari G P, *Ann. New York Acad. Sci.*, 279 (1976), 117.
9. Segel S L & Mansingh A, *J. chem. Phys.*, 51 (1969), 4578.

Indian Journal of Pure & Applied Physics
Vol. 18, August 1980, pp. 588-592

Relaxation Time & Activation Energy for Viscosity from Radiofrequency Conductivity Measurements

A K Ghosh & S N Sen

Department of Physics, North Bengal University, Darjeeling

Received 19 *April* 1979

From the measurement of radiofrequency conductivity of a number of polar molecules such as methyl alcohol, ethyl alcohol, benzyl alcohol, aniline and benzyl chloride at different temperatures and over a frequency range 400-800 kHz, the relaxation time, the number of free ions per unit volume and the variation of activation energy of viscosity with frequency have been obtained. The results prove the validity of the equation deduced earlier by S N Sen and R Ghosh [*J. phys. Soc. Japan*, **36** (1974), 743] and give a quantitative estimate of the imperfection in liquid polar dielectrics. The variation of activation energy of viscosity with frequency of the applied field indicates that viscosity is connected with the nature of charge distribution in a molecule and it is pointed out this should be taken into account to find the nature of internal frictional force acting in a liquid.

1. Introduction

The experimental determination of radio frequency conductivity of polar liquids and its variation with temperature and also when the polar liquid is dissolved in non-polar solvents has evoked considerable interest as it provides a method for the determination of dipole moment and the time of relaxation (τ) of the polar molecule. Determination of dipole moment can give an insight into the properties like distinguishing functional groups whereas the relaxation time gives us information regarding the activation energy, intermolecular field and structure of the molecule concerned. In an ideal dielectric, there should be present no free ions or electrons. In this case, displacement current is the only factor contributing to the conductivity as has been assumed by Murphy and Morgan.[1] But in practice, all dielectrics fall far short of this ideal due to the existence of free ions and electrons. The evidence for the existence of free ions and electrons has been shown by many workers such as Standhammer and Seyer,[2] Lohneyson and Nageral,[3] and Adamczewski and Jachkym.[4] Assuming the existence of free ions, Sen and Ghosh[5] have deduced a mathematical expression for the radio frequency conductivity of polar dielectrics which has satisfactorily explained the observed experimental results and it has been shown that it is possible to calculate the number of free ions per unit volume in some pure polar liquids. In a recent paper Sen and Ghosh[6] have shown that by utilizing the expression for radio frequency conductivity, it is possible to calculate the time of relaxation accurately when the polar molecule is dissolved in non-polar solvents and also to determine the free ion concentration in the liquid. The generation of free ions in both polar and non-polar liquids has been attributed to various factors such as cosmic rays, natural conductivity, thermal dissociation, etc. Thus when a radio frequency field is applied to a polar liquid, the total heat produced is due to the combined effect of displacement current and conduction current. The object of the present study is to extend the investigations to a number of pure polar liquids in order to establish the general validity of the expression deduced by Sen and Ghosh.[5] Considering the existence of free ions, Sen and Ghosh[7] have shown recently that the activation energy for electrical conductivity and that for viscosity are related to one another, both being functions of frequency and gradually decreasing almost linearly with the increase of frequency. The results are similar to those observed by Andrade and Dodd[8] where it has been found that viscosity decreases upto a certain frequency which they termed as critical frequency. Again it is now generally accepted that η which has been assumed to be the coefficient of macroscopic viscosity in the Debye expression $\tau = 4\pi\eta a^3/kT$ cannot adequately represent the internal friction term. The observation by Sen and Ghosh[7] that the activation energy for viscosity varies with frequency should be taken into consideration to examine the nature of

the internal force and this may help to develop a theory whose origin lies with some process closely connected with the charge distribution in molecules. Though the activation energy for electrical conductivity and that for viscosity have been calculated by Sen and Ghosh[7] in case of only three polar liquids, viz. nitrobenzene, *n*-propyl alcohol and acetone, it will be worthwhile to observe whether the same result is valid for other polar liquids as well. In the present investigation, the variation of activation energy with frequency of the applied field will also be investigated by measuring the radio frequency conductivity of a number of polar molecules over a range of frequencies.

2. Experimental Arrangement

The method of determining the radio frequency conductivity has been described in detail in a previous communication by Sen and Ghosh.[9] The dielectric cell used is a cylindrical glass tube of a diameter 2·62 cm fitted with two circular gold electrodes 1·08 cm apart. Each gold plate is connected with a platinum wire which is sealed with the glass tube. The liquids investigated are methyl alcohol, ethyl alcohol, benzyl alcohol, aniline and benzyl chloride and measurements have been made for a wide range of temperatures and the frequency of the applied radio frequency field has been varied from 400 kHz to 800 kHz.

3. Results and Discussion

The real part of the radio frequency conductivity (K') has been measured in case of ethyl, methyl and benzyl alcohol from 25 to 60°C and in case of aniline and benzyl chloride from 30 to 80°C under the application of a radio frequency field whose frequency is varied from 400 kHz to 800 kHz. The experimental values of K' where K' is the radio frequency conductivity at different temperatures are plotted against the corresponding values of $1/\eta$ where η is the coefficient of viscosity at the corresponding temperature and the results are shown in Fig. 1. for different frequencies. It is observed that curves are straight lines with different intercepts for different frequencies for the liquids studied and this shows that the equation deduced by Sen and Ghosh[5] namely

$$K' = \frac{1}{4\pi}(\epsilon_0 - \epsilon\infty)\,\omega^2\,\tau + \frac{n e^2}{6\pi a \eta} = A + \frac{B}{\eta} \qquad \ldots(1)$$

is generally valid. The values of A for different frequencies for the liquids are entered in the second column in Table 1 and from the third column it is noted that A/f^2, where f is the frequency of the applied radio frequency field, is almost a constant for a particular liquid. This shows the quantitative validity of Eq. (1). Taking the mean average value of A/f^2 for each liquid, the value of τ has been calculated and the results are entered in the 4th column of Table 1. The average slope of the curves for each liquid has also been entered in the 4th column of Table 1 and the value of a the molecular radius calculated from the kinetic theory has also been entered in the 4th column of Table 1. Utilizing these values, the value of n the free ion concentration has been calculated for each liquid and the results are entered as the last entry in column 4 of Table 1.

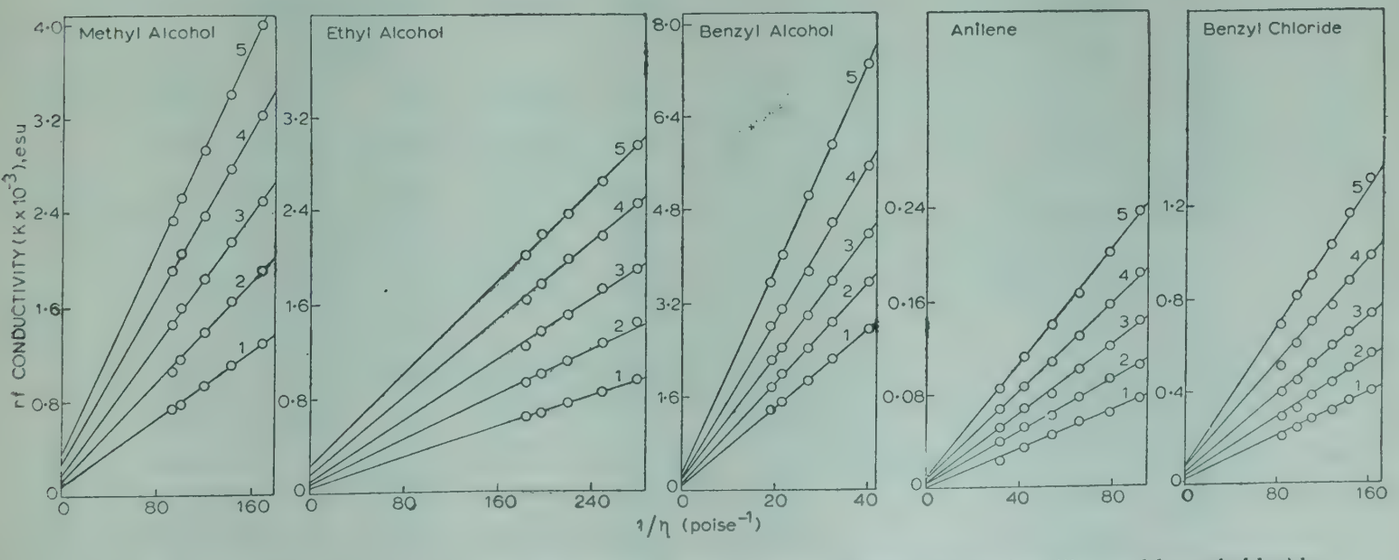

Fig. 1—Variation of K' with $1/\eta$ for ethyl alcohol, methyl alcoh ol, benzyl alcohol, aniline and benzyl chloride

It is observed from Table 1 that the number of ions per cc in case of liquids studied here is of the order of 10^{12} to 10^{14}. It is minimum (of the order of 10^{12}) in case of aniline and is maximum (of the order of 10^{14}) in case of benzyl alcohol. The value of free-charge carrier density in case of benzyl alcohol has been found to be $2{\cdot}8 \times 10^{16}$ per cc by Loheneysen and Nageral[8] which shows that free-charge density depends upon the state of purity of the liquid. In the case of nitrobenzene, acetone and propyl alcohol as previously studied by Sen and Ghosh,[5] the charge carrier density is of the order of 10^{12} to 10^{13}/cc. In case of alcohols, it is seen that the time of relaxation increases with the increasing molecular size. Such a behaviour has been noted before by many workers such as Cole and Cole[10] on

Table 1—Values of A, A/f^2, B, a, η and n at Different Temperatures for the Polar Molecules Studied

Frequency in kHz	Value of $A\times10^{-3}$	$A\times10^{7}/f^{2}$	Values of B, a, τ and n
		Ethyl alcohol	
400	0·08	0·0050	$B=$ 4·063
500	0·13	0·0052	$a=$ $2{\cdot}8537\times10^{-8}$
600	0·18	0·0050	$\tau=$ $0{\cdot}75\times10^{-11}$ sec
700	0·27	0·0055	$n=$ $3{\cdot}28\times10^{13}$
800	0·36	0·0056	
		Ave : 0·00526	
		Methyl alcohol	
400	0·05	0·0031	$B=$ 6·551
500	0·08	0·0032	$a=$ $2{\cdot}5266\times10^{-8}$
600	0·10	0·0028	$\tau=$ $0{\cdot}33\times10^{-11}$ sec
700	0·16	0·0033	$n=$ $1{\cdot}35\times10^{13}$
800	0·24	0·0037	
		Ave : 0·00324	
		Benzyl alcohol	
400	0·08	0·0050	$B=$ 113·10
500	0·14	0·0056	$a=$ $3{\cdot}4516\times10^{-8}$
600	0·20	0·0056	$\tau=$ $1{\cdot}66\times10^{-11}$ sec
700	0·24	0·0049	$n=$ $3{\cdot}19\times10^{14}$
800	0·32	0·0050	
		Ave : 0·00522	
		Aniline	
400	0·002	0·00017	$B=$ 1·554
500	0·005	0·00020	$a=$ $3{\cdot}3141\times10^{-8}$
600	0 006	0·00017	$\tau=$ $1{\cdot}31\times10^{-11}$ sec
700	0·009	0·00018	$n=$ $4{\cdot}21\times10^{12}$
800	0·011	0·00017	
		Ave : 0·00018	
		Benzyl chloride	
400	0·020	0·0013	$B=$ 4·443
500	0·035	0·0014	$a=$ $3{\cdot}5838\times10^{-8}$
600	0·050	0·0014	$\tau=$ $1{\cdot}17\times10^{-11}$ sec
700	0·05	0·0015	$\eta=$ $1{\cdot}30\times10^{13}$
800	0·090	0·0014	
		Ave : 0·0014	

Table 2—Values of A/K_0, B/K_0D, ΔE_c and ΔE_v for Different Frequencies at 30 C

Frequency in kHz	$\frac{A\times10^{3}}{K_0}$	$\frac{B}{K_0D}$	ΔE_c eV	ΔE_v eV	ΔE_v (eV) at zero frequency
			Ethyl alcohol		
400	0·4356	2·3246	0·285	0·167	
500	0·5192	1·7034	0·281	0·157	
600	0·6844	1·6218	0·267	0·149	0·188
700	0·9288	1·4673	0·259	0·143	
800	1·0769	1·2/59	0·255	0·138	
			Methyl alcohol		
400	1·4327	1·7158	0·206	0·119	
500	1·6985	1·2714	0·201	0·109	
600	1·6367	0·9801	0·200	0·101	0·141
700	2·2321	0·8351	0·194	0 095	
800	3·0900	0·7709	0·187	0·090	
			Benzyl alcohol		
400	0·0821	1·9703	0·337	0·186	
500	0·1212	1·6631	0·332	0·181	
600	0·1489	1·4303	0·330	0·177	0·206
700	0·1634	1·3076	0·322	0·170	
800	0·1749	1·0500	0·319	0·163	
			Aniline		
400	0·0296	0·5224	0·409	0·189	
500	0·0538	0·3794	0·407	0·182	
600	0·0534	0·3138	0·402	0·174	0·215
700	0·0662	0·2593	0·397	0·167	
800	0·0703	0·2255	0·392	0·161	
			Benzyl chloride		
400	0·8055	1·4949	0·252	0·141	
500	1·0866	1·1524	0·248	0·131	
600	1·2710	0·9435	0·242	0·123	0·169
700	1·5766	0·7803	0·236	0·115	
800	1·5960	0·6582	0·230	0·108	

the measurements of Slevogt[11] and Baz[12] particularly in case of alcohols and that of Smyth and collaborators[13-15] in case of other series of compounds. The actual value of τ calculated for the liquids presently studied though of the same order of magnitude as reported in the literature, will be different from that calculated from dielectric constant measurements, because the value of τ here corresponds to a state of the liquid in which $\eta \to \infty$ (infinity) and Murphy-Morgan equation will lose its validity long before this stage is reached.

It has been shown by Sen and Ghosh[7] that as $K' = K_0 \exp\{-\Delta E_c/2kT\}$, the activation energy for electrical conductivity can be obtained by plotting log K' against $1/T$. Further, it has been deduced (Sen and Ghosh[7]) that

$$\exp\{-\Delta E_c/2kT\} = \frac{A}{K_0} + \frac{B}{K_0 D} \exp\{-\Delta E_v/kT\} \quad .. (2)$$

where A and B are the same constants as in Eq. (1) and D is the constant in the equation

$$\eta = D \exp\{\Delta E_v/kT\}$$

The values of ΔE_v for different frequencies for the liquids investigated have thus been calculated and entered in the last column of Table 2. From Table 2, it is seen that the activation energy for electrical conductivity and that for viscosity become a function of frequency, both gradually decrease with the increase of frequency. The results are plotted in Fig. 2 and it is observed that there is a tendency of saturation towards higher frequencies as was reported earlier by Andrade and Dodd.[8] It is further observed that in case of alcohols both ΔE_c and ΔE_v increase with the increase of molecular size. Though there is a general tendency for τ and ΔE_v to increase with the increasing molecular size or weight, the results for aniline and benzyl chloride indicate that a definite conclusion cannot be drawn regarding the variation of time of relaxation and activation energy with the size, shape and nature of the molecules. Such a behaviour of τ has been observed by LeFevre and Sullivan[16] where measurements of τ have been made in order to observe the variation of τ with molecular size or weight for 32 different solutes mainly in carbon tetrachloride solvent and they found that τ value at infinite dilution shows no smooth variation with the size or shape of the molecule. When the activation energy for viscosity is plotted against the frequency (Fig. 2), it is found that the curve is almost linear and by extrapolation to zero frequency, the value of activation energy obtained agrees well with that found in literature.

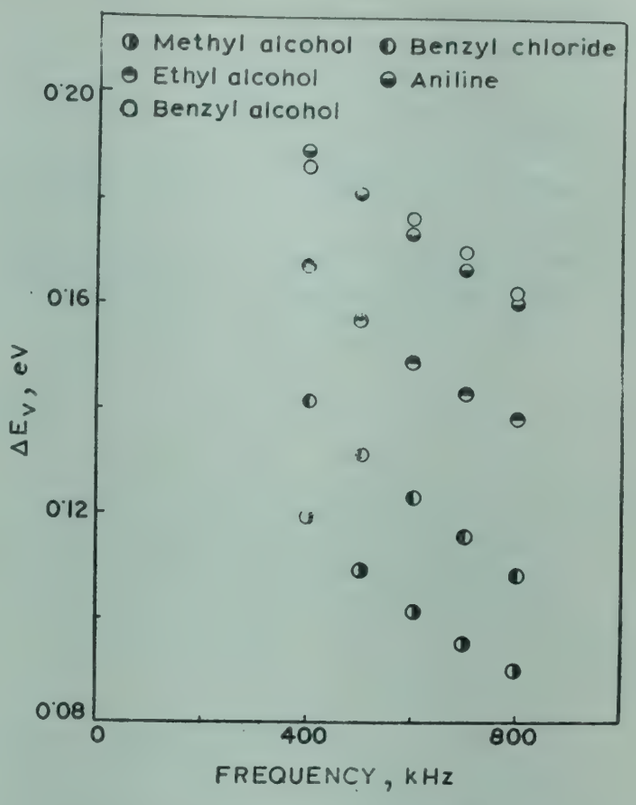

Fig. 2—Variation of ΔE_v with frequency

We can thus conclude that the expression for radio frequency conductivity deduced by Sen and Ghosh[5] has general validity for a large number of polar molecules and the equation can be utilized for calculating the time of relaxation and the number of free-charge carriers in polar liquids. Though the number of free ions is very small (percentage of ionization of the order of 10^{-6}), it gives a measure of the imperfection in pure liquid dielectrics. Another point that emerges is that viscosity of a polar dielectric becomes a function of the frequency of the applied radio frequency field and must have some bearing on the experimental results of Andrade and Dodd regarding the effect of electric field on viscosity. The nature of the internal frictional force which has been taken to be analogous to viscous force in Debye's expression for relaxation time can be reviewed in the light of the result that activation energy for viscosity becomes a function of the frequency of the applied radio frequency field.

References

1. Murphy E J & Morgan S C, *Bell Syst. Tech. J.*, **18** (1939), 502.
2. Standhammer P & Seyer W F, *J. appl. Phys.*, **28** (1957), 405.
3. Loheneysen H V & Nageral H, *J. Phys.*, **D4** (1971), 1718.
4. Adamczewski I & Jachym B, *Acta phys. Polon*, **34** (1968), 1015.

5. Sen S N & Ghosh R, *J. phys. Soc. Japan*, 36 (1974), 743.

6. Sen S N & Ghosh A K, *J. phys. Soc. Japan*, 48 (1980), 1219.

7. Sen S N & Ghosh R, *Indian J. pure appl. Phys.*, 16 (1978), 665.

8. Andrade E N D & Dodd C, *Proc. R. Soc.*, A187 (1946), 296.

9. Sen S N & Ghosh R, *J. phys. Soc. Japan*, 33 (1972), 838.

10. Cole K S & Cole R H, *J. chem. Phys.*, 9 (1941), 341.

11. Slevogt K E, *Ann. Phys.*, (5), 36 (1939), 141.

12. Baz G, *Phys. Z.*, 40 (1939), 394.

13. Hennelly E J, Heston (Jr) W M & Smyth C P, *J. Am. chem. Soc.*, 70 (1948), 4102.

14. Kalmann O F & Smyth C P, *J. Am. chem. Soc.*, 82 (1960), 783.

15. Grub E L & Smyth C P, *J. Am. chem. Soc.*, 83 (1961), 4122.

16. LeFevre R J W & Sullivan E P A, *J. chem. Soc.*, Part-III (1954), 2874.

Indian Journal of Pure & Applied Physics
Vol. 18, August 1980, pp. 593-596

Characteristics of Fireballs Produced in 200 GeV/c Proton-Nucleus Interactions

Y V Keshava Rao & R K Puri

Department of Physics, Indian Institute of Technology, New Delhi 110 029

Received 13 *July* 1979

The parameters of fireballs produced in 200 GeV/c proton-nucleus interactions in nuclear emulsion have been estimated. The identification of fireballs has been made from the Duller-Walker plots and target diagrams for individual interactions, applying Berger's quantitative measure for clustering of particles. The average mass of the fireballs is found to be $(2{\cdot}01 \pm 0{\cdot}12)$ GeV/c and the average momentum of the emitted pions is (231 ± 14) MeV/c. The results have been compared with the data at other energies.

1. Introduction

A significant feature of the multiple production in hadron-hadron interactions, at high energy, is the production of high multiplicity clusters, i.e. fireballs, besides the prominent low-mass resonances. The fireball model[1-3] which was postulated to explain the apparent double lump structure of the angular distribution of cosmic ray jets, has been extensively studied theoretically. Frautschi[4] had predicted various general characteristics of isobars and fireballs in high energy hadron-hadron collisions. The study of decay of fireballs after production[5] and the effect of the transverse momentum of the fireball on its subsequent decay[6,7] were also considered.

The analysis of cosmic ray jets (energy $\geqslant 10^{12}$ eV) indicated that at these energies, events with one fireball existed which decay isotropically and have a mass distribution of 2-5 GeV/c. The multi-peripheral approach to the production of fireballs revealed that correlated groups of pions (clusters) should be produced besides the well known resonances.[8] The present experimental results on short-range correlations point to the conclusion that pion production is mediated by the production of pionic clusters with the mean mass of 2 GeV/c^2 decaying on an average into 3-4 pions. The fact that these parameters are certainly higher than those expected from low-mass resonance decay justifies the assumption that clusterization observed in accelerator experiments is an averaged effect of pionic resonances and fireball. The present analysis aims at the study of characteristics of fireballs produced in proton-nucleus collision at 200 GeV/c primary energy.

2. Identification of Fireballs

A number of methods have been proposed for the detection of clusters.[8] We have adopted the most plausible method for identification of fireballs in the individual interactions by comparing the angular distributions of secondaries in the Duller-Walker plot and the plot of natural coordinates of points of emission of the particle in the azimuthal plane (target diagram). A criterion for quantitative measure for cluster formation as suggested by Berger[9] has been applied.

The trace of a nucleon-nucleon collision in the azimuthal plane is shown in Fig. 1, wherein the

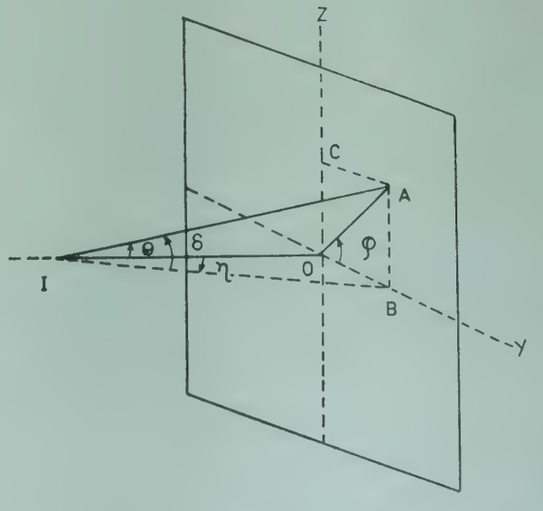

Fig. 1—The trace of an interaction in the emulsion. [I is the point of interaction in the XY-plane of the emulsion and IA is the direction of emission of a secondary]

point of emission of the secondary particle has the coordinates $y = \tan\theta \cos\phi = \tan\eta$

and $z = \tan\theta \sin\phi = \sec\eta \tan\delta$

where θ and ϕ are respectively the space and azimuthal angles and η and δ are respectively the projection and dip angles of the secondary particle. A plot of $\tan\eta$ versus $\sec\eta \tan\delta$ shows a grouping of the points corresponding to a fireball emission. A comparison of the target diagram and the Duller-Walker plot is made to decide the exact number of clusters and the number of particles belonging to a cluster. This is feasible because there exists a one-to-one correspondence between the points referring to the same secondary in both the plots. All the points forming a group in the target diagram should lie on a straight line in the Duller-Walker plot. Likewise all points lying on a straight line should form a group in the target plot. Such points which do not conform to the above criteria are rejected. The presence of such points in either of the plots may be due to the following reason. As the fireball is also considered as a secondary particle emitted with a short life-time, the decay products of the fireball may be emitted in close proximity to other particles produced during the interaction. These particles may, therefore, have angles of emission very close to those emitted from the fireball.

According to Berger,[9] a group of particles will appear to form a cluster if its extension along the rapidity axis is small compared to the total range of rapidity available. For the production of single isotropic cluster, the dispersion parameter of the rapidity $\Delta \leqslant 0{\cdot}91$. The dispersion is defined by

$$\Delta = \left[\frac{1}{N-1}\sum_{i=1}^{N}(\bar{y}-y_i)^2\right]^{1/2}$$

where N is the number of charged particles in the cluster, $\bar{y}$ the average rapidity of N particles and y_i the rapidity of the ith particle.

3. Determination of Fireball Parameters

The fireball parameters are determined by the method suggested by Agnese *et al.*[10] The identification of fireball, described in the previous section, gives the exact number of particles included in the cluster. From the projection and dip angles of the particles constituting the cluster say (η_i, δ_i) the centre of gravity $(\eta_g, \delta_g,)$ of the angles is calculated. The Euler angle of emission $(\alpha, \phi, 0)$ of the fireball with respect to the laboratory system is then calculated as

$$\tan\alpha = (\tan^2\eta_g + \tan^2\delta_g + \tan^2\eta_g \tan^2\delta_g)^{1/2}$$

and $\psi = \pi/2 - \tan^{-1}(\sin\eta_g/\tan\delta_g)$

The angle of emission of each particle emitted from the cluster is then transformed to the coordinate system defined by $(\alpha, \phi, 0)$. The polar rotated angle θ_{Rj} of the particles in the cluster is given by

$$\cos\theta_{Rj} = \sin\alpha \sin\theta_j \sin(\phi + \phi_j) + \cos\alpha \cos\theta_j$$

The quantities θ_j and ϕ_j are the space and azimuthal angles of the tracks belonging to the cluster in the laboratory system. The azimuthal angle ϕ_j can be calculated from

$$\sin\phi_j = \sin\delta_j/\sin\theta_j.$$

Assuming an isotropic decay of the fireball in its rest system and for the case $\alpha = 0$ (i. e. in the rotated laboratory system) the integral polar rotated angular distribution can be shown to be of the form

$$F(\theta_R) = 1 - \frac{[1-(m^2-1)\gamma_b^2 \tan^2\theta_R]^{1/2}}{1+\gamma_b^2\tan^2\theta_R}$$

where $F(\theta_R)$ is the fraction of particles within an angle θ_R in the fireball system, γ_b is the Lorentz factor of the fireball and the ratio $m = \beta_b \Big/ \left\langle \beta_j^* \right\rangle$ is the ratio of the velocity of the fireball to the average velocity of the emitted particles.

The method of successive approximation is used to calculate the value of m and γ_b from the above distribution from least square fit method. The average momentum of the pions p_0 and the mass of the fireball m_F are calculated from the relations

$$p_0 = \frac{m_\pi}{(m^2/\beta_b^2 - 1)^{1/2}}$$

and

$$m_F = 3/2\, N\,(p_0^2 + m_\pi^2)^{1/2}$$

The emission angle $\bar{\alpha}$ of the fireball in the c. m. system is calculated as

$$\tan\bar{\alpha} = \pm \frac{\sin\alpha}{(\cos\alpha - \beta_c/\beta_b)} \cdot \frac{1}{\gamma_c}$$

where γ_c is the Lorentz factor of the cm system. The inelasticity of the interaction is given by $\rho = \bar{E}_F/E_{av}$ where $\bar{E}_F = (\bar{p}_F^2 + m_F^2)^{1/2}$ is the energy of the fireball in the c. m. system and E_{av} is the energy available in the c.m. system (19·02 GeV/c).

4. Experimental Details

Line scanned data of 200 GeV/c proton interactions in nuclear emulsions have been used. The details of exposure are given elsewhere.[11] The interactions have been analyzed after selecting the events satisfying the criteria* $N_h \leqslant 5$ and $N_s \geqslant 8$. The

*Tracks satisfying the criterion $\beta < 0{\cdot}7$ are termed heavy tracks (N_h) and the tracks satisfying the criterion $\beta > 0{\cdot}7$ are termed shower tracks (N_s).

former criterion is used to select the probable proton-nucleon events with a minimum excitation given to the target nucleus. The latter condition ensures the identification of fireballs from a cluster comprising a minimum of three secondaries, thus providing a sufficient statistical significance to the data.

Angular measurements were made on Cooke's microscope under a magnification of $\times 1000$. Tracks emitted at an angle exceeding 90° from the beam direction are not included in the analysis A comparison of the Duller-Walker plot and the target diagram is made for an interaction to identify a possible fireball emission and Berger's criterion is applied for all such clusters. The clusters satisfying these criteria are accepted as fireballs. The Duller-Walker plot and the target diagram for a typical fireball case are shown η in Figs. 2(a) and 2(b) respectively. In the target plot, although the points denoted by open circles form the group, these do not form a straight line in the Duller-Walker plot. The points denoted by solid circles form the cluster and satisfy Berger's criterion also.

5. Results and Discussion

A total of 50 events from 200 GeV/c proton-nucleus interactions satisfying the criteria $N_h \leqslant 5$ $N_s \geqslant 8$ were analyzed. There is no evidence of fireball production in three events whereas six events indicate emission of two fireballs as per our criteria. One fireball emission has been identified in each of the remaining events. The mass distribution of the fireballs and the distribution of momenta of the pions, are displayed in Figs 3(a) and 3(b) respectively.

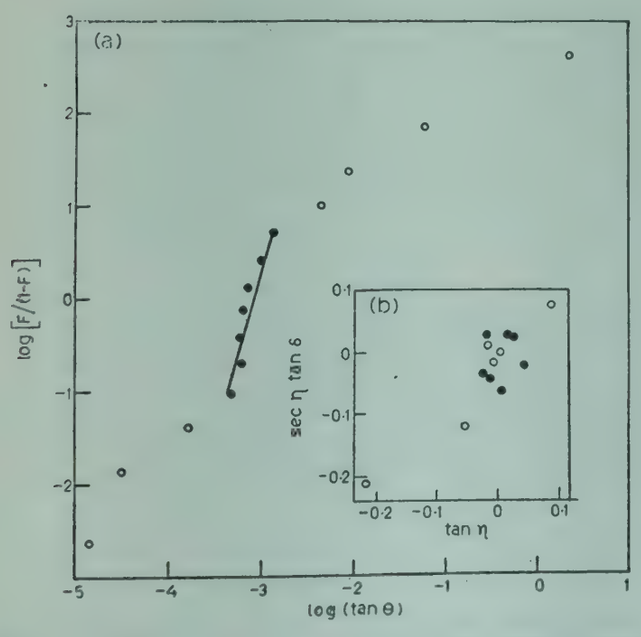

Fig. 2—(a) Duller-Walker plot for a typical fireball event and (b) target diagram for the same event

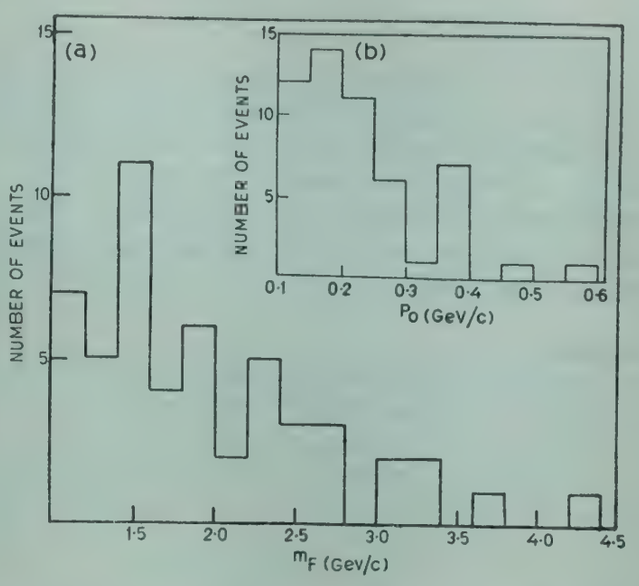

Fig. 3—(a) Distribution of fireball mass, and (b) distribution of the momenta of pions

Table 1—Average Values of Mass of Fireball (m_F) and Momentum of Pions (p_0) and the Inelasticity of Collisions (ρ) at 200 GeV/c as Compared to Those at Different Energies

Primary energy & particle	No. of events	Average No. of particles per fireball	m_F, GeV/c	p_0, MeV/c	Inelasticity (ρ)
200 GeV/c (present work)	53	4·98±0·2	2·01+0·12	231±14	0·24±0.03
p-N 60 GeV/c π^-−N (Ref. 10)	9	6·88±0·4	2.61±0·37	213±59	0·33±0·04
50 GeV/c π^-−N (Ref. 13)	12	—	3·47±0·42	344±52	—
70 GeV/c p-N (Ref. 14)	2	—	2·8±0·1	169	—

The value of the average charged multiplicity of the fireballs, average mass of the fireball and the average momentum of pions, are shown in Table 1. The inelasticity of collision is peaked around 0·24. This seems to be slightly less than the maximum value of 1/3 predicted by Satz[12] on the basis of quark model.

From the data, we observe rather weak dependence of the fireball mass on the charged multiplicity. More data at other energies are necessary to draw any inferences about the energy dependence of the fireball parameters.

Acknowledgement

We wish to thank the members of Bombay-Chandigarh-Jammu Collaboration for the loan of 200 GeV/c emulsion plates. Thanks are due to Dr Sardar Singh for helpful discussions. We thank Prof. A Agnese and A Wataghin of the University of Genova, Italy for their prompt correspondence and clarification of some points.

References

1. Niu K, *Nuovo Cim.*, **10** (1958), 994.
2. Ciok P, *et al.*, *Nuovo Cim.*, **10** (1958), 741.
3. Cocconi G., *Phys. Rev.*, **111** (1958), 1699.
4. Frautschi S C, *Nuovo Cim.*, **28** (1963), 409.
5. Nahm W, *Nucl. Phys.*, **68B** (1974), 111.
6. Agnese A., *et al.*, *Nuovo Cim.*, **59A** (1969), 71.
7. Agnese A, *et al.*, *Nuovo Cim.*, **62A** (1969), 174.
8. Dremin I M, P N Lebedev Institute preprint **18**, 1977.
9. Berger E L, *Physics Lett.*, **43B** (1973), 132.
10. Agnese A, *et al.*, *Nuovo Cim.*, **13A** (1973), 144.
11. Gurtu A, *et al.*, *Physics Lett.*, **50B** (1974), 391.
12. Satz H, *Physics Lett.*, **25B** (1967), 220.
13. Shabratova G S, *et al.*, *Lett. Nuovo Cim.*, **18** (1977), 511.
14. Daftari I K *et al.*, *Annln Phys., Lpz.*, **32** (1975), 471.

Indian Journal of Pure & Applied Physics
Vol. 18, August 1980, pp. 597-600

Forward-Backward Asymmetry in Proton-Nucleus Interaction at 70 GeV/c in Emulsion

D K Bhattacharjee, S Naha & T Roy

High Energy Physics Division, Department of Physics, Jadavpur University, Calcutta 700 032

Received 24 *August* 1979; *revised received* 12 *November* 1979

Forward-backward rapidity correlation and asymmetry in proton-nucleus interactions in emulsion are observed to be consistent with the expectation of the fragmentation notion of particle production. The boundary value η_0 of rapidity separating the projectile and target hemispheres is 2·5. The asymmetry parameter is observed to be exponentially dependent on η_0.

1. Introduction

The spurt of interest in the study of proton-nucleus interaction is mainly caused by the suggestion that the study of multiparticle production in such interaction can provide informations which are not available in elementary nucleon-nucleon processes.

Forward-backward multiplicity fluctuations were considered in a number of papers.[1-6] Lal *et al.*[7] have studied the multiplicity distribution of forward charged secondaries in cosmic ray pion and proton interaction in carbon target at energies of about 50 GeV. A symmetric configuration is typical for multiperipheral models, while in a fragmentation picture, asymmetric events with unequal number of particles produced in the forward (projectile) and backward (target) hemispheres follow as a rule.

A study of asymmetry in proton-nucleus interaction in emulsion can be made through quantities which are invariant to the Lorentz transformation and are estimated in the laboratory system. An analysis through such quantities gives for the interpretation of elementary processes, information that is free from the inaccuracies arising in transformations to the centre of mass system due to the uncertainty about the target nucleus.

A quantity possessing the property of additivity under Lorentz transformation and characterizing the dynamics of the interaction process is the pseudorapidity variable $\eta = -\ln \tan(\theta/2)$ which approaches the laboratory rapidity y for $P_T^2 \gg m^2$.

The study of forward-backward multiplicity fluctuations necessitates the splitting up of secondaries in the projectile and target hemispheres. In case of p-p collision $\eta_0^{Cm}\, N - N = 0$ can define the two hemispheres in view of the symmetry of the initial state. In the case of proton-nucleus collision, however, there is asymmetry in the initial colliding system. Jain *et al.*[8] considered the problem of splitting up of secondaries into inner and outer cones in laboratory system (l.s.) defining the boundary through the centre of mass (c.m.) Lorentz factor.

In this paper, we call attention to a mode of data presentation, which, although in a somewhat different context, has been applied by Wosiek,[9] to determine the boundary value in the laboratory rapidity space. The method can reasonably separate the secondaries ($\beta \geqslant 0{\cdot}7$) in p-nucleus interaction into projectile (forward) and target (backward) hemispheres. The correlation between associated multiplicities in the two hemispheres and the asymmetry in the final state are studied by using the value of η_0 so obtained. An empirical relationship between the asymmetry parameter α defined in terms of the average multiplicities in the respective hemispheres and the value of η_0 has been obtained.

The presentation of data is based on 179 events which satisfy usually accepted criterion ($N_h \geqslant 2$) for nucleon-nucleus collision. The whole sample of data has been divided into two sub-groups characterized by $2 \leqslant N_h \leqslant 6$ and $N_h > 6$ because of the usually accepted suggestion that these are the features exhibited by the collision suffered by the proton with the light (CNO) and heavy (AgBr) groups of nuclei respectively.[10]

2. Experimental Material

The pellicles of nuclear emulsions used for this analysis are a set of photoemulsion plates of dimensions 20 cm × 10 cm × 600 μm, which were exposed to 70 GeV/c proton beam at Serpukov. Scanning of the plates by 'along the track' method were performed

on an Leitz-Wetzlar microscope. Events which were clear and without any blob at the point of production were selected for analysis. The method of classification of the tracks and the exclusion of the coherently produced events have been made as described by Daftari *et al.*[10]

The angles (θ) of the shower tracks were measured by the coordinate method. In a sample of events, the results so obtained were checked by measuring the projected angle of the secondary tracks relative to the primary direction by using a goniometer attached to one of the oculars of the microscope. An error of $\sim 3\%$ was calculated from these two measurements.

3. Projectile and Target Hemispheres

Our approach is to split the secondaries into two hemispheres on the basis of a few selected values of η_0 and to study the distributions. The necessary bias for selection of appropriate values of η_0 has been provided by comparison of values obtained for η^{cm}N—N computed from our measured angles through their conversion from laboratory to p-p centre of mass system.[11] The results are given in Table 1 and Fig. 1 where the variation of $D/\bar{N}$ with η_0 for the two hemispheres has been shown. The ratio of the dispersion (D) to the average shower multiplicity ($\bar{N}$) is an important parameter which can effectively distinguish between a hadron-nucleon and hardon-nucleus interaction.[12] Since η_0 defines the boundary between the two hemispheres in the rapidity space, the shower particles (n_s) of an event can, therefore, be split up into two parts denoted by N_P and N_T as associated with the projectile and target hemispheres respectively, such that $n_s = N_P + N_T$. We define $\bar{N}_T$ (or $\bar{N}_P$) as the average value of N_T (or N_P) averaged over all events having the same N_P (or N_T) for a chosen value of η_0.

It is seen that in the target hemisphere the $D/\bar{N}$ ratio increases with η_0 while in the projectile hemisphere the behaviour gets modified and approaches

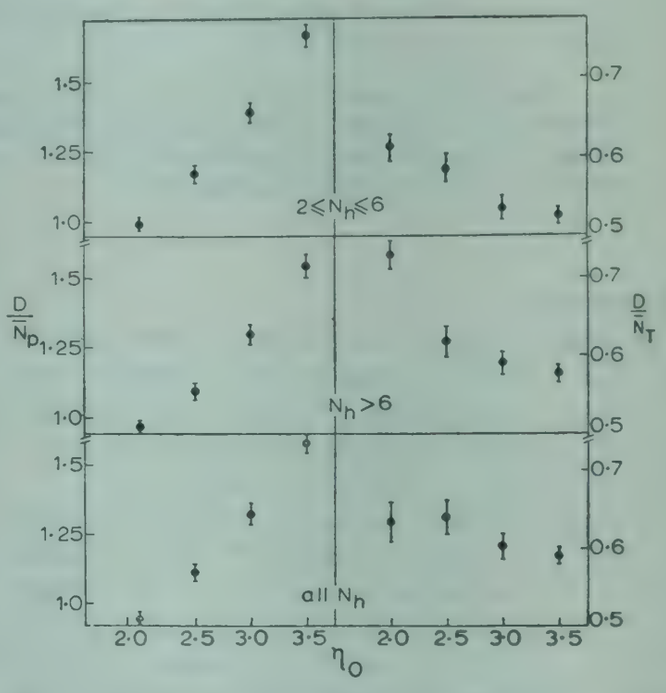

Fig. 1—Graphical representation of the dependence of $D/\bar{N}_P$ (left) and $D/\bar{N}_T$ (right) on the value of η_0

Table 1—Variation of $D/\bar{N}_P$ and $D/\bar{N}_T$ in the Projectile and Target Hemispheres

η_0	Projectile hemisphere			Target Hemisphere		
	$\bar{N}_P$	D	$D/\bar{N}_P$	$\bar{N}_T$	D	$D/\bar{N}_T$
			(a) $2 \leqslant N_h \leqslant 6$			
2·0	2·24±0·05	2·23±0·04	0·99±0·05	2·36±0·05	1·45±0·03	0·61±0·09
2·5	1·73±0·03	2·03±0·05	1·17±0·05	2·87±0·04	1·68±0·03	0·58±0·08
3·0	1·18±0·04	1·64±0·04	1·39±0·07	3·42±0·09	1·83±0·08	0·54±0·04
3·5	0·81±0·01	1·35±0·03	1·65±0·09	3·79±0·13	1·99±0·07	0·52±0·02
			(b) $N_h > 6$			
2·0	2·70±0·09	2·61±0·03	0·96±0·05	3·38±0·11	2·45±0·07	0·72±0·11
2·5	1·82±0·06	1·99±0·03	1·09±0·06	4·26±0·11	2·63±0·04	0·61±0·11
3·0	1·23±0·04	1·60±0·01	1·29±0·08	4·85±0·12	2·84±0·08	0·58±0·08
3·5	0·76±0·01	1·17±0·02	1·54±0·09	5·32±0·14	3·07±0·10	0·57±0·06
			(c) all N_h			
2·0	2·57±0·06	2·42±0·08	0·94±0·05	3·11±0·10	1·97±0·04	0·63±0·13
2·5	1·79±0·03	2·00±0·06	1·11±0·06	3·89±0·10	2·49±0.04	0·64±0·12
3·0	1·22±0·03	1·61±0·06	1·32±0·07	4·47±0·11	2·68±0·06	0·61±0·06
3·5	0·77±0·01	1·22±0·02	1·57±0·07	4·91±0·13	2·90±0·10	0·59±0·06

a value within 0·5 and 0·6 as is expected in a pp collision. It can also be ascertained that $D/\bar{N}_P$ and $D/\bar{N}_T$ differ from each other. This difference is found to be increasing with η_0. Table 2 and Fig. 2 show the dependence of forward-backward correlations on the values of η_0. It is evident from Table 2 that for $\eta_0 = 2{\cdot}0$, the correlations between $\bar{N}_P$ and N_T as well as $\bar{N}_T$ and N_P are strong. One can also see that correlations at $\eta_0 = 3{\cdot}0$ and $3{\cdot}5$ are very small indicating their near independence. This might lead one to suggest. $\eta_0 = 2{\cdot}5$ to be the point where the parameters start to be independent. This definition seems to be quite reasonable to suggest that with the higher incident proton energy the projectile hemisphere would be bound by higher η_0 values where the jet structure is more pronounced. This value of η_0 agrees well with the value of $\eta_0 = 2{\cdot}47$ obtained through the procedure adopted by Jain *et al.*[7] In fact, a principal axis variable method of analysis of a part of our data showed clear evidence of jet structure at 70 GeV/c.[13]

4. Correlation between Associated Multiplicities in the Projectile and Target Hemispheres

The variation of the average multiplicity in one hemisphere with the multiplicity in the other for the two sub-groups and for the whole sample of data are given in Table 2. Fig. 2 shows the relationship between these for $\eta_0 = 2{\cdot}5$.

It is thus observed that the average multiplicity in the target hemisphere is dependent on the multiplicity in the projectile hemisphere in a stronger manner than the dependence of the average multiplicity in the projectile hemisphere on the multiplicity in the target hemisphere.

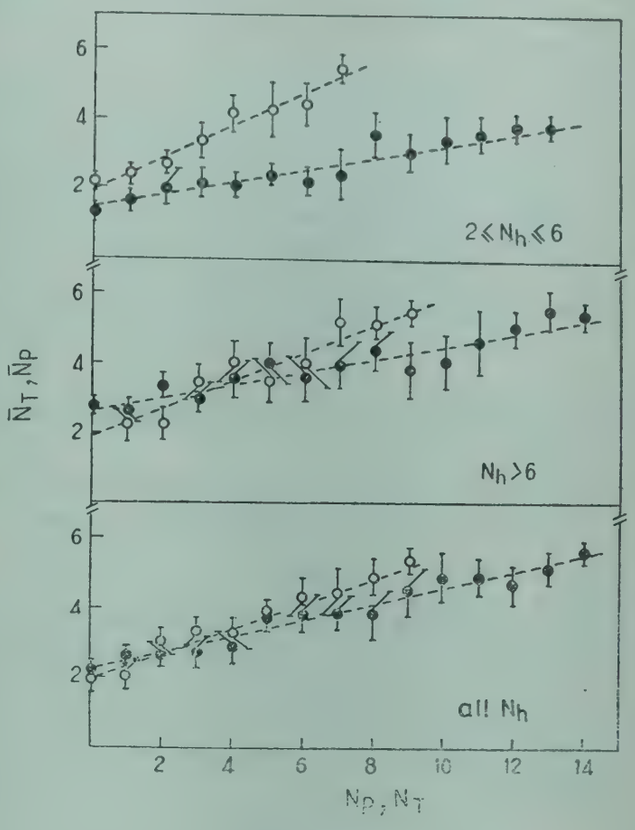

Fig. 2—Average multiplicity ($\bar{N}_P$) in the projectile hemisphere plotted against multiplicity in the target hemisphere (N_T) and vice-versa at $\eta_0 = 2{\cdot}5$ [○ $\bar{N}_T$ vs N_P; ● $\bar{N}_P$ vs N_T]

Table 2—Variation of Forward-backward Correlations with the Value of η_0

η_0	$\bar{N}_T = a(\eta_0) + N_P + b(\eta_0)$		$\bar{N}_P = a(\eta_0)\, N_T + b(\eta_0)$	
	$a(\eta_0)$	$b(\eta_0)$	$a(\eta_0)$	$b(\eta_0)$
	(a) $2 \leqslant N_h \leqslant 6$			
2·0	0·18±0·01	0·21±0·20	0·29±0·03	2·45±0·07
2·5	0·45±0·04	1·96±0·12	0·18±0·02	1·48±0·08
3·0	0·13±0·01	3·41±0·42	0·10±0·02	0·61±0·05
3·5	0·08±0·01	5·14±0·37	0·02±0·01	0·74±0·06
	(b) $N_h > 6$			
2·0	0·21±0·02	0·19±0·20	0·31±0·12	2·72±0·06
2·5	0·38±0·03	1·94±0·13	0·20±0·02	2·60±0·31
3·0	0·16±0·05	4·12±0·11	0·09±0·04	1·42±0·05
3·5	0·13±0·04	5·13±0·23	0·02±0·01	0·62±0·01
	(c) all N_h			
2·0	0·15±0·02	0·23±0·12	0·27±0·03	2·41±0·08
2·5	0·40±0·03	2·05±0·41	0·19±0·02	2·30±0·27
3·0	0·11±0·01	4·52±0·50	0·08±0·02	1·52±0·12
3·5	0·04±0·02	5·71±0·04	0·01±0·01	0·84±0·07

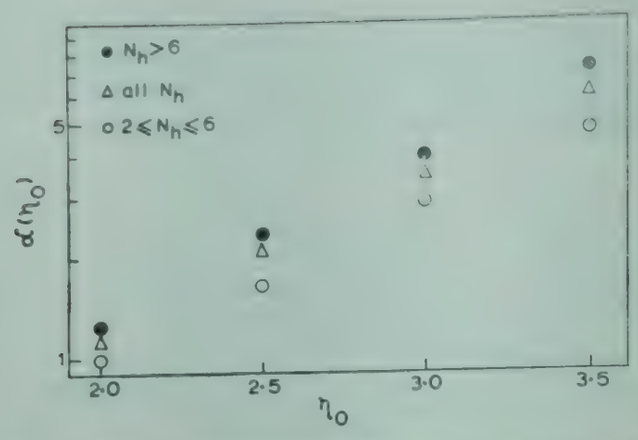

Fig. 3—Variation of asymmetry parameter α (η_0 as a function of η_0

5. Asymmetry between Projectile and Target Hemispheres

We study the asymmetry between the two hemispheres with the help of an asymmetry parameter

$$\alpha(\eta_0) = \overline{N}_T/\overline{N}_P$$

where $\overline{N}_T$ and $\overline{N}_P$ are the mean associated multiplicities in the target and projectile hemispheres as a function of η_0. The variation of the asymmetry parameter with η_0 is shown in Fig. 3. An exponential fit to the data yields a relation between α and η_0 of the form

$$\alpha(\eta_0) = a \exp(b\,\eta_0)$$

The values of a and b for the first sub-group ($2 \geqslant N_h \leqslant 6$) are respectively $0{\cdot}148 \pm 0{\cdot}011$ and $0{\cdot}984 \pm 0{\cdot}029$. The values of a and b for the second sub-group ($N_h > 6$) and for the whole set of data (All N_h) are $0{\cdot}127 \pm 0{\cdot}008$ and $1{\cdot}149 \pm 0{\cdot}020$ and $0{\cdot}118 \pm 0{\cdot}009$ and $1{\cdot}152 \pm 0{\cdot}022$ respectively. As has been discussed earlier, it is expected that with the rise in the primary energy, η_0 would approach to an asymptotic value η_0^{max} setting the kinematical limit. This would result in a growth of $\alpha(\eta_0)$ and this is found to be consistent with the relation obtained above.

6. Discussion

The results show that the splitting up of secondaries in the projectile and target hemispheres brings out distinguishing features of the proton-nucleus collision

It is observed that the multiplicity distribution in the two hemispheres suggest an asymmetric behaviour which persists with different values of η_0 (Fig. 3) and for both light and heavy group of nuclei. Small differences in the forward and backward multiplicities and observed near independence of asymmetry parameter on the target size disfavour an explanation on the basis of a native classical intra-nuclear cascade. The backward asymmetry and the nature of variation of asymmetry parameter with η_0 have implications for the fragmentation vs independent-emission issue. However, a kinematical analysis[14] of a part of our data shows that the region of phase space where most of the secondaries appear contains both pionization and target fragmentation regions.

Acknowledgement

The authors are deeply indebted to Prof. K D Tolstov, Joint Institute for Nuclear Physics, Dubna for providing them with exposed emulsion plates and to Prof. A Subramanian, Tata Institute of Fundamental Research, Bombay, for his interesting remarks.

References

1. Caneschi L, *Phys. Rev.*, D3 (1971), 2865.
2. Belletini C, *Proc. 16th int. Conf. on high energy Physics Batavia*, Vol. 1, (1972), 279.
3. Jacob M, *Proc. 16th Int. Conf. on high energy Physics Batavia*, Vol. 3, (1972), 373.
4. Berger E L & Jacob M, *Phys. Rev.*, D6 (1972), 1930.
5. Nussinov S, Quigg C, Wang J M, *Phys. Rev.*, D6 (1972), 2713.
6. Atanelishvili M I *et al.*, *Proc. 14th Int. cosmic ray Conf. Munich*, Vol. 7, 1975, 2286.
7. Lal S, Raghavan R, Sreekantan B V, Rangaswamy T N, Subramanian A & Verma S D, *Proc. Int. Conf. high energy Physics, CERN*, (1962), 641.
8. Jain P L, Girard B, Kazuno M & Thomas G, *Phys. Rev. Lett.*, 34 (1975), 972.
9. Wosiek B, *Krakow Rep.*, (1976), 930/PH.
10. Daftari I K, Bhattacharjee D K, Naha S, Ghosh D C & Roy T, *Fortschr. Phys.*, 26 (1978), 609.
11. Hagedorn R, *Relativistic kinematics*, (Addison Wesley) 1964.
12. Bialas A *et al.*, *Nucl. Phys.*, **B100** (1975), 103.
13. Ghosh D C, Bhattacharjee D K, Daftari I K, Roy Chowdhury A & Roy T, *Phys. Rev.*, **D19** (1979), 391.
14. Daftari I K, Bhattacharjee D K & Roy T, *Czech. J. Phys.*, (1979), in press.

Communications

Relativistic Correction for the NPL (India)-PTB (West Germany) Clock Synchronization Experiments

B S Mathur & G M Saxena

Time & Frequency Section, National Physical Laboratory
Hillside Road, New Delhi 110 012

Received 27 *March* 1980

The Einstein's relativistic correction due to earth's rotation has been derived and its value for the NPL-PTB clock synchronization experiments calculated to be 179·5 nsec. In view of the precision of 10 nsec achieved in the measurements this correction factor is significant and explains a part of the path delay anomaly.

The precision achieved[1] in the recent time transfer experiments between the National Physical Laboratory (NPL), New Delhi, and Physikalisch-Technische Bundesanstalt (PTB), West Germany, was of the order of 10 nsec. This encouraged us to calculate the Einstein's relativistic correction to the clock settings. This correction in case of NPL-PTB measurements is 179·5 nsec, an easily measurable quantity in view of the precision achieved. The details of the derivation and calculation for the correction factor are given below.

Derivation and calculation—The NPL-PTB clock sychronization experiments were performed using the interface facilities at New Delhi Earth station in India and Raistings Earth Station in West Germany and the coordinates referred to in this paper are for these two places, i.e. New Delhi (N) and Raistings (R). The relativistic correction to be applied to the two-way clock synchronization experiment has been calculated as follows.

In a two-way method, assuming that the earth is stationary, the time difference (τ_{NR}) between the clock pulse at N and received pulse from R and vice versa (τ_{RN}) are given by

$$\tau_{NR} = T_N - (D_{NR} + T_R) \doteq \Delta T - D_{NR}$$

$$\tau_{RN} = T_R - (D_{RN} + T_N) = -\Delta T - D_{RN}$$

Here D_{RN} is the total delay, i.e. sum of propagation, transmitter and receiver delays from R to N. From the above two relations we have

$$\frac{1}{2}\left(\tau_{NR} - \tau_{RN}\right) = \Delta T + \frac{1}{2}\left(D_{RN} - D_{NR}\right) \quad ...(1)$$

The actual difference ΔT between the two clocks can be obtained from Eq. (1). If the rotation of the earth is taken into account, the propagation delay, while considering transmission from R to N, will increase, because due to earth's rotation New Delhi will be moving eastward thus taking more time. While for the reverse transmission, the delay will be shortened. If $|\delta|$ is the increase or decrease in time of propagation due to earth's rotation the above formula is modified to

$$\frac{1}{2}\left(\tau_{NR} - \tau_{RN}\right) = \Delta T + \frac{1}{2}\left(D_{RN} - D_{NR}\right) + \delta \quad ...(2)$$

The electromagnetic waves could be identified with light propagation, both having the same velocity in vacuum. To find δ, we treat the problem in Minkowski Space Time coordinates.

Signal propagation in the rotating coordinates—Consider (x, y, z, ct) as the coordinates in the stationary frame of reference and (x', y', z', ct') as those in the rotating frame having angular velocity ω about the z-axis. Assuming that the two z-axes are coincident, the two sets of coordinates are related as

$$\left.\begin{aligned} x &= x' \cos \omega t' - y' \sin \omega t' \\ y &= x' \sin \omega t' + y' \cos \omega t' \\ z &= z' \\ t &= t' \end{aligned}\right\} \quad ...(3)$$

In Minkowski's space, the metric is defined as

$$dS^2 = -c^2 T^2 = dx^2 + dy^2 + dz^2 - c^2 dt^2 \quad ...(4)$$

Transforming dx, dy and dz into dx', dy' and dz' gives

$$dx = \frac{dx}{dx'} dx' + \frac{dx}{dy'} dy' + \frac{dx}{dz'} dz' + \frac{dx}{dt'} dt' \quad ...(5)$$

with similar expressions for dy and dz. On putting the value of dx/dx' etc. in Eq. (4) and using Eq. (3), dx etc. get transformed into dx' etc. The metric dS^2 in rotating coordinates thus becomes

$$dS^2 = -\left[1 - \frac{\omega^2 (x'^2 + y'^2)}{c^2}\right] c^2 dt^2 + 2\omega (x' dy' - y' dx') dt + (dx')^2 + (dy')^2 + (dz)^2 \quad ...(6)$$

For light or electromagnetic wave propagating in vacuum, $dS^2 = 0$

Table 1—Data used in the Calculation of δ

Location	Latitude	Longitude	Spherical coordinates			Cartesian coordinates	
			r km	θ, deg	θ, deg	x, km	y, km
Raisting (R)	48·30°	11·1°	6378	41·6	11·10	4154	815
*Symphonie (S)	−0·15°	48·88°	42151	90·15	48·88	27720	31754
New Delhi (N)	28·57°	77·32°	6378	61·43	77·32	1229·5	5464·8

* Data obtained from Symphonie, France.

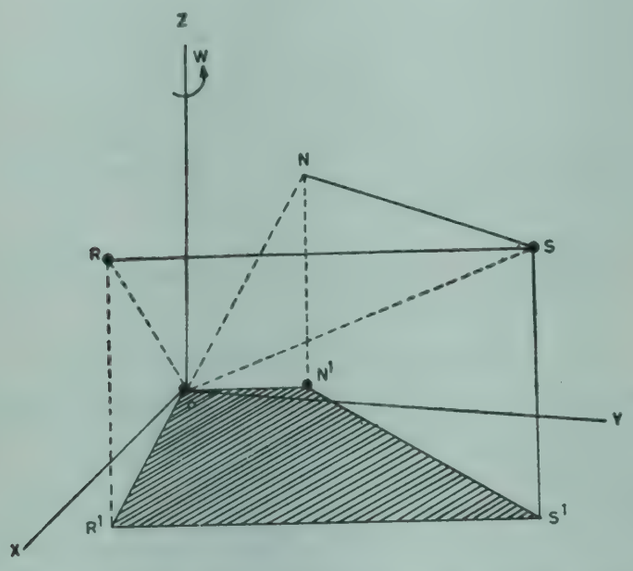

Fig. 1—Coordinates transformation to the rotating frame

therefore, $c^2\ dt^2 = dx^2 + dy^2 + dz^2$, and in the rotating frame

$$-\left[1 - \omega^2 \frac{(x'^2 + y'^2)}{c^2}\right] c^2\ dt^2 + 2\,\omega\,(x'\,dy' - y'\,dx')\,dt + (dx')^2 + (dy')^2 + (dz)^2 = 0 \qquad ...(7)$$

This quadratic equation in dt could be solved assuming

$\omega^2\,(x'^2 + y'^2) \ll c^2$. The solution is

$$dt_1 = \frac{1}{c}\left[\left\{1 - \omega^2 \frac{(x'^2 + y'^2)}{c^2}\right\}\left\{(dx')^2 + (dy')^2 + (dz)^2\right\}\right]^{1/2} + \omega \frac{(x'\,dy' - y'\,dx')}{c^2}$$

$$dt_2 = \frac{1}{c}\left[\left\{1 - \omega^2 \frac{(x'^2 + y'^2)}{c^2}\right\}\left\{(dx')^2 + (dy')^2 + (dz)^2\right\}\right]^{1/2} - \omega \frac{(x'\,dy' - y'\,dx')}{c^2}$$

It is seen that $|\,dt_1\,| = |\,dt_2\,|$, except for the term $\omega \dfrac{(x'\,dy' - y'\,dx')}{c^2}$ which arises due to earth's rotation.

To find the total effect, an integration has to be performed for the finite path according to the direction of the signal propagation.

$$\text{The delay } \delta = \frac{1}{2}\left[\int_{R\to N} dt_1 - \int_{N\to R} dt_2\right]$$

$$= \frac{\omega}{2c^2}\left[\int_{R\to N}(x'\,dy' - y'\,dx') - \int_{N\to R}(x'\,dy' - y'\,dx')\right]$$

Keeping in view the limits of integration the two terms will be added up and the delay is

$$\delta = \frac{\omega}{c^2}\int (x'\,dy' - y'\,dx')$$

$$= \frac{\omega}{c^2}\,(\text{Total loop area projected on the } x' - y' \text{ plane})$$

$$= \frac{2\,\omega\,A}{c^2}$$

Here $A = \dfrac{1}{2}\int (x'\,dy' - y'\,dx')$

= Area OR′ S′ N′ as shown in Fig. 1.

Knowing the coordinates of R′, S′, N′; the projections on the earth's surface of R, S, N; the area can be calculated as follows.

If (x'_R, y'_R), (x'_S, y'_S) and (x'_N, y'_N) are the coordinates of R, the satellite and N respectively as transformed to the rotating frame with the centre of earth as origin of the coordinate system, the area A from Fig. 1 is

$$A = \text{Area of } \Delta\,OR'\,S' + \text{Area of } \Delta\,S'\,N'\,O$$

$$= \frac{1}{2}\left[(x'_R\,y'_S - x'_S\,y'_R) + (x'_S\,y'_N - x'_N\,y'_S)\right]$$

$$\text{or } 2A = \left[y'_S\,(x'_R - x'_N) - x'_S\,(y'_R - y'_N)\right]$$

Putting this value of A in Eq. (8), δ arising due to the earth's rotation is obtained.

Calculation of δ for the experiment conducted between Raistings (West Germany) and New Delhi (India) can be made using the above derivation. The necessary data used are compiled in Table 1.

For the rotating earth, $\omega/c^2 = 8{\cdot}091 \times 10^{-16}$ sec/km^2

On putting the values of x_R, x_N, etc. the delay δ is :

$$\delta = 8{\cdot}091 \times 10^{-16}\Big[(4154 - 1229.5)$$

$$31754 - (815 - 5464{\cdot}8)\, 27720 \Big]$$

$$= (92864573 + 128950668)\, 8{\cdot}091 \times 10^{-16}$$

$$= 221815241 \times 8{\cdot}091 \times 10^{-16}$$

$$= 179{\cdot}5 \text{ nsec.}$$

The relativistic correction factor calculated for the NPL (India)-PTB (West Germany) clock synchronization experiment explains to a great extent the anomaly in the total path delay time. The other anomalous factors being the transmitter and receiver delays along with the ionospheric delay arising due to different electron densities along the path of the signal. The relativistic correction factor calculated in this communication could be generalized and made use of in the projected time transfer experiments with Indian satellites APPLE and INSAT.

References

1. Becker G, Fisher B, Mathur B S & Xiao Cuiging, *Time and frequency comparisons by means of Symphonie*, presented at the seminar on Symphonie at Berlin, February 1980.
2. Soburi Y, *JRRL*, **23** (Nov) (1976), 255.

Calculation of Spectroscopic Characteristics of Some Acetophenones Using Pariser-Parr-Pople SCF-CI Approximation

V P Gupta

Department of Physics, University of Jammu
Jammu Tawi 180 001

Received 11 *February* 1980

Pariser-Parr-Pople SCF-CI calculations on acetophenone derivatives have been used to explain the position and intensity of electronic transitions. Calculated π-electron densities and bond-order values have been used quite successfully to discuss the proton NMR chemical shifts and carbonyl stretching frequencies in the infrared region.

In earlier communications,[1-3] we have reported studies concerning the spectroscopic and physicochemical properties of acetophenone and its hydroxy, methyl and methoxy derivatives. A detailed experimental analysis of the infrared spectra of substituted acetophenones was conducted and characteristic frequencies of the various functional groups established.[1] Electronic spectra and physical and chemical parameters of acetophenone and some of its hydroxy derivatives vere calculated in the molecules-in-molecules and Pariser-Parr-Pople approximations.[2,3]

In this communication, we make use of our calculated π-electron densities, bond orders, transition energies and oscillator strengths to discuss the available proton NMR chemical shifts, electronic spectra and shifts in carbonyl stretching frequencies in hydroxy acetophenones (Fig. 1).

The method of calculation and procedures for obtaining various integrals needed for the calculations in Pariser-Parr-Pople SCF-CI approximation are similar to those described earlier in our theoretical works.[2,3]

It has been recognized[4-6] that in aromatic systems with π-electronic net charges, the electrostatic polarization of the CH— bond density is the main cause for the proton chemical shifts. The chemical shift on this account should be added to the ring current contribution to obtain the true chemical shift. Assuming the ring current contribution to remain constant for a series of acetophenones one would expect a linear relationship between the proton chemical shift (δ_H) and the π-electron density (q_π). A least squares fit analysis is carried out and a least square fit of the form given by Eq. (1) is obtained for all acetophenones presently studied.

$$\delta_H = 12{\cdot}8\,(q_\pi - 1) - 7{\cdot}32 \qquad \ldots(1)$$

Calculated electron densities and predicted proton chemical shifts are given in Table I along with available experimental data.[7-10] It may be observed that the two are in good agreement.

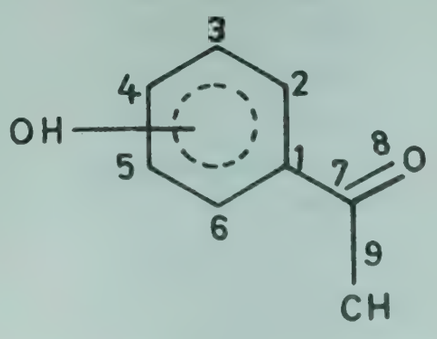

Fig. 1—General structure of hydroxy actophenones

A relationship similar to Eq. (1) was obtained by Ahuja[11] for chromones with proportionality constant of 13·95 ppm/electron. It is, however, found that Eq. (1), which is true for acetophenones, is applicable even to chromones with almost equal accuracy.

In our earlier communication,[3] we had calculated transition energies and oscillator strengths of some monosubstituted acetophenones. It is observed that the same set of parameters can explain the spectra of di- and tri-hydroxy-substituted acetophenones. Experimentally observed[12-15] and calculated values of electronic transition energies and oscillator strengths of 2,4-dihydroxy and 2,4,6-trihydroxy acetophenones are reported in Table 2. It may be seen that they are in good agreement with each other.

It was shown by Coulson and Longuet-Higgins[16] and Berthier *et al.*[17] that a correlation exists between the bond order (P_{C-O}) of the carbonyl group and its stretching vibrational frequency (ν_{C-O}) in the infrared region. In the case of acetophenone derivatives presently studied, it is observed that a linear relationship exists between the two. A least squares fit analysis gives a relation of the form

$$\nu_{C-O}\ (cm^{-1}) = 4000\ P_{C-O} - 1739 \qquad ...(2)$$

The carbonyl stretching frequencies obtained using Eq. (2) are given in Table 3 along with the available experimental data.[1] It may be observed that the two are in good agreement.

From the present study, it appears that the results of molecular orbital calculations in the PPP approximation can be successfully used not only in predicting the electronic spectra of acetophenone and its hydroxy derivatives but also the proton NMR chemical shifts and the carbonyl stretching frequencies in the infrared region.

Table 1—PPP π-Electron Densities (σ_π) and Proton NMR Chemical Shifts (δ_H) in Some Acetophenones

Position	(σ_π^{-1})	δ_H	
		Calc.[a]	Obs.[b]
	Acetophenone		
2	−0·0135	7·486	7·86
3	+0·001	7·308	7·37
4	−0·019	7·563	7·45
5	−0·003	7·350	7·37
6	−0·041	7·844	7·86
	2-OH-acetophenone		
3	+0·032	6·91	6·75
4	−0·023	7·614	7·11
5	+0·013	7·154	7·27
6	−0·045	7·896	7·52
	4-OH-acetophenone		
2	−0·017	7·537	8·05
3	+0·032	6·911	6·90
5	+0·028	6·962	6·90
6	−0·045	7·896	8·05
	2,4-di-OH-acetophenone		
3	+0·063	6·514	6·35
5	+0·043	6·77	6·50
6	−0·048	7·934	7·76
	2,4, 6-tri-OH-acetophenone		
3	+0·079	6·309	6·20
5	+0·076	6·348	6·20

[a] Obtained using Eq. (1)

[b] Obtained from Ref. 7-10

Table 2—Electronic Transitions in Hydroxy-Acetophenones

Position of substituent	Energy, eV		Oscillator strength	
	Exptl.	PPP	Exptl.	PPP
2,4	3·948	4·206	(3·840)	0·032
	4·475	4·788	(4·140)	0·435
	—	5·690	—	0·531
	—	5·950	—	0·484
2,4,6	3·72	4·065	(3·399)	0·037
	4·260	4·610	(4·250)	0·334
	5·559	5·472	(4·100)	0·346
	—	5·750	—	0·576

Values in parentheses are log ϵ

Table 3—Calculated Carbonyl Bond Orders and IR Carbonyl Stretching Frequencies of Acetophenone and Its Hydroxy Derivatives

Position of the substituent	P_{C-O}	ν_{C-O}, cm^{-1}	
		Calc.[a]	Obs.[b]
—	0·8534	1674	1680
2-	0·8507	1663	1650
3-	0·8533	1674	1670
4-	0·8507	1663	1655
2,4-	0·8379	1613	1622
2,4,6-	0·8395	1619	1620-1625

[a] Obtained using Eq. (2)

[b] Obtained from Ref. 1

References

1. Gupta V P, Gupta D & Jain S M, *Indian J. pure appl. Phys.*, 14 (1976), 846.

2. Gupta D & Gupta V P, *Indian J. pure appl. Phys.*, **16** (1978), 968.
3. Gupta V P, *Indian J. pure appl. Phys.*, **18** (1980), in press.
4. Fraenkel G K, Carter R E, McLachlan A D & Richards J M, *J. Am. chem. Soc.*, **82** (1960), 5846.
5. Maclean C, Mackor E L, *Molec. phys.*, **4** (1961), 241.
6. Spiesecke H, Schneider W G, *Tetrahedron Lett.*, **14** (1961), 468.
7. Szymanski H A & Yelin R E, *NMR band handbook*, (Plenum Press, New York), 1968.
8. Dyer J R, *Applications of absorption spectroscopy of organic compounds*, (Prentice-Hall, New Delhi), 1978.
9. Harborne J B & Mabry T J, *The flavanoids*, (Pergamon Press, New York), 1975.
10. *High resolution NMR spectra*, (Sadtler Research Laboratories Inc., Philadelphia), 1967.
11. Ahuja V K, *Indian J. Chem.*, **16A** (1978), 531.
12. Scott A I, *International series of monograph on organic chemistry*, (Pergamon Press, London), 1964.
13. Morton R A & Stubbs A L, *J. chem. Soc.*, (1940), 1092.
14. Kamlet M J, *Organic electronic spectral data*, Vol I (Interscience, New York), 1960.
15. Morton R A & Stubbs A L, *J. chem. Soc.*, (1940), 1347.
16. Coulson C A & Longuet-Higgins H C, *Proc. R. Soc.*, **A193** (1948), 456.
17. Berthier G, Pullman B & Pontis J, *Bull. Soc. Chem. Fr.*, **18** (1952), 271.

Notes

One-Spin Cross-Relaxation in Dilute Nickel Fluosilicate

A K Sikri & M L Narchal

Physics Department, Punjabi University, Patiala

Received 18 *January* 1979; *revised received* 9 *January* 1980

Grant's theory of a single-spin cross-relaxation has been extended so as to include the effect of lattice temperature and crystal field. It is applied to compute the one-spin cross-relaxation time for the transition (1→0) observed in nickel fluosilicate at 2K. The result is found to be in fair agreement with experiment.

In a series of five papers,[1,2] Grant has developed the statistical theory of cross-relaxation (CR) in the high temperature approximation. The theory has been applied by Grant himself to explain the two-spin CR experiment of Mims and McGee[3] in ruby and three-spin CR experiment of Pershan[4] in LiF. Other workers[5-7] have attempted to apply Grant's theory to explain two- and three-spin CR experiments in various other samples. In the first of his papers where Grant builds up the conceptual and mathematical framework of his theory, he calculates the probability of a CR process involving a single spin flip. Such a phenomenon of CR, in which a single spin flips, has been observed in many samples.[8-10] We shall confine our attention to the CR experiment performed by Van Duynevedt *et al.*[8] at $H = 1315$ Oe, and $T = 2$K in nickel fluosilicate diluted with isomorphous zinc fluosilicate because theoretically it is the simplest to deal with. To the best of the author's knowledge, Grant's theory has not so far been applied to understand the results of the above experiment. Since the temperature at which the experiment has been done is low enough (2K), we first make suitable modifications in Grant's original theory[1] to dispense with the high-temperature approximation and then apply the final formula to the experiment under consideration.

The Structure of nickel fluosilicate crystal is rhombohedral and the unit cell contains only one paramagnetic ion. The six water molecules arranged in an octahedron with Ni^{2+} ion at the centre cause a crystalline field of nearly cubic symmetry with a trigonal distortion parallel to the C axis of the crystal. In the experiment under consideration the external magnetic field has been applied parallel to the C axis. All ions are equivalent and have a spin $s=1$ and $g = 2{\cdot}25$. The magnetic properties of each such ion are described by the spin Hamiltonian.[11]

$$\mathcal{H} = g\beta HS_z + DS_z^2 \qquad \ldots(1)$$

We adopt the following theoretical model for the computation of the one-spin CR time. Consider a set of N identical particles with the above description occupying a spherical volume V in dipolar interaction with one another and in thermal interaction with a bath of infinite heat capacity at a temperature T. Each spin experiences the dipolar perturbation produced by all other spins in the sample and exchanges energy with all the other spins in the sample and also with heat bath.

We focus our attention on a particular spin say 1 fixed at the centre of the spherical volume assumed to be the origin. The static part of the dipolar interaction at the spin 1 produced by all the other spins labelled 2, 3...N having position vectors $\mathbf{r}_2$, $\mathbf{r}_3 \ldots \mathbf{r}_N$ relative to spin 1 and instantaneous magnetic quantum numbers m_2, $m_3 \ldots m_N$ respectively is given by

$$\mathcal{H}_{st} = \sum_{i=2}^{N} \frac{g^2\beta^2 (1-3\cos^2\theta_i)}{r_i^3} I_{iz} I_z \qquad \ldots(2)$$

where θ_i is the zenith angle of the radius vector $\mathbf{r}_i$, I_{iz} and I_z are the zth components of the spin vector $\mathbf{I}_i$ and $\mathbf{I}_1$ respectively.

The sets of position vectors $\mathbf{r}_2 \ldots \mathbf{r}_N$ and $m_2 \ldots m_N$ define an instantaneous configuration of the total system. The spin state of the total system at any given time may be represented by $| m\, m_2\, m_3 \ldots m_N >$ where m is the magnetic quantum number of spin 1, $m_2 \ldots m_N$ fluctuate due to spin-spin and spin-lattice interactions. However, statistically speaking the average spin populations are maintained constant and consistent with the appropriate Boltzmann factors at temperature T of the heat bath with which the spin system is considered to be in thermal equilibrium. The probability per unit time that the spin 1 makes a transition from $| m >$ to $| m-1 >$ is

$$W = \frac{2\pi}{\hbar} \left| \left\langle (m-1)\, m_2 \ldots m_N \right| \mathcal{H}_{dip} \left| m\, m_2 \ldots m_N \right\rangle \right|^2 \delta(\Delta E) \qquad \ldots(3)$$

where ΔE is the energy difference between initial and final states including the dipolar contribution. The energies corresponding to the three spin states at the experimental value of the static field $H =$ 1315 Oe are $E(1) = 0{\cdot}16 \times 10^{-17}$ ergs, $E(0) = 0$, $E(-1) = -5{\cdot}328 \times 10^{-17}$ ergs. It is evident that the energy imbalance $E(1) - E(0)$ is small enough so that it can be compensatad by the dipolar interaction. Other energy imbalances are too large to be compensated. We therefore presume that the experiment observes the relaxation time for the transition $1 \leftrightarrow 0$. The dipolar interaction $\mathscr{H}_{dip}$ which connects the final state $|1>$ with the initial state $|0>$ is given by

$$\mathscr{H}_{dip} = -\sum_{i=2}^{N} \frac{3g^2\beta^2 \sin\theta_i \cos\theta_i}{2r_i^3} \exp(i\phi_i)\, I_{iz}\, I^{+} \qquad \ldots(4)$$

The matrix element of transition is

$$M = -\sum_{i=2}^{N} \frac{3\, g^2\beta^2 \sin\theta_i \cos\theta_i\, m_i}{\sqrt{2}\, r_i^3} \exp(i\phi_i)$$

and the energy ΔE is

$$\Delta E = E_{r_1 r_2 \cdots r_N, 1, m_2 \ldots m_N} - E_{r_1 r_2 \cdots r_N, 0, m_2 \ldots m_N}$$

$$\Delta E = g\beta H + D + \sum_{i=2}^{N} \frac{g^2\beta^2 (1 - 3\cos^2\theta_i)\, m_i}{r_i^3} \qquad \ldots(5)$$

Since the configurations of the system change with time due to fluctuations in $m_2 \ldots m_N$ the transition probability given by Eq. (3) is a function of time. We are primarily interested in a long time average of this transition probability. From the ensemble theory of statistical mechanics the long time average is identical with appropriately weighted average over a canonical ensemble. The statistical weight of a particular configuration in the ensemble is given by $\exp(-E/kT)$ where E is the total energy of the whole system in a given configuration. Thus the expectation value of transition probability given by Eq. (3) is

$$\langle W \rangle = \frac{\iint \cdots \int W \exp(-E/kT) \prod_{i=2}^{N} dr_i dm_i}{\iint \cdots \int \exp(-E/kT \prod_{i=2}^{N} dr_i dm_i} \qquad \ldots(6)$$

we may approximate the weight function as

$$\exp\left[-\sum_{j=2}^{N} \frac{(g\beta H m_j + D m_j^2)}{kT}\right] \prod_{j=2}^{N} \sum_{t=-1}^{1} \delta(m_j - t) \qquad \ldots(7)$$

Substituting this weight function in Eq. (6), and using the fact that all cross terms when integrated give zero and replacing the δ function by its Fourier integral representation, we obtain

$$\langle W \rangle = \sum_{j} \frac{9\, g^4\beta^4}{2\hbar^2 v f}\left[\exp\left(-\frac{\alpha}{kT}\right)\iint \frac{C_i dr_i}{r_j^6} \exp\left[-i\rho\left(\omega + \frac{g^2\beta^2 b_i}{\hbar r_i^3}\right)\right] \times \phi(\rho)\, d\rho + \exp\left(-\frac{\gamma}{kT}\right)\iint \frac{C_i dr_i}{r_i^6} \exp\left[-i\rho\left(\omega - \frac{g^2\beta^2 b_i}{\hbar r_i^3}\right)\right] \times \phi(\rho)\, d\rho \qquad \ldots(8)$$

where

$$\alpha = g\beta H + D$$

$$\gamma = D - g\beta H$$

$$b_i = (1 - 3\cos^2\theta_i)$$

$$C_i = \sin^2\theta_i \cos^2\theta_i$$

$$f = \exp\left(-\frac{\alpha}{kT}\right) + 1 + \exp\left(-\frac{\gamma}{kT}\right) \qquad \ldots(9)$$

$$\phi(\rho)\left[\frac{1}{vf}\int \exp\left(-\frac{i\rho g^2\beta^2 b m_s}{hr^3}\right) \exp\left\{-\frac{(g\beta H m_s + D m_s^2)}{kT}\right\} \times \sum_{q=-1}^{1} \delta(m_s - q)\, dr\, dm_s\right]^{N-2} \qquad \ldots(10)$$

Integrating over ρ and assuming $\Phi(\omega)$, which is the Fourier transform of $\phi(\rho)$ as Lorentzian for the dilute sample, we obtain

$$\langle W \rangle = \frac{9g^4\beta^4 a}{\hbar^2 f}\left[\exp\left(-\frac{\alpha}{kT}\right)\int \frac{C_i dr_i}{r_i^6\left\{\left(\omega + \frac{g^2\beta^2 b_i}{\hbar r_i^3}\right)^2 + a^2\right\}} + \exp\left(-\frac{\gamma}{kT}\right)\left[\frac{C_i dr_i}{r_i^6\left\{\left(\frac{\omega - g^2\beta^2 b_i}{\hbar r_i^3}\right)^2 + a^2\right\}}\right]\right] \qquad \ldots(11)$$

where n is the concentration of nickel ions per unit volume and a is half-width of Lorentzian line. Integration over r_i by making the substitution $\frac{1}{r_i^3} = t$ and substitution of the experimental condition $\omega = 0$ in the above expression [Eq. (11)] leads to

$$\left\langle W \right\rangle = \frac{6\pi n g^2\beta^2 \{\exp(-\alpha/kT) + \exp(-\gamma/kT)\}}{\hbar f}$$

$$\int_0^{\pi} \frac{C_i \sin\theta_i}{b_i} \times d\theta_i \tan^{-1}\left(\frac{g^2\beta^2 b_i}{\hbar a r_0^3}\right) \qquad ...(12)$$

where r_0 is the nearest neighbour distance. The experimentally observed one-spin CR transition probability W_{cr} is obtained by multiplying Eq. (12) with the average of Boltzmann probabilities for the initial and final states of particle 1. Thus

$$W_{cr} = 3\pi n g^2\beta^2 \{\exp(-\alpha/kT) + \exp(-\gamma/kT)\}\{1 + \exp(-\alpha/kT)\}/\hbar f^2$$

$$\times \int_0^{\pi} \frac{C_i \sin\theta_i \, d\theta_i}{b_i} \tan^{-1}\left\{\frac{g^2\beta^2 b_i}{\hbar a r_0^3}\right\} \qquad ...(13)$$

The integral over θ_i in Eq. (13) has been evaluated numerically [using $a = 6$ Oe. and $r_0 = 6{\cdot}27$ Å] obtaining a value 1·08.

The theoretically calculated one-spin CR time τ from Eq. (13), using $n^* = 2{\cdot}3 \times 10^{20}$ cm^{-3}, $D = -0{\cdot}13$ cm^{-1}, $H = 1315$ Oe. and $T = 2$K, is $0{\cdot}25 \times 10^{-8}$ sec. This is in reasonable agreement with experimentally measured value of $\tau^* \cong 2 \times 10^{-8}$ sec. (*These values of n and τ have been obtained in a private communication with Van Duyneveldt.). We therefore conclude that the temperature-dependent statistical theory of one-spin CR, as developed in this note, explains the experimental results of Van Duyneveldt.

References

1. Grant W J C, *Phys. Rev.*, **134A** (1964), 1554, 1565, 1574; **135A** (1964), 1265.
2. Grant W J C, *J. Phys. Chem. Solids*, 25 (1964), 751.
3. Mims W B & McGee J D, *Phys. Rev.*, 119 (1960), 1233.
4. Pershan P S, *Phys. Rev.*, 117 (1960), 109.
5. Squire P T, *Proc. phys. Soc.*, 86 (1965), 573.
6. Weissfloch C F, *Can. J. Phys.*, 45 (1967), 93.
7. Minkowski J M, *Phys. Rev.*, 168 (1968), 348.
8. Van Duyneveldt A J, Tromp H R C & Gorter C J, *Physica*, 38 (1968), 205.
9. Van Duyneveldt A J & Soeteman J, *Physica*, 45 (1969), 227.
10. Vantol M W, Eijkelhof H M C & Van Duyneveldt A J, *Physica*, 60 (1972), 223.
11. Penrose R P & Stevens K W H, *Proc. phys. Soc.*, 63 (1950), 29.

Mechanoluminescence Spectra of Sodium Bromate & Sodium Chlorate Crystals

B P Chandra* & R D Verma

Department of Physics, Government College of Science
Raipur 492 002

Received 5 *June* 1979

The mechanoluminescence spectra of sodium bromate and sodium chlorate crystals correspond to the second positive group ($^3\Pi_u \rightarrow {}^3\Pi_g$) of molecular nitrogen. The ML activity of sodium chlorate crystals is nearly two orders less as compared to that of sodium bromate crystals. It is concluded that either the piezoelectrification or the electrification due to the separation of the crystal regions of microscopically disturbed electrical equilibrium is responsible for the mechanoluminescence excitation in sodium bromate and sodium chlorate crystals.

The luminescence produced during mechanical action on solids, is known as mechanoluminescence or triboluminescence. Due to the weak intensity and short duration of mechanoluminescence (ML), it has been studied spectroscopically in a limited number of substances.[1] Sodium bromate crystals have been reported to be mechanoluminescent[2] and we have also found a weak ML also in sodium chlorate crystals. The interest in ML of sodium bromate and sodium chlorate crystals is primarily because of their simple structure among the piezoelectric mechanoluminescent crystals. The present communication reports on the ML spectra of sodium bromate and sodium chlorate crystals and discusses the possible origin of ML.

Single crystals of sodium bromate and sodium chlorate were grown from the aqueous solution of the reagent grade materials. For the determination of the ML spectra, the crystals were fractured in a glass vial with a stainless steel rod. The spectra of the light emitted as a result of the application of the mechanical stress were determined with the help of EMI 9558 RF photomultiplier tubes and a Bausch and Lomb 1-m excitation monochromator by following the method described by Hardy and Zink.[3] The ML activity per gram mole of the crystals was determined from the total intensity of ML for a given mass of a crystal. For the measurement of the total intensity of ML, the crystals were fractured impulsively by dropping a load of 800 g from a height of 4 cm. The total intensity of ML was monitored by an IP21 photomultiplier tube connected to a ballistic galvanometer.

* Present address : Department of Chemistry, University of California, Los Angeles, California 90024, USA

Fig. 1 shows the ML spectra of sodium bromate crystals. It is seen that the ML spectra correspond to the second positive group ($^3\Pi_u \rightarrow {}^3\Pi_g$) of molecular nitrogen. The ML spectra of sodium chlorate crystals are also similar to that of sodium bromate crystals. The ML activity per gram mole of sodium bromate crystals is found to be nearly $(2{\cdot}2 \pm 0{\cdot}3) \times 10^2$ times higher than that of sodium chlorate crystals.

The appearance of ML only during crystal fracture and its origin from excited molecules of nitrogen suggest that the mechanism of excitation may involve creation of charged surfaces during fracture followed by excitation of nitrogen molecules by electrons accelerated between the surfaces.[5] There are several possible mechanisms of charging the newly created surfaces, such as the motion of charged dislocations, frictional electrification caused by rubbing two dissimilar materials together, internal electrification at cleavage or shear planes in the crystals, piezoelectrification caused by the deformation of non-centrosymmetric crystals and the electrification due to the separation of the crystal regions of microscopically disturbed electrical equilibrium.

The ML intensity increases with decreasing temperature; however, as the motion of dislocations is blocked at low temperature, the ML excitation due to the motion of the charged dislocations can be ruled out. Because the ML intensity does not depend on the materials used for crushing the crystals, the ML excitation due to the frictional electrification between the crushing materials and the crystal can also be eliminated. First, the ML intensity of sodium bromate and sodium chlorate crystals does not vary considerably with the direction of cleavage, and secondly, in spite of the same type of bonding and structure of sodium bromate and sodium chlorate crystals, the ML activity differs by two orders of magnitude. Hence there seems no ground for accepting the ML excitation due to the internal electrification at cleavage shear planes of the crystal. Thus, we conclude that either the piezoelectrification or the electrification due to the separation of the crystal regions of microscopically disturbed electrical equilibrium as a result of the chemical defects, is responsible for the ML excitation. We have studied ML in 18 crystals of bromate, chlorate and iodate, and have found ML even in centrosymmetric crystals. Hence the piezoelectrification cannot be the only reason for the ML excitation. The ideas on the ML excitation in bromate, chlorate and iodate crystals will be explored fully in the future work.

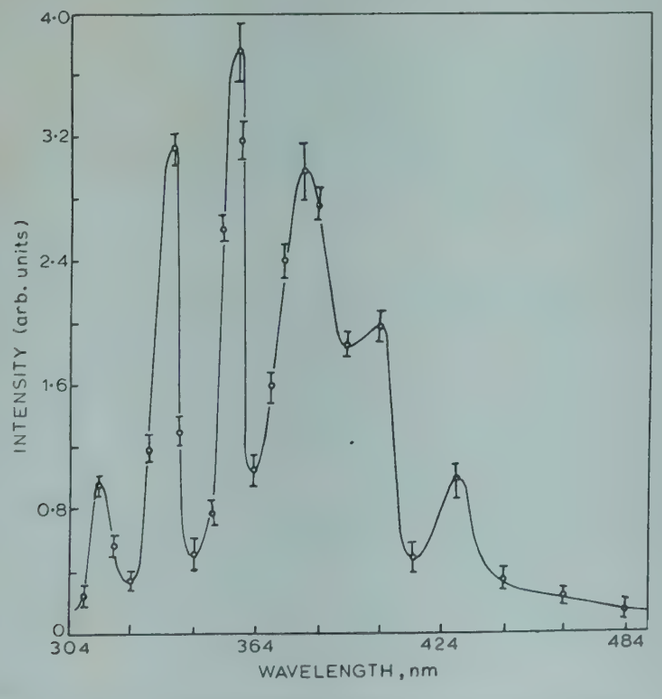

Fig. 1—Mechanoluminescence spectra of sodium bromate crystals

The authors wish to thank the Vice-Chancellor, Ravishankar University, Raipur for the financial assistance. The authors also wish to thank Prof. Jeffrey I Zink of the University of California, Los Angeles, California, USA, for providing the facilities for ML spectra.

References

1. Zink J I, *Accounts Chem. Res.*, 11 (1978), 289.
2. Wolff G, Gross G & Stranski I, *Z. Electrochem.*, 56 (1952), 420.
3. Hardy G E & Zink J I, *Inorg. Chem.*, 15 (1976), 3061.
4. Herzberg G, *Molecular spectra and molecular structure.* 1-Spectra of diatomic molecules (Van Nostrand, New York), (1950), 324.
5. Chandra B P, *Czech J. Phys.*, B28 (1978), 84.

Effect of Acid Concentration & Temperature on the Selective Etch Rate & Etch Pit Morphology of {111} Faces of CaF_2 Crystals

A R Patel & M D Kotak*

Department of Physics, Sardar Patel University
Vallabh Vidyanagar, Gujarat 388 120

Received 30 *May* 1979

The effect of the concentration and temperature of HCl on the etch pit morphology and selective etch rate in CaF_2 crystals has been investigated and the values of activation parameters computed. Correlation between the etch pit morphology and activation energy of dissolution is established.

The effects of the concentration of an acid on etch pit morphology[1,2] and of the temperature of the

*Present address : Department of Physics, Banaskantha Arts and Science College, Pabanpur 385 001

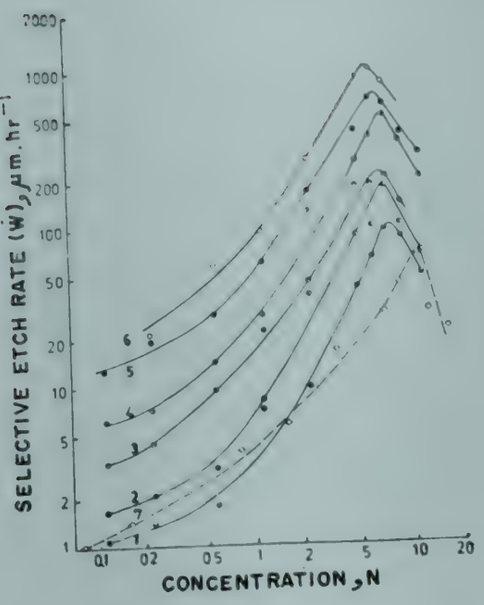

Fig. 1—Dependence of etch rate w on acid concentration c of HCl (curves 1-6) and HNO_3 (curve 7) at different temperatures [curves : 1 and 7, 29°C; 2, 35°C; 3, 40°C; 4, 50°C; 5, 60°C and 6, 72°C]

etchant on selective etch rate[2] [2] have been reported in CaF_2 crystals. Such an investigation is useful not only in estimating the values of activation parameters, but also in establishing a correlation between the etch pit morphology and the value of activation energy of dissolution. Since the activation energy is influenced by the adsorption processes taking place at the dissolution steps and the nature of reactants and the reaction products, the study may also shed light on the processes responsible for the change in the morphology of dislocation etch pits. In this note, the results of an investigation dealing with the influence of concentration and temperature of HCl on the selective etch rate and etch pit morphology, are reported.

Freshly cleaved {111} faces of natural CaF_2 single crystals were etched at different temperatures, in about 25 ml HCl of different concentrations in 50 ml beakers. After etching for appropriate durations, the samples were rinsed in distilled water, dried and examined under an optical microscope. The distance between the corner of a triangular etch pit and its opposite side and the distance between the opposite sides of hexagonal pits, were measured with the help of a filar eye-piece fitted to an optical microscope, and from these dimensions the lateral etch rate, w, was computed.

The concentration dependence of etch rates at different temperatures is shown in Fig. 1. It may be noted from the figure that the lateral etch rate, w at dislocations increases with an increase in the acid concentration and attains a maximum value, w_{pk}, at a particular concentration, c_{pk}, and thereafter decreases with a further increase in the concentration. The values of w_{pk} and c_{pk} depend on the nature and temperature of the acid. For HCl and HNO_3, at 29°C, the value of c_{pk} is 7·5 N and 10·5 N, respectively. It is seen that the value of c_{pk} slowly decreases with an increase in the temperature of etching. It is also found that the etch pit morphology varies with an increase in the acid concentration. The morphology at low acid concentrations is triangular and becomes hexagonal in HCl and rounded in HNO_3 around and beyond c_{pk}. The photographs of the change in the morphology of etch pits in HCl are presented in Fig. 2. The dependence of etch rate, w, on temperature (29-72°C) of HCl is shown in Fig. 3, in the form of Arrhenius plots. It may be noted that despite a scatter in the experimental points, the trend of the graphs indicates that the value of activation energy changes with concentration. The scatter is quite large in the case of weak solutions at high temperature.

The calculated values of activation energy, (E_t), and pre-exponential factor (A_t) of dissolution for different HCl concentrations are given in Table 1.

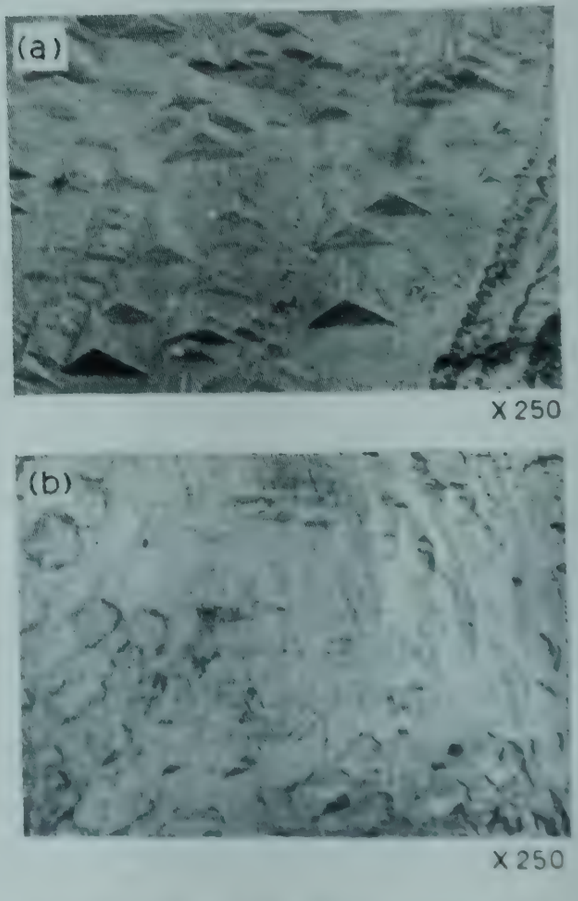

Fig. 2—Morphology of etch pits in 5·65 N (a) and 11·3N (b) HCl at 29 C. [Etching time, 30 min; (× 250)]

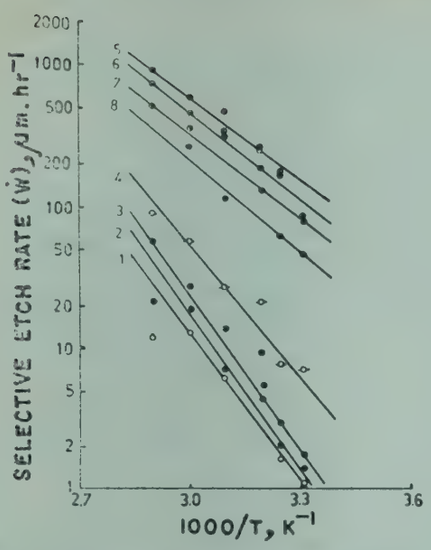

Fig. 3—Arrhenius-type plots of the dependence of etch rate $\dot{w}$ on T conc. of HCl (in N): Curve (1) 0·11, (2) 0·23, (3) 0·57, (4) 1·13, (5) 5·65, (6) 6·78, (7) 8·48 and (8) 11·3

Table 1—Activation energy and Pre-exponential Factor for Lateral Etching in HCl

Acid normality N	E_t (eV)	A_t (μm/hr)
0·11	0·70	$4·9 \times 10^{11}$
0·23	0·70	$6·0 \times 10^{11}$
0·57	0·72	$2·2 \times 10^{12}$
1·13	0·63	$2·3 \times 10^{11}$
5·65	0·38	$3·5 \times 10^{8}$
6·78	0·42	$1·0 \times 10^{9}$
8·48	0·41	$1·0 \times 10^{8}$
11·30	0·46	$2·3 \times 10^{10}$

It was reported[2] that the values of activation energy of dissolution for 4·52 and 9·04 N HCl are 0·90 and 0·58 eV, respectively. The morphology of etch pits in these solutions was found to be triangular and hexagonal, respectively. Except for a difference that the values of E_t are less in the present study, the present and the previously reported results show a positive correlation between the etch pit morphology and the value of E_t.

If it is assumed that the dissolution of CaF_2 involves chemical reactions, the change in the values of E_t and the morphology of etch pits may be understood considering the adsorption of the complexes and reaction products. The dependence of c_{pk} on T also indicates the adsorption of the complexes and reaction products on the crystal surface.[5] The different values of c_{pk} for HCl and HNO_3 at the same temperature are also not unexpected because the two acids should form two different activated complexes.

References

1. Patel A R & Desai C C, *Z. Krist.*, **121** (1965), 55.
2. Sangwal K, *Kristallografiya*, **20** (1975), 116.
3. Sangwal K & Arora S K, *J. Mater. Sci.*, **13** (1978), 1977.
4. Sangwal K, Desai C C & John V, *Kristall und Technik*, **14** (1979), 63.
5. Sangwal K, *J. mater. Sci.*, **15** (1980), 522.

Analysis of the Diamagnetic Anisotropy of Thermo- & Magneto-Electret States

M L Maji, M Saha* & S D Chatterjee

Department of Physics, Jadavpur University
Calcutta 700 032

Received 16 *March* 1979; *revised received* 17 *December* 1979

Experimental results show that the magnetic anisotropy of the assemblage of molecules oriented in the liquid or semi-liquid state cannot be attributed to individual molecules but rather to groups of molecules forming cybotactic state, liquid crystals or cluster of molecules.

It is known that free molecules in gaseous or a liquid medium possessing magnetic anisotropy tend to align themselves along the uniform magnetic field against zig-zag thermal agitation, keeping minimum energy and maintaining minimum daimagnetic susceptibility along the direction of the magnetic field. Such rotation of molecules in the liquid state was actually observed during the study of magnetic birefringence of liquids.[1-2] The free molecules possessing electric dipole moment would also try to align themselves in the direction of the electric field against random thermal agitation in a gaseous or liquid state as formulated by Debye.[3] If, however, any liquid or semi-liquid medium having its molecules oriented by the electric or magnetic field could be frozen gradually by slowly reducing the temperature, the orientation effect would continue to remain frozen in the solid state and the solid would exhibit diamagnetic anisotropy as was first shown by Chatterjee *et al.*[4,5] It would indeed be interesting to calculate theoretically the magnetic anisotropy of a thermo-or magneto-electret.

Theory—Let us consider the simple case of a type of molecule whose three principal volume susceptibilities are represented by k_1, k_2 and k_3 respectively and which are mutually perpendicular to each other. In this particular case, k_2 and k_3 may be considered equal to each other. The components of magnetic susceptibilities of a molecule making angles θ and ϕ with the corresponding electret-forming electric or magnetic field (Fig. 1) are given by

$$k_{\parallel} = k_1 \cos^2 \theta + k_2 \sin^2 \theta \quad \ldots(1)$$

*Present address : Barasat Government College, Barasat

and $k_\perp = k_1 \sin^2\theta \sin^2\phi + k_2 \cos^2\theta \sin^2\phi + k_3 \cos^2\phi$ ...(2)

where $k_{\parallel}$ and $k_\perp$ are parallel and perpendicular components of magnetic susceptibility respectively with regard to the forming field.

The potential energy U of the molecules in the magnetic field H is given by

$$U = -\tfrac{1}{2} v H^2 (k_1 \cos^2\theta + k_2 \sin^2\theta) \quad ...(3)$$

$$= -\tfrac{1}{2} v H^2 (\Delta k \cos^2\theta + k_2) \quad ...(4)$$

where $\Delta k = k_1 - k_2$ and v = volume of the molecule. If P is the dipole moment of the molecule, the potential energy of the molecule, in the electric field E is

$$U = -P E \cos\theta \quad ...(5)$$

The anisotropy between $\parallel$ and $\perp$ components is given by

$$\Delta K = (k_1 \cos^2\theta + k_2 \sin^2\theta) - (k_1 \sin^2\theta \sin^2\phi + k_2 \cos^2\theta \sin^2\phi + k_3 \cos^2\phi) \quad ...(6)$$

According to statistical mechanics, the probability for the molecule to stay within angles θ to $\theta + d\theta$ and ψ to $\psi + d\psi$ with regard to the field is proportional to

$$\sin\theta \, d\theta \, d\phi \exp(-U/k_B T) \quad ...(7)$$

where k_B is the Boltzmann's, constant and T the absolute temperature. Hence the average value of the anisotropy is

$$\langle \Delta K \rangle = \frac{\int_0^{\pi} \int_0^{2\pi} \Delta K \exp(-U/k_B T) \sin\theta \, d\theta \, d\phi}{\int_0^{\pi} \int_0^{2\pi} \exp(-U/k_B T) \sin\theta \, d\theta d\phi} \quad ...(8)$$

For magneto-electret, the value of $\langle \Delta K \rangle$ is given by $\langle \Delta K \rangle = \frac{M}{N}$ where M and N are as follows.

$$M = \int_0^{\pi} \int_0^{2\pi} \left\{ (k_1 \cos^2\theta + k_2 \sin^2\theta) - (k_1 \sin^2\theta \sin^2\phi + k_2 \cos_2\theta \sin^2\phi + k_2 \cos^2\phi) \right\} \exp\left\{ \tfrac{1}{2} v H^2 (\Delta k \cos^2\theta + k_2) \Big/ k_B T \right\} \sin\theta \, d\theta \, d\phi$$

$$\text{and } N = \int_0^{\pi} \int_0^{2\pi} \exp\left\{ \tfrac{1}{2} v H^2 (\Delta k \cos^2\theta + k_2) \Big/ k_B T \right\} \sin\theta \, d\theta \, d\phi$$

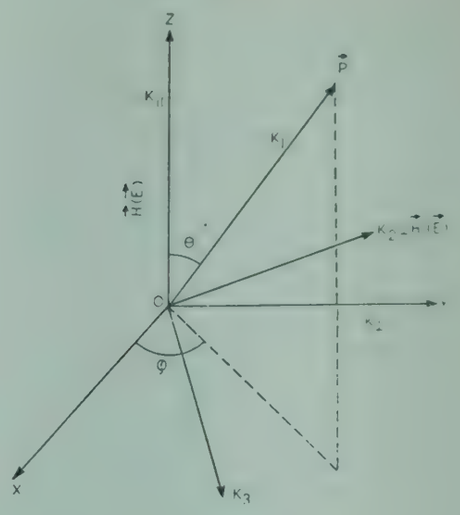

Fig. 1— Diagrammatic representation of the components of magnetic susceptibilities of a molecule with respect to the electret-forming electric or magnetic field

$$\langle \Delta K \rangle = \frac{\Delta k}{2} \left[\frac{3}{2a} \left(\sum_{n=0}^{\infty} \frac{e^a}{\frac{a^n}{n(2n+1)}} - 1 \right) - 1 \right] \quad ...(9)$$

where $a = \frac{1}{2} v H^2 \Delta / k_B T$.

For individual molecules, we have v of the order of 10^{-23} cc and Δk of the order of 10^{-7} cgs emu per cc. Thus when H is of the order of 10^3 Oe and T is between 350 and 400 K,

$$\langle \Delta K \rangle \simeq \frac{1}{15} \frac{v H^2}{k_B T} (\Delta k)^2 \approx 10^{-18} \text{ cgs emu per cc}$$

and molar anisotropy comes out to be of the order of 10^{-17} cgs emu per g mole which is not very significant. If we consider the case for which $k_2 \neq k_3$, then the orientation of the molecule will depend on the maximum values of the differences between k_1, k_2 and k_3. The molecule will align itself keeping the maximum susceptibility along the field. In that case also, the calculated value of anisotropy of the material would not differ much. And so, for $\langle \Delta K \rangle$ to be about $\sim 10^{-7}$ cgs emu per cc as obtained from actual experimental data, the magnetic anisotropy of the assemblage of molecules which are oriented in the liquid or semi-liquid state cannot be attributed to the rotation of individual molecules but rather to big groups of molecules forming cybotactic state, liquid crystals on cluster of molecules. Each domain may be assumed to contain as many as 10^{10} to 10^{11} molecules.

Correspondingly, for the thermo-electret state, one can write $\langle \Delta K \rangle = R/Q$ where R and Q are

as follows.

$$R = \int_0^{\pi} \int_0^{2\pi} \{(k_1 \cos^2\theta + k_2 \sin^2\theta) - (k_1 \sin^2\theta \sin^2\phi + k_2 \cos^2\theta \sin^2\phi + k_2 \cos^2\phi)\} \exp.\ (P E \cos\theta / k_B T) \sin\theta \, d\theta \, d\phi$$

$$\text{and } Q = \int_0^{\pi} \int_0^{2\pi} \exp.\ (P E \cos\theta / k_B T) \sin\theta \, d\theta \, d\phi$$

$$\langle \Delta K \rangle = \Delta k \left[1 - \frac{3}{\alpha} \left(\frac{e^{\alpha} + e^{-\alpha}}{e^{\alpha} - e^{-\alpha}} - \frac{1}{\alpha} \right) \right] \quad \ldots(10)$$

where $\alpha = \dfrac{P E}{k_B T}$

For individual molecules, $P \sim 10^{-18}$cgs unit. When, however, $E \approx 10^3$ V or about 10cgs units and $T \approx 350$ K, $\alpha \approx 10^{-3}$. then $\langle \Delta K \rangle = \dfrac{1}{15} \Delta k \left(\dfrac{PE}{k_B T} \right)^2 \sim 10^{-14}$ cgs emu per cc which is rather too small to be experimentally measurable. The different values of k_2 and k_3 cannot change the order of the calculated values of anisotropy of the material. The experimental value of $\langle \Delta K \rangle$ is actually of the order of 10^{-7} cgs emu per cc which shows that magnetic anisotropy of the assemblage of molecules oriented in the liquid or semi-liquid state cannot be attributed to the orientation of individual molecules but rather to groups of molecules forming cybotactic state or clusters. Such groups should possess electric dipole moment of the order of 10^{-15} cgs unit.

Results and discussion — Table 1 indicates the values of magnetic anisotropy as measured experimentally in the thermo- and the magneto-electret states.

Table 1—Experimental Values of Magnetic Anisotropy of Thermo- and Magneto-Electret States

Substance	Forming temp. °C	Forming field k gauss	Molar anisotropy 10^{-6} cgs emu/g mole
		Thermo-Electret	
Carnauba-wax	80	10*	16
		Magneto-Electret	
Carnauba-wax	80	4·4	5
Polystyrene	122	4·5	0·063 *M*
Shellac-wax	78	6·0	0·015 *M*
Naphthalene	79	4·0	1

*The forming field is in kV/cm weight

M, Molecular

The measurement of magnetic anisotropy of thermo- and magneto-electret states indicates the state of polarization of the materials. The additivity of average susceptibilites of organic compounds shows that, even in the solid state, the mutual influence of neighbouring molecules on the magnetic susceptibility is negligible. This has been substantiated by Raman and Krishnan[6] according to whom magnetic anisotropy of a unit-cell in a crystal depends upon the relative orientation of the molecules within the cell. However, the diamagnetic moments induced in neighbouring cells are so feeble that their mutual influences are negligible. Thus it seems unlikely that clusters of isotropic molecules would produce magnetic anisotropy in the crystalline phases.

During his study of Tyndall scattering of light by liquids, Krishnan[7] provided evidences of molecular clustering in liquids, which may be either isotropic or anisotropic. But no evidence has been furnished that clusters of isotropic molecules could yield magnetic anisotropy in crystals. Further, Bates[8] emphasized that the magnetic anisotropy of a bulk material is solely due to the anisotropy of individual molecules and their cumulative orientation.

Thus, it is evident that the diamagnetic anisotropy of molecules forming domains or cybotactic groups depends only on the resultant anisotropy of the individual molecules in the material. If the individual molecules are essentially magnetically isotropic, the crystal or medium would show no anisotropy. But if the molecules are anisotropic, the resultant anisotropy of the material would depend on the relative orientation of molecules. If, however, the magnetically anisotropic dipole molecules are arranged randomly so that their anisotropies cancel each other, the specimen, in general, appears to be isotropic. But when the thermo-electret is prepared in the liquid or semi-liquid state, the electric field causes the magnetically anisotropic dipolar molecules possessing resultant electric dipole moment to align themselves towards the field against thermal agitation. Thus the material exhibits magnetic anisotropy in the solid state, when the lattices are frozen. Similarly, when magneto-electret is prepared, the magnetic field causes the molecules or groups of molecules possessing magnetic anisotropy to align themselves towards the field so that the minimum diamagnetic susceptibility lies along the field. Thus the material exhibits magnetic anisotropy in the solid state.

Thanks are due to Dr S Saha for valuable discussions.

References

1. Raman C V & Krishnan K S, *Proc. R. Soc.*, A 113 (1927), 5111.
2. Chinchalkar S W, *Indian J. Phys.*, 6 (1931), 173.
3. Debye P, *Polar molcules* (Dover, New York), (1945).
4. Chatterjee S D, Banerjee K, Roychoudhuri K D & De H, *Physics Lett.*, A 29 (1969), 183.
5. Chatterjee S D, Roychoudhuri K D & Banerjee K, *Acta Phys. Pol.*, A 51 (1977), 643.
6. Raman C V & Krishnan K S, *Proc. R. Soc.*, A115 (1927), 549.
7. Krishnan R S, *Proc. Indian Acad. Sci.*, 1A (1934), 211.
8. Bates L F, *Modern magnetism* (Cambridge University Press, Cambridge), 1939, 134.

In situ Resistivity Measurements on Thin Silver Films

M Saleem Iqbal, Ijaz-ur-Rehman & S Beg
Department of Physics, Quaid-i-Azam University
Islamabad, Pakistan

Received 19 *July* 1979; *revised received* 17 *September* 1979

Continuous measurement of resistivity during the growth of thin silver film has been made *in situ*. The data are plotted using EE Mola and J M Heras [*Thin Solid Films*, 18 (1973), 137] equation. The bulk mean free path l_0 and the probability of reflection of conduction electrons at grain boundaries are calculated.

Mola and Heras,[1] derived a linear approximation to the expression for the resistivity (ρ_f) of a thin poly-crystalline film, which can be used over the thickness range $0{\cdot}2 < K < 0{\cdot}5$. According to them,

$$\rho_f t = \rho_g t + \rho_g N(p, \alpha) l_0 \quad \ldots(1)$$

with the assumption that the grain size is independent of thickness. In Eq. (1), ρ_g is the resistivity of the polycrystalline film of infinite thickness having the same structure; l_0, the bulk mean free path of the conduction electrons; t, the film thickness; p, specularity parameter (represents the probability of secular scattering at the surface); r the probability of the reflection of a conduction electron at a grain boundary; $N(p, \alpha)$ is a function, [tabulated by Mola and Heras for different α values], given in Table 1, for $p = 0$ and

$$\alpha = \frac{r}{1-r}, \quad K = \frac{t}{l_0} = \frac{\text{Film thickness}}{\text{Bulk mean free path}}$$

Table 1—Values of the Function $N(p, \alpha)$ for Different Values of α and $p = 0$ as given by Mola and Heras[1]

α	0·0	0·5	1·0	1·5	2·0
$N(p, \alpha)$	0·46	0·26	0·173	0·135	0·11

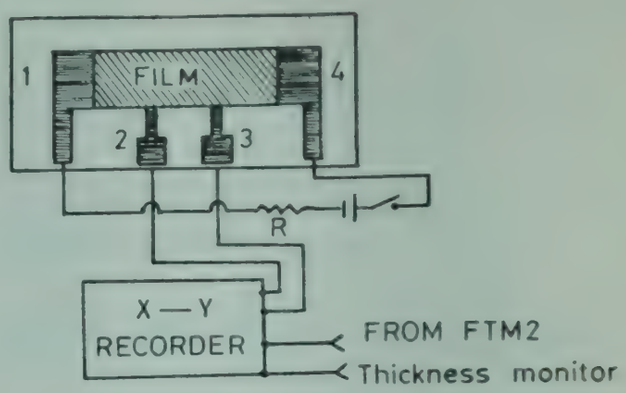

Fig. 1—Schematic diagram of the experimental set-up

A straight line should result if $\rho_f t$ is plotted against t in the region of the validity of Eq. (1), from which ρ_g and $N(p, \alpha)$ can be evaluated respectively from the slope and the intercept of the line of best fit. This approach has been made by several other authors.[1,2]

Films were grown on ultrasonically cleaned, microscopic glass slides. Fig. 1 shows four contacts (1-4) each of thickness greater than 2000 Å, and evaporated first using the same material as that of the film. The substrate was then fixed in the vacuum chamber at a suitable distance from the evaporation source and fine copper wires were attached to the contacts by means of conducting silver paint and then connected to the outer circuits through proper feed-throughs as shown in Fig. 1. The film thickness was monitored by a piezoelectric quartz crystal connected to an Adwards FTM 2 film thickness monitor, which was placed close to the substrate in the vacuum chamber so that the rate of evaporation over the crystal and the substrate was very nearly the same. The analogue output of the FTM2 was used to provide the necessary horizontal input signal to the two-pin X-Y recorder, the vertical signal being the voltage developed between the contacts 2 and 3. By plotting the voltage developed across resistance R placed between contacts 1 and 4, it has been observed that the current through the film rose sharply as the film became continuous and reached its maximum value (limited by R) at about 100 Å of its thickness. Thus for the rest of the experiment, the current was essentially constant. The pressure during evaporation varied between 2 and 3×10^{-5} torr. The rate of evaporation in case of all films was between 10 and 20 Å per second. The rate was kept high in view of poor vacuum. The final thickness was verified by using a Tolansky interferometer.

Fig. 2 shows a plot of $\rho_f t$ versus t which gives a straight line fit for data obtained from two different silver films.

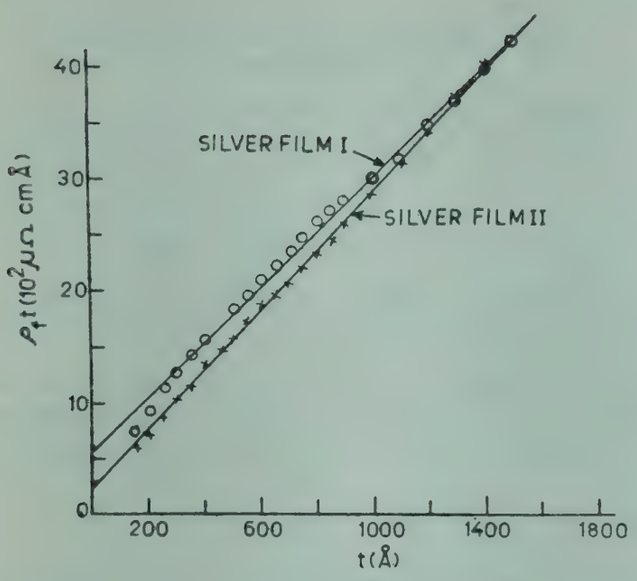

Fig. 2—Plot of $\rho_f t$ versus t for two thin silver films

Table 2—Values of ρ_g and $N(p, \alpha)$ using Eq. (1) and the Calculated Values of l_0 [Resistivity of pure bulk material (ρ_0) is 1·6 Ω-cm]

Film	ρ_g (μ Ω-cm)	(l_0 Å)	$N(p, \alpha)$	α	r
Silver I	2·5	560	0·38	0·15	0·13
Silver II	2·7	560	0·4	0·11	0·1
Silver I	2·5	463	0·38	0·0	0·0
Silver II	2·7	487	0·46	0·0	0·0

The values of ρ_g and $N(p, \alpha)$ obtained by fitting our data to Eq. (1) (using known values of l_0 are given in Table 2. The highest value of $N(p, \alpha)$ for $p = 0$ is 0·46 which gives a lower limit to the mean free path in silver film, viz. 460 Å.

From our experimental data the highest value of $N(p, \alpha)$ is taken and the corresponding l_0 is calculated which is also shown in Table 2. These values of l_0 are in good agreement with the value 460 Å.

The resistivity versus thickness graphs of the thin silver films have shown no significant deviations from a continuous curve, most probably a consequence of automation and instantaneous measurement. A striking feature of all film data is that the asymptotic resistivity ρ_g, is much higher than the bulk value ρ_0, (Table 2). However, the difference in resistivities of two films, at the same thickness, may be due to structural differences.

References

1. Mola E E & Heras J M, *Thin Solid Films*, 18 (1973), 137.
2. Singh B, Ling C C & Surplice N A, *Thin Solid Films*, 23 (1974), 550.

Application of Glauber Approximation to Feshbach-type Resonance Scattering

K N Joshipura
M B Patel Science College, Anand 388 001
and
H S Desai
Physics Department, Faculty of Science, M S University of Baroda, Baroda 390 002

Received 2 *July* 1979

The calculation of the lifetime of a temporarily formed negative ion, in Turners mechanism, is modified by using the Glauber approximation. The results of the calculations are compared with those of other workers. The present calculations support longer lifetime.

The particular behaviour of the resonance scattering of slow electrons by the polar molecules like H_2O, D_2O, H_2S, etc. has long since received attention. Many investigations[1-6,9] have been reported to explain the large diffusion cross-sections for these molecules. Turner's mechanism[1] explains this by means of a two-step process. The electron of the incident swarm is first captured in the dipole field of the target molecule, forming a loosely bound momentary state, and exciting the rotational state of the target. Then, the natural decay of the negative ion thus formed returns the electron back to the swarm and contributes to the diffusion or momentum transfer cross-section. The lifetime of the temporary negative ion is estimated to be of the order of the rotational period of the target molecule. In all these calculations, Born approximation has been used to find the elastic scattering amplitude. However, the dipole field, due to its long-range nature, involves distant encounter with the electron. Hence eikonal approximation is expected to be more appropriate. Although this is basically a high-energy approximation it has been successfully applied in low-energy problems.[7,8] The direct calculation of diffusion cross-section using Glauber amplitude, suggests a much higher value of the quantity. This favours the higher value of the lifetime. In this note, we report the calculation of the lifetime of the temporarily formed negative ion, by making use of the Glauber approximation.

Theory—The Glauber amplitude for the elastic scattering is given by

$$f(\hat{\mathbf{s}}, q) = \frac{i k_i}{2\pi} \int e^{i\mathbf{q}\cdot\mathbf{b}} \left(1 - e^{i\chi(\mathbf{b}\cdot\hat{\mathbf{s}})}\right) d^2b \qquad \ldots(1)$$

where $\mathbf{b}$ is the impact parameter measured from the centre of mass of the rigid rotator; $\mathbf{q} = (\mathbf{k}_i - \mathbf{k}_f)$, $\mathbf{k}_i$

and $\mathbf{k}_f$ being respectively the momenta of the incident and scattered electron; θ, ϕ are the angles of scattering and $\hat{\mathbf{s}}$ denotes the orientation of the molecular axis. The phase shift $\chi(\mathbf{b}, \hat{\mathbf{s}})$ is of the form,

$$\chi(\mathbf{b}, \hat{\mathbf{s}}) = -\frac{1}{\hbar v_i} \int_{-\infty}^{\infty} V_D(\mathbf{r}, \hat{\mathbf{s}})\, dz \qquad ...(2)$$

where v_i is the velocity of the incident electron and $\mathbf{r}$ denotes the position vector of an incoming electron relative to the centre of mass,

$$\mathbf{r} = \mathbf{b} + \hat{\mathbf{n}} z$$

$\hat{\mathbf{n}}$ being the unit vector along the incident direction. The potential V_D is expressed as

$$V_D(\mathbf{r}, \hat{\mathbf{s}}) = -\frac{D e}{r^2} \cos \mathbf{r} \qquad ...(3)$$

where D is the dipole moment of the molecule, which is considered as a rigid rotator and Υ is the angle made by the position vector of the incoming electron with the molecular axis.

Substituting Eq. (3) in Eq. (1) and carrying out elementary integration, we obtain

$$\chi(\mathbf{b}, \hat{\mathbf{s}}) = \frac{2 e D}{\hbar v_i b} (\hat{\mathbf{s}} \cdot \hat{\mathbf{b}}), \qquad ...(4)$$

where e is the electronic charge, $\hbar = h/2\pi$, h the Planck's constant and $\hat{\mathbf{b}}$ is the unit vector along the direction b. Using Eq. (4), the amplitude factor $f(\hat{\mathbf{s}}, q)$ is evaluated as done by Ashihara *et al.*[8] The result is

$$f(\hat{\mathbf{s}}, q) = \frac{i k_i}{2\pi} \left(\frac{2\xi}{q}\right)^2 \Bigg[2 \sin \theta_s \cos(\phi_s - \phi_q) \times \left\{\frac{1}{4\xi} - \frac{\xi}{40}\right\} - 2 \ln\left(\frac{\xi}{2}\right) + \left\{\frac{1}{4}\psi(5/2) + \frac{1}{4}\psi(2) + \frac{1}{2}\psi(1)\right\}\Bigg] \qquad ...(5)$$

where $\xi = \left(\frac{m e D}{\hbar^2 k_i}\right) q$, m being the mass of the electron, θ_s, ϕ_s being the orientation of the molecular axis relative to the fixed frame, ψ is a digamma function and ϕ_q is the angle made by $\mathbf{q}$ vector in the (x, y) plane. Using Eq. (5), calculations for the lifetime of the temporary bound states are made exactly in the manner of Turner.[1] The matrix element for the decay from the final state $(L_f\, M_f')$ to the initial state $(L_i\, M_i)$ is

$$T_{fi} = \left(\frac{\hbar^2}{I\sqrt{6}}\right)\left(\frac{Z}{a_0}\right)^{3/2}\left(I_1 + I_2 + I_3\right) \qquad ...(6)$$

Table 1—Results of $|T_{fi}|^2$ and τ Calculated by Different Methods

Quantity	Turner's value (Ref. 1)	Variation method (Ref. 6)	Finite dipole correction (Ref. 9)	Glauber's Approximation (present study)
$\lvert T_{fi}\rvert^2 \times 10^{-47}$	1·183	1·182	1·248	0·27
$\tau \times 10^{-14}$ sec	3·488	3·490	3·307	15·0

Explicit expressions for I_1, I_2 and I_3 are given in the Appendix. Using Eq. (6) the life-time of the temporary bound state is calculated by using the formula

$$\tau = \frac{\pi \hbar^4}{m(2Em)^{1/2}} \cdot \frac{1}{|T_{fi}|^2}. \qquad ...(7)$$

Results and discussion—All the quantities are evaluated in cgs system, for the typical H_2O molecule. The dipole moment $D \sim 2{\cdot}0 \times 10^{-18}$ esu cm and the moment of inertia $I \sim 10^{-40}$ g × cm^2. The results for T_{fi} matrix element are evaluated for the initial state $L_i = 2$ of the rotator to the final state $L_f = 3$, $M_i = M_f = 0$ and for the electron of incident energy 0·025 eV. Our calculated results are compared with the results of other workers[9] and are shown in Table 1.

It is observed that the lifetime of the captured state is shorter than the period of rotation of the target molecule, which is nearly equal to $3{\cdot}82 \times 10^{-13}$ sec. The calculation using Glauber approximation supports the existence of long-lived negative ions. This, in turn, can reduce the capture cross-section and increase momentum transfer cross-section, a fact that is supported by experiments.

Appendix

The integrals I_1, I_2 and I_3 are as follows (Ref. 1):

$$I_1 = \left[\frac{5}{4\pi}\right]^{1/2} \int\int e^{-Zr/a_0}\, Y^*_{L_f, M_f}(\hat{\mathbf{s}})\, \textcircled{H}^2 f(\hat{\mathbf{s}}, q)\, \frac{e^{ikr}}{r}\, Y_{L_i, M_i}(\hat{\mathbf{s}})\, d\nu\, d\Omega$$

$= 0$ for the case considered.

I_2 is the same as in Ref. 1.

$$I_3 = \left(\frac{4\pi}{3}\right)^{1/2} \int\int e^{-Zr/a_0} \Big\{ Y^*_{1,-1}(\hat{\mathbf{r}})\, Y_{1,-1}(\hat{\mathbf{s}}) + Y^*_{1,0}(\hat{\mathbf{r}})\, Y_{1,0}(\hat{\mathbf{s}})\, Y_{1,1}(\hat{\mathbf{r}})\, Y_{1,1}(\hat{\mathbf{s}}) \Big\}\, Y^*_{L_f, M_f}(\hat{\mathbf{s}}) \times \textcircled{H}^2 f(\hat{\mathbf{s}}, q)\, \frac{e^{ikr}}{r}\, Y_{L_i, M_i}(\hat{\mathbf{s}})\, d\nu\, d\Omega$$

$$= \frac{2iP}{k_i}\left(3\pi\right)^{1/2} Q\left[1 - R\right] S^3_{fi}$$

$$+ \frac{4i}{5}\left(\frac{2\pi}{3}\right)^{1/2}\frac{P^3\hbar^3}{k_i}Q\left[1-R\right]S_{fi}^3$$

$$+ \frac{14i}{ki}\left(\frac{3\pi}{4}\right)^{1/2}P^2 L_i\,(L_i+1)\,Q\,[1-R]\,S_{fi}^3$$

$$\times\left[\left\{\frac{(L_f+1+M_f)\,(L_f+1-M_f)}{(2L_f+1)\,(2L_f+3)}\right\}^{1/2}\right.$$

$$\delta L_{f+1}, L_i\,\delta_{M_f, M_i} + \left\{\frac{(L_f+M_f)\,(L_f-M_f)}{(2L_f+1)\,(2L_f-1)}\right\}^{1/2}$$

$$\left.\delta_{L_f-1, L_i}\,\delta_{M_f, M_i}\right]$$

where $\frac{m\,e\,D}{\hbar^2} = P,\ Q = \left(\frac{Z\,a_0}{Z^2+k_i^2\cdot a_0^2}\right)^2$

and $R = \left[\left(\frac{k_i\,a_0}{Z}\right)^2 + 2i\left(\frac{k_i\,a_0}{Z}\right)\right]$

References

1. Turner J E, *Phys. Rev.*, **141** (1966), 21.
2. Hadjaintoniou A, Christophorou L G & Carter J G, *J. chem. Soc. Faraday Trans.*, 69 (Pt I) (1973), 1991.
3. Itikawa Y, *Physics Lett.*, 24A (1969), 495.
4. Takayanagi K & Itikawa, *J. phys. Soc. Japan*, **24** (1968), 160.
5. Desai H S & Maru M P, *Indian J. pure appl. Phys.*, **10** (1972), 750.
6. Desai H S, Maru M P & Pandya S R, *Z. Naturf.*, **29A** (1974), 1229.
7. Takayanagi K, *Prog. theor. Phys.*, 52 (1974).
8. Ashihara O & Shimamura Takayanagi, *J. phys. Soc. Japan*, 38 (1975).
9. Maru M P & Desai H S, *Indian J. pure appl. Phys.*, 16 (1978), 705.

Vibrational Spectrum of 2,6-Dichlorobenzamide

D V Ramanamurti, P Venkatacharyulu & D Premaswarup

Department of Physics, Nagarjuna University
Nagarjunanagar 522 510

Received 16 *April* 1979; *revised received* 6 *December* 1979

The infrared absorption spectrum of 2,6-dichlorobenzamide has been recorded in the region 600-4000 cm^{-1}. The vibrational assignments of all the observed frequencies have been made assuming C_{2v} symmetry.

Vibrational spectrum of benzamide[1] has been reported. However, no work has been reported on 2,6-dichlorobenzamide (hereafter denoted as A for convenience). Hence the vibrational spectrum of the compound was recorded in solid phase. The compound is a solid at room temperature and obtained from M/s K and K Laboratories Inc., USA. The commercial sample was purified by the method of recrystallization using acetone as solvent. The spectrum was recorded in the region 600-4000 cm^{-1} using the KBr pellet technique. The accuracy of measurement is estimated to be $\pm$ 5 cm^{-1}.

The observed bands have been analyzed in terms of fundamentals, their combinations and overtones on the basis of the intensity considerations and comparison with the spectra[1-7] of 1-substituted 2,6-dichlorobenzenes, in particular 2,6-dichlorotoluene, 2,6-dichlorophenol, 2,6-dichloroanisole, 2,6-dichlorophenetole, which hereafter are denoted as B,C,D and E respectively, and are given in Table 1. The mass of the substituent group in position 1 of benzene ring increases as one goes from C to E with the rest of the molecules remaining identical. A similar change occurs between B and A. Keeping the different bands of these compounds C,D,E in view, the observed bands in A had been analyzed, comparing with those of B. Vibration numbers are given in Wilson's notation. The figures in brackets represent the intensities of vibrational bands on an arbitrary scale. Table 2 represents assignment of overtones and combination frequencies. Assuming the molecule 2,6-dichlorobenzamide as planar, it would belong to C_{2v} point group. The molecule belongs to the category 1,3-di-'heavy' and -2-'light' and the expected ranges of frequencies for all modes are given by Varsanyi.[1]

Benzene has 6 modes of C—H stretching vibrations denoted in Wilson's notation by 20a, 20b, 2, 13, 7a and 7b. Two modes, 20 and 7, are degenerate and have the frequencies 3080 cm^{-1} (e_{1u}) and 3046 cm^{-1} (e_{2g}) while the other two modes 2 and 13 have the frequencies 3062 cm^{-1} (a_{1g}) and 3060 cm^{-1} (b_{1u}) respectively. In the case of trisubstituted benzene, out of these 6 modes, 3 modes viz. 20a, 20b and 2, remain as C—H stretching and the other three, 13, 7a, 7b, become C—X stretching, where X is substitution for H atom in benzene. The three C—H stretching frequencies almost retain their values in benzene and lie in the region 3000-3100 cm^{-1}. These vibrations appear generally with weak intensity and are not well resolved. In the present case the frequency 3075 cm^{-1} has been assigned to the C—H stretching mode 20b. The modes 20a and 2 are not observed. The frequency 1185 cm^{-1} has been assigned as C—X stretching frequency corresponding to the mode 13. For this mode 13, the frequency decreases as one goes from C to E, similarly the observed frequency for this mode in the compound A is less than that of B as expected. C—Cl stretching frequencies corresponding to 7a and 7b are expected to fall below 600 cm^{-1} and hence are not observed.

Table 1—Assignment of Fundamental Vibrations in Compounds A-E

Vibration No.	Vibrational frequency, cm^{-1} A	B	C	D	E
1	1045(3)	1056	1067	1036	1023
2	—	3075	—	3070	3074
3	1295(3)	1269	1269	—	1273
4	700(5)	694	715	—	686
5	970(11)	963	963	966	951
6a	730(33)	765	799	743	734
6b	—	805	824	788	788
7a	—	373	404	377	—
7b	—	401	417	397	—
8a	1550(36)	1561	1577	1558	1550
8b	1575(16)	1580	1585	1566	1576
9a	—	222	—	—	—
9b	1150(21)	1156	1142	1154	1147
10a	—	—	—	—	—
10b	—	—	—	—	—
11	770(49)	776	769	775	770
12	—	589	—	603	616
13	1185(44)	1204	1240	1204	1197
14	—	—	1337	1254	1244
15	—	256	—	—	—
16a	—	530	484	—	—
16b	—	575	548	541	535
17a	895(16)	896	900	898	—
17b	—	114	—	—	—
18a	1085(25)	1092	1096	1070	1065
18b	—	493	373	—	—
19a	1445(31)	1496	1463	1470	1467
19b	1420(49)	1470	1450	1420	1430
20a	—	—	—	—	—
20b	3075(5)	3068	3075	3008	—
$CONH_2$ group internal vibrations					
A_3	1370(49)				
A_2	1635(8) 1640(3)				
A_1	1650(3) 1660(5)				
N—H stretching	3160(17)				
N—H stretching	3425(43)				

Table 2—Assignment of Overtones and Combination Frequencies in 2,6-Dichlorobenzamide

Vibrational freq. cm^{-1}	Overtones and combinations
1075(29)	700+ 375*
1495 (3)	730+ 770
1600 (9)	700+ 895
1700(38)	730+ 970
1810 (3)	730+1075
1885 (5)	700+1185 or 1150+ 730
1960 (6)	770+1185 or 1075+ 895
2490(12)	1045+1445
2750 (6)	1295+1445 or 1185+1575 or 2×1370
3280(10)	1635+1650

*This value is taken basing on the observed 7a from the other compounds.

The in-plane bending vibrations for trisubstituted benzene are derived from the C—H in-plane bending vibrations of benzene. There are 6 modes of these vibrations for benzene denoted by 3, 9a, 9b, 15, 18a and 18b having the magnitudes 1326 (a_{2g}), 1178 (e_{2g}), 1150 (b_{2u}) and 1033 (e_{1u}) cm^{-1} respectively. In trisubstituted derivatives 3 modes of vibrations, 3, 9b, 18a designated as C—H in-plane bending vibrations remain almost unaltered and 3 modes 9a, 15 and 18b change considerably in frequency assuming the character of C—X in-plane bending vibrations. The frequencies of these three modes fall below 600 cm^{-1} and hence cannot be observed in the present case. The frequencies 1085 cm^{-1}, 1150 cm^{-1}, 1295 cm^{-1} have been assigned to the C—H in-plane bending modes 18a, 9b and 3 respectively. The frequency of the modes 18a, 9b and 3 decreases, does not change and increases respectively, as the mass of the 1 substituent increases.

There are six C—H out-of-plane bending vibrations in benzene corresponding to the modes 5, 17a, 17b, 10a, 10b and 11 whose frequencies are 985 (b_{2g}), 970 (b_{2u}), 849 (e_{1g}) and 671 (e_{2u}) cm^{-1} respectively. In trisubstituted benzene derivatives three modes 5, 17a, 11 remain as C—H out-of-plane bending vibrations and three modes 17b, 10a, 10b become C—X out-of-plane bending vibrations. The frequencies of these three modes fall below 300 cm^{-1} and hence are not observed. The frequencies 770, 895 and 970 cm^{-1} have been assigned to the C—H out-of-plane bending vibrations 11, 17a and 5 respectively. The frequency of the mode 11 is of the same

order in all the five compounds. Similar is the case with 17a. The mode 5 is not following any order.

The vibration modes 8a, 8b, 19a, 19b, 14 and 1 of benzene with frequencies 1535 (e_{2g}), 1485 (e_{1u}), 1310 (b_{2u}) and 992 (a_{1g}) cm^{-1} are the C—C stretching vibrations. On substitution, the frequencies of the first five modes remain almost unchanged whereas the frequency of mode 1 (ring breathing) is increased in C_{2v} symmetry.[1] The frequencies 1045, 1445, 1550 and 1575 cm^{-1} are assigned as C—C stretching vibrations 1, 19b, 19a, 8a and 8b respectively. The vibration mode 14 is not observed. The modes 19a, 19b and 8b are not following any order in the different compounds. The frequencies of modes 8a and 1 decrease as one goes from C to E and the observed frequencies for these two modes in A are less than those corresponding in B as expected.

The normal modes 6a, 6b and 12 are regarded as the C—C—C in-plane bending vibrations. The benzene frequencies for these modes are 606 (e_{2g}) and 1010 (b_{1u}) cm^{-1} respectively. The frequency 730 cm^{-1}, assigned to the mode 6a, decreases as one goes from C to E. The observed frequency in A is less than the corresponding one in B, as expected; 6b and 12 are not observed. The mode 12 is not within the range of observed spectrum. The normal modes 4, 16a and 16b are the C—C—C out-of-plane bending vibrations of benzene. The corresponding frequencies being 703 (b_{2g}) and 405 (e_{2u}) cm^{-1} respectively. The frequency 700 cm^{-1} is assigned to the mode 4. This mode is not following any order.[5] The modes 16a and 16b are not observed because their frequencies fall below 600 cm^{-1}.

All amides show a carbonyl absorption, termed as Amide I (A_1) band, and is observed near 1650 cm^{-1}. The NH_2 deformation mode in primary amides is to be expected in the 1600 cm^{-1} region and this absorption is termed as Amide II (A_2) band. The C—N stretching mode near 1400 cm^{-1} is termed as Amide III (A_3) band. In the present case, two close frequencies 1650 and 1660 cm^{-1} with almost equal intensity were observed and one of these should be A_1 band. Similarly two other close frequencies 1635 and 1640 cm^{-1} were observed and one of these should be A_2 band. The frequency with strong intensity 1370 cm^{-1} is assigned as A_3 band. Primary amides show two N—H stretching modes near 3180 cm^{-1} and 3350 cm^{-1} corresponding to the symmetric and asymmetric motions of the hydrogen atoms. In the present case, the frequencies 3160 cm^{-1} and 3425 cm^{-1} are assigned as N—H stretching frequencies. These assignments find support from the work on benzamide.[1]

One of the authors (DVR) is grateful to the CSIR, New Delhi, for offering the post of Pool-Officier. Their thanks are due to the staff of the Regional Research Laboratory, Hyderabad, where the spectrum was recorded.

References

1. Varsanyi G, Assignments for vibrational spectra of Benzene *derivatives*, Vol. 1 (Adam Hilger, London), 1974.
2. Bellamy L J, *Infrared spectra of complex molecules*, (Methuen, London), 1966.
3. Green J H S, *Spectrochim. Acta*, 26A (1970), 1523.
4. Green J H S, Harrison D J & Kynaston W, *Spectrochim. Acta*, 27A (1971), 793.
5. Singh R N & Prasad S C, *Indian J. pure appl. Phys.*, 15 (1977), 264.
6. Singh V B & Singh I S, *Indian J. pure appl. Phys.*, 6 (1968), 81.
7. Singh R N, Prasad S C & Prasad R K, *Spectrochim. Acta*, 34-A (1978), 39.

Vibrational Spectra of *p*-Methoxy Benzonitrile

A N Pathak

Department of Physics, Bhagalpur University
Bhagalpur 812 007
and
B K Sinha

Department of Physics, TNB College
Bhagalpur 812 007

Received 22 *August* 1979; *revised received* 16 *November* 1979

The infrared absorption spectra of *p*-methoxy benzonitrile has been recorded. Vibrational assignments have been made on the basis of C_s symmetry.

The vibrational spectra of benzonitrile,[1] benzonitrile d_5^2, *para*-substituted benzonitriles,[3] pentafluoro benzonitrile[4] and *s*-trichloro benzonitrile[5] have been studied and their fundamental modes characterized. In this study, the spectrum of *p*-methoxy benzonitrile has been investigated in the region 4000-300 cm^{-1}. The observed frequencies and their assignments are given in Table 1.

Assuming that —OCH_3 and —CN behave as single atoms, as has been done by many previous workers,[6-8] this molecule may be classified under C_{2v} symmetry. Benzonitrile is planar and belongs to C_{2v} symmetry.[9] But Rai and Upadhya[10] in their studies of *p*-fluoroanisole and *p*-chloroanisole suggest that the attachment of the methoxy and halogen groups in the benzene ring in *para* position reduces the symmetry to the C_s point group. Making the same assumption, we have also taken up the vibrational assignments on the basis of C_s symmetry. However, it is not difficult to pick up the benzene ring vibrations in

Table 1—Vibrational Frequencies (in cm^{-1}) of the Bands of *p*-Methoxy Benzonitrile and Their Assignments

Frequency (cm^{-1})	Assignment
322 w	C—OCH_3 bend, out-of-plane
368 w	C—O—C bend, in-plane
386 w	C—C bend, in-plane
500 m	C—OCH_3 bend, in-plane
550 s	C≡N bend, in-plane
680 m	C—C bend, in-plane
720 vw	C—H bend, out-of-plane
809 w	322 + 500
830 s	ring breathing
1020 s	O—CH_3 stretching
1115 vw	2 × 550
1128 vw	CH plane deformation
1172 s	CH plane deformation
1255 s	Phenyl—O stretching
1300 m	C—C ring stretching
1375 m	methyl CH deformation sym.
1430 w	C—C ring stretching
1455 s	methyl CH deformation asym.
1500 m	C—C ring stretching
1572 m	550 + 1020
1600 s	C—C ring stretching
1855 vw	830 + 1020
2205 s	C≡N stretching
2835 s	methyl CH stretching sym.
2890 s	methyl CH stretching sym.
2930 s	methyl CH stretching asym.
3080 m	C—H ring stretching

s=strong, m=medium, w=weak, vw=very weak

this molecule. The absorption at 3080 cm^{-1} is attributed to C—H stretching of benzene ring. C—C stretching bands usually occur between 1650-1300 cm^{-1}. The bands at 1300, 1420, 1500 and 1600 cm^{-1} have been attributed to this type of vibration. A combination band of comparable intensity at 1572 cm^{-1} might be due to Fermi resonance. The two bands at 1375 and 1455 cm^{-1} are attributed to methyl C—H deformation. The band at 1255 cm^{-1} is due to phenyl-O stretching while that at 1020 cm^{-1} is due to O—CH_3 stretching. The C≡N stretching frequency is easily identified near 2230 cm^{-1} in aromatic nitriles. According to Varsanyi,[11] *para*-substitution in benzonitrile lowers this frequency accompanied by an intensity increase of C≡N stretching. In the present case, this band has been observed at 2205 cm^{-1}. The band at 550 cm^{-1} is attributed to C≡N in-plane bending. The strong absorption at 830 cm^{-1} is attributed to ring breathing mode. Indeed, it would have been very helpful in making the vibrational assignments if Raman spectra were also recorded but it could not be possible for want of such facilities. However, considerable guidance has been taken in making the vibrational assignments of this molecule, by comparing their frequencies with the frequencies of other related molecules.

We are grateful to Dr P D Singh of Instituto Astronomico e Geofisico, University of Sao Paulo (Brazil) and Dr K P Sharma, Prof. of Physics, Bhagalpur University for their interest in the work. One of us (BKS) is grateful to the University Grants Commission, New Delhi, for financial help.

References

1. Green J H S, *Spectrochim. Acta*, 17 (1961), 607.
2. Jakobsen R J, *Spectrochim. Acta*, 21 (1965), 127.
3. Wilson H W & Bloor J E, *Spectrochim. Acta*, **21** (1965), 45.
4. Shurvell H F, Blair A S & Jakobsen R J, *Spectrochim. Acta*, **24A** (1968), 1257.
5. Faniran J A, *J. Cryst. molec. Struct.*, 5 (1975), 191.
6. Mooney E F, *Spectrochim. Acta*, **19** (1963), 877.
7. Green J H S, *Spectrochim. Acta*, 18 (1962), 39.
8. Stephenson C V, *Spectrochim. Acta*, 17 (1961), 933.
9. Lide D R, *J. chem. Phys.*, **22m** (1954), 1577.
10. Rai J N & Upadhya K N, *Spectrochim. Acta*, **22** (1966), 1427.
11. Varsanyi G, *Vibrational spectra of benzene derivatives* (Academic Press, New York), 1969.

Vibrational Analysis of Monomeric Trihalides of Gallium & Indium

V Sengodan & K G Srinivasacharya

Postgraduate Department of Physics, P S G College of Arts & Science, Coimbatore 14, Tamil Nadu

Received 12 *January* 1979

The kinetic constants method is applied to evaluate a fresh set of potential constants (in-plane) in the case of monomeric trihalides of gallium and indium, using recent vibrational frequencies [I R Beattie & J R Horder, *J. chem. Soc.*, A (1969), 2655]. The calculated potential constants are, in turn, used to evaluate other molecular constants, such as compliance constants, mean amplitudes of vibration and Coriolis coupling constants. The values of mean amplitudes of vibration obtained by this method are in good agreement with the experimental values in the case of gallium iodide.

In continuation of our studies on the evaluation of potential constants using the kinetic constant method[1] we have presently undertaken the study of gallium and indium trihalide monomers, and the results are reported in this note. The molecules

belong to the D_{3h} point group of the planar symmetrical XY_3 type. The six normal modes of vibrations of this model are classified as, one totally symmetric (A_1'), two doubly degenerate (E') and one non-totally symmetric (A_2'').

Beattie and Horder[2] have recently reported the vibrational analysis of in-plane frequencies of these molecules from an experimental study of the Raman spectra in gaseous form. They have given a complete vibrational assignment for the molecules GaI_3 and $InBr_3$. In case of other monomers the ν^3 frequency was not reported by them. However, recently Cyvin and Phongsatha[3] have calculated this missing frequency. In the present investigation the vibrational frequency data are taken from Refs. 2 and 3.

Based on the method already discussed in our earlier paper,[1] we have presently evaluated the kinetic and potential constants for the gallium and indium trihalide monomers which are presented in Tables 1 and 2 respectively. From Tables 1 and 2 it is observed that the kinetic constants in general increase as the mass of the Y atom increases for the same X atom, whereas in the case of force constants a reverse trend is observed, except in the case of the interaction constants f_{rr}, $f'_{r\alpha}$ and $f_{r\alpha}$. As the mass of the X atom increases keeping the Y atom same, the kinetic constants show an increase except the interaction constants k_{rr}, $k'_{r\alpha}$, and $k_{r\alpha}$ which show a reverse trend, whereas all the force constants show a decrease.

By observing the trend of variation for the stretching force constant f_r we can infer the strength of chemical bonding as follows :

(i) Ga—Y_3>In—Y_3—This is in accordance with the decrease in electronegativity and increase in atomic radii from Ga to In.

(ii) X—Cl_3> X—Br_3> X—I_3—This is also in accordance with the decrease in the electronegativity and increase in atomic radii from Cl to I. In Table 2 the values of force constants obtained by Phongsatha[4] are also included for comparison. A good agreement between the two could be observed which shows a systematic set of force constants could be obtained employing the kinetic constant method.

The compliance constants C_r are also determined for these molecules based on the procedure given by Decius[5] and are given in Table 3. The values of C_r are in the order: C_r (Ga—Y_3) $< C_r$ (In—Cl_3) and also C_r (X—Cl_3) $< C_r$ (X—Br_3) $< C_r$ (X—I_3) which also supports the trend of variation in the strength of chemical bonding. The compliance constant, in general, increases as the mass of the X atom increases for the same Y atom, and also increases as the mass of the Y atom increases for the same X atom.

The mean amplitudes of vibration for the bonded and non-bonded atom pairs for seven temperatures ranging from 0 to 2000 K, are evaluated using the method given by Cyvin[6] and are presented in

Table 1—Values of Kinetic Constants (in amu)

Molecule	k_r (k_{rr})	k_α ($-k_{\alpha\alpha}$)	$-k'_{r\alpha}$ ($k_{r\alpha}$)
$GaCl_3$	27·9432 (3·5184)	5·4277 (2·7139)	4·0626 (2·0313)
$GaBr_3$	59·2455 (10·3487)	10·8659 (5·4330)	11·9497 (5·9748)
GaI_3	91·1163 (17·9142)	16·2671 (8·1336)	20·6855 (10·3428)
$InCl_3$	29·4151 (2·7824)	5·9184 (2·9592)	3·2129 (1·6064)
$InBr_3$	61·9287 (9·0071)	11·7603 (5·8802)	10·4005 (5·2002)
InI_3	94·4397 (16·2525)	17·3749 (8·6875)	18·7663 (9·3832)

Table 2—Values of Force Constants (in mdyne/Å)

Molecule	f_r	f_{rr}	f_α	$-f_{\alpha\alpha}$	$-f'_{r\alpha}$	$f_{r\alpha}$
$GaCl_3$	3·0990 (3·1317)	−0·0430 (−0·0423)	0·0527 (0·0533)	0·0263 (0·0267)	0·0393 (−0·0400)	0·0197 (−0·0200)
$GaBr_3$	3·1503 (3·1580)	−0·2497 (−0·2570)	0·0440 (0·0440)	0·0220 (0·0220)	0·0487 (−0·0480)	0·0243 (−0·0240)
GaI_3	1·5830 (1·5870)	0·0180 (0·0140)	0·0240 (0·0240)	0·0120 (0·0120)	0·0307 (−0·0300)	0·0153 (−0·0150)
$InCl_3$	2·4717 (2·4927)	0·0287 (0·0327)	0·0307 (0·0313)	0·0153 (0·0157)	0·0167 (−0·0170)	0·0083 (−0·0087)
$InBr_3$	1·9350 (1·9290)	0·0930 (0·0930)	0·0267 (0·0267)	0·0133 (0·0133)	0·0233 (−0·0234)	0·0117 (−0·0117)
InI_3	0·9590 (0·9587)	0·3750 (0·3727)	0·0200 (0·0200)	0·0100 (0·0100)	0·0213 (−0·0214)	0·0107 (−0·0107)

Values in parenthesis are from Ref. 4.

Table 4, along with the experimental values for GaI_3. It can be noted that the calculated mean amplitude values for GaI_3, at 500 K are in good agreement with the observed values.[8] Also it is found that the mean amplitudes of vibration, for both bonded and non-bonded atom pairs, increase as the temperature increases. The mean amplitudes of vibration will be useful for the electron diffraction study of these molecules.

Table 3—Values of Compliance Constants (in Å/mdyne)

Molecule	C_r (C_{rr})	C_α ($-C_{\alpha\alpha}$)	$C'_{r\alpha}$ ($-C_{r\alpha}$)
$GaCl_3$	0·3258 (0·0030)	8·5846 (4·2923)	0·1613 (0·0807)
$GaBr_3$	0·3266 (0·0254)	10·0579 (5·0290)	0·2209 (0·1104)
GaI_3	0·6484 (−0·0154)	18·6839 (9·3420)	0·5626 (0·2813)
$InCl_3$	0·4062 (−0·0054)	14·4789 (7·2394)	0·1489 (0·0745)
$InBr_3$	0·5254 (−0·0269)	16·9433 (8·4717)	0·3256 (0·1628)
InI_3	1·4010 (−0·4078)	23·9722 (12·0161)	1·2932 (0·6466)

The Coriolis coupling constants are obtained by the vector method of Meal and Polo.[9] The calculated Coriolis coupling constants are listed in Table 5. It is observed from Table 5 that

$$\zeta^x_{33} = -\zeta^x_{44}$$

and also the square sum rule $(\zeta^x_{33})^2 + (\zeta^x_{34})^2 = 1$ is satisfied for all molecules. The Coriolis coupling coefficients are useful in vibration-rotation interaction studies.

The authors wish to thank Prof. D K P Varadarajan, Principal, P S G College of Arts & Science, Coimbatore and the management for their kind encouragement.

Table 5 – Values of Coriolis Coupling Coefficients

Molecule	$\zeta^z_{33} = -\zeta^z_{44}$	ζ^z_{34}
$GaCl_3$	0·4320	0·9013
$GaBr_3$	0·6347	0·7725
GaI_3	0·7340	0·6791
$InCl_3$	0·3134	0·9496
$InBr_3$	0·5106	0·8598
InI_3	0·6236	0·7819

Table 4—Values of Mean Amplitudes (in Å) of Vibration

	Temp. (K)	$GaCl_3$	$GaBr_3$	GaI_3	$InCl_3$	$InBr_3$	InI_3
	0	0·0390	0·0343	0·0390	0·0399	0·0368	0·0444
	298	0·0434	0·0425	0·0550	0·0464	0·0494	0·0774
	400	0·0471	0·0475	0·0617	0·0511	0·0558	0·0862
	500	0·0509	0·0521	0·0682	0·0557	0·0616	0·0990
				(0·0720)*			
X—Y				(0·067*			
				±0·004)†			
	800	0·0618	0·0645	0·0853	0·0684	0·0769	0·1248
	1000	0·0684	0·718	0·0951	0·0759	0·0857	0·1393
	2000	0·0954	0·1008	0·1365	0·1063	0·1206	0·1968
	0	0·0650	0·0553	0·0572	0·0717	0·0612	0·0672
	298	0·1050	0·1110	0·1481	0·1326	0·1403	0·1082
	400	0·1198	0·1279	0·1725	0·1522	0·1619	0·1878
	500	0 1331	0·1426	0·1911	0·1695	0·1807	0·2099
				(0·1390)*			
Y—Y				(0·163			
				±0·010)†			
	800	0·1671	0·1798	0·2290	0·2133	0·2282	0·2653
	1000	0·1864	0·2009	0·2699	0·2382	0·2550	0·2966
	2000	0·2630	0·2839	0·3846	0·3364	0·3604	0·4193

*Observed values from Ref. 7 †Observed values from Ref. 8

References

1. Ramasamy R, Sengodan V & Srinivasacharya K G, *Spectrosc. Lett.*, 11 (1978), 625.
2. Beattie I R & Horder J R, *J. chem. Soc.*, A (1969), 2655.
3. Cyvin S J & Phongsatha A, *Spectrosc. Lett.*, 8 (1975), 71.
4. Phongsatha A, thesis No. 18, The University of Trondheim, Norway.
5. Decius J C, *J. chem. Phys.*, 38 (1963), 241.
6. Cyvin S J, *Molecular vibrations and mean square amplitudes* (Universitet sporlaset, Oslo/Elsevier), 1968.
7. Akishin P A, Naumov V A & Tatevskii, *Kristallogr.*, 4 (1959), 194.
8. Morino Y, Ukaji T & Ito T, *Bull. chem. Soc. Japan*, 39 (1966), 71.
9. Meal J H & Polo S R, *J. chem. Phys.*, 24 (1956), 1119.

Centrifugal Distortion Constants of Cyclobutane & Cyclobutane-d_8

T A Karuppannan, R Ramasamy & K Venkateswarlu

Department of Physics, P S G Autonomous College of Arts & Science, Coimbatore 641 014

Received 3 *December* 1978

The centrifugal distortion constants of cyclobutane and cyclobutane-d_8 molecules have been evaluated using the force constants obtained on the basis of general valence force field. The results have been discussed in relation to the structure and molecular weight of the molecules.

Two possible models are mainly discussed, relating to the structure of the cyclobutane, one with a plane carbon ring (D_{4h}) and the other with a puckered ring (D_{2h}). The observed vibrational spectrum of cyclobutane agrees with the D_{4h} symmetry.[1,3] In the present investigation, the D_{4h} symmetry is assumed for cyclobutane and such a configuration exhibits 30 normal vibrations distributed as $3a_{1g} + 1\,a_{1u} + 1\,a_{2g} + 2\,a_{2u} + 2\,b_{1g} + 3\,b_{1u} + 3\,b_{2g} + 1\,b_{2u} + 3\,e_g + 4\,e_u$. The species a_{1g}, b_{1g}, b_{2g} and e_g are Raman active; a_{2u} and e_u are infrared active; a_{1u}, a_{2g}, b_{1u} and b_{2u} are inactive in both Raman and infrared.

The normal coordinate analysis of these two molecules has been carried out by Venkateswarlu and Bhamambal[4,5] and some of the molecular constants have been evaluated. However, no attempt has so far been made to evaluate the centrifugal distortion constants of these molecules. In the present investigation, these constants have been calculated for the first time, using the force constants evaluated on the basis of general valence force field. These constants may be useful to the investigators of the microwave spectra of these molecules.

Centrifugal distortion constants — The bonds between atoms in a molecule are not rigid. The interatomic distances will vary with the speed of rotation, giving rise to centrifugal distortion. According to the notation used by Kivelson and Wilson,[6] the Hamiltonian for the rotational energy of a semi-rigid molecule can be expressed as

$$\mathscr{H} = \frac{1}{2}\sum_{\alpha} \sigma_{\alpha\alpha}\, P_\alpha^2 + \frac{1}{4}\sum_{\alpha\beta\gamma\delta} \tau_{\alpha\beta\gamma\delta}\, P_\alpha\, P_\beta\, P_\gamma\, P_\delta$$

In the above equation, the first term on the right hand side represents the rigid rotor term, while the second term gives the correction for the centrifugal distortion effect. P_α is the operator for the component of the angular momentum along the α axis ($\alpha, \beta, \gamma, \delta = x, y$ or z), $\sigma_{\alpha\alpha}$ is a constant for a given vibrational state. The distortion coefficients $\tau_{\alpha\beta\gamma\delta}$ are given as

$$\tau_{\alpha\beta\gamma\delta} = -\frac{t_{\alpha\beta\gamma\delta}}{2\, I_{\alpha\alpha}\, I_{\beta\beta}\, I_{\gamma\gamma}\, I_{\delta\delta}}$$

Where I s are the principal moments of inertia evaluated at equilibrium. $t_{\alpha\beta\gamma\delta}$ are given in terms of partial derivatives of the inertia tensor. Cyvin *et al.*[7] have developed an easier method for the calculation of the centrifugal distortion constants in which $t_{\alpha\beta\gamma\delta}$ are given as

$$t_{\alpha\beta\gamma\delta} = T_s'\, \theta\, T_s$$

Where $\theta = G^{-1}\, F^{-1}\, G^{-1}$ and T_s is a matrix consisting of six columns $T_{xx,s}$, $T_{yy,s}$, $T_{zz,s}$, $T_{xy,s}$. $T_{yz,s}$ and $T_{zx,s}$. The column vectors $T_{\alpha\alpha,s}$ and $T_{\alpha\beta,s}$ are given as

$$T_{\alpha\alpha,s} = 2\, Bi^{\alpha\alpha} \cdot R^e$$

$$T_{\alpha\beta,s} = -Bi^{\alpha\beta} \cdot R^e$$

where B is the symmetry coordinate transformation matrix and R^e is a column vector, consisting of the equilibrium position vector components of the atoms ($3N$ elements), and $i^{\alpha\alpha}$ and $i^{\beta\beta}$ consist of N, (3×3) matrices, one for each atom along the main diagonal.

The centrifugal stretching coefficients D_j, D_k, D_{jk}, R_5, R_6 and δ_j are the linear combinations of $\tau_{\alpha\beta\gamma\delta}$ elements.

Results and discussion—The force constants and the molecular parameters used in this investigation have been taken from Refs. 4 and 5. The centrifugal distortion constants of C_4H_8 and C_4D_8 molecules are given in Table 1. They are observed to be low as expected from the consideration of the force constants of the molecules. The centrifugal distortion constants are characteristic of the force constants. In the case of C_4H_8 and C_4D_8 molecules, even though the C—H and C—D stretching force

Table 1—Centrifugal Distortion Constants ($\tau_{\alpha\beta\gamma\delta}$) of C_4H_8 and C_4D_8 Molecules in kHz

$\tau_{\alpha\beta\gamma\delta}$	C_4H_8	C_4D_8
τ_{xxxx}	−3·2119	−4·0363
τ_{xxyy}	−1·1994	−0·7244
τ_{xxzz}	−1·1372	−0·7510
τ_{xxxy}	0·0102	0·0332
τ_{xxyz}	−0·0008	−0·0056
τ_{xxzx}	−0·2000	−0·9893
τ_{yyyy}	−2·4511	−1·4588
τ_{yyzz}	−1·0071	−0·6238
τ_{yyxy}	−0·0556	−0·0717
τ_{yyyz}	0·0049	0·0049
τ_{yyzx}	−0·0046	−0·0077
τ_{zzzz}	−0·3310	−0·5275
τ_{zzxy}	−0·0399	−0·0335
τ_{zzyz}	0·0004	−0·0007
τ_{zzzx}	−0·0004	−0·0020
τ_{xyxy}	−0·4267	−0·1831
τ_{xyyz}	−0·0056	−0·0015
τ_{xyzx}	0·0018	−0·0006
τ_{yzyz}	−0·0418	−0·0144
τ_{yzzx}	−0·0120	−0·0118
τ_{zxzx}	−0·1046	−0·4571

constants have normal values, the C—C stretching force constant and the force constant corresponding to the out-of-plane bending of the ring are considerably low.[5,8,9] Thus cyclobutane and cyclobutane-d_8 possess a low rigidity and are more flexible for the bond elongation during the rotation of the molecule. According to the theory[7] of rotational distortion constants, the two important factors which govern the rotation are the force constants and the moments of inertia. The centrifugal distortion constants vary directly with the force constants and inversely with the fourth power of the moments of inertia. Hence the moments of inertia are the more predominant factors affecting the rotational distortion constants. The low force constants of the molecules result in higher values of the moments of inertia and lower values of the centrifugal distortion constants. In the case of ethylene oxide and ethylene oxide-d_4 molecules, which contain a three membered ring, the force constants are relatively higher[10] and consequently the centrifugal distortion constants are also high.[11]

The centrifugal stretching coefficients of cyclobutane and cyclobutane-d_8 are given in Table 2. It

Table 2—Centrifugal Stretching Coefficients of C_4H_8 and C_4D_8 Molecules in kHz

Coefficient	C_4H_8	C_4D_8
D_J	0·6967	0·5833
D_K	0·1702	0·1357
D_{JK}	0·7842	−0·5871
R_5	0·0078	0·0173
R_6	−0·0243	−0 0518
δ_J	0·0476	0·1611

is observed that D_J is positive in the case of both the molecules which indicates that the centrifugal forces about any given axis will always tend to increase the moment of inertia about that axis which in turn decreases the effective rotational constant. The values of D_J, D_K and D_{JK} are slightly larger in the case of C_4H_8 than in the case of C_4D_8 indicating that they are sensitive to the mass, varying inversely with the mass of the molecule. These molecules being symmetric top type, the coefficients R_5, R_6 and δ_J are very small.

Since no experimental values of the rotational constants of these molecules are available in the literature, it has not been possible to compare the calculated values with the experimental ones. However, from the fact that the centrifugal distortion constants yield a satisfactory set of force constants for these molecules, the former can be considered to be reliable in the absence of the experimental values. These centrifugal distortion constants, would be of much use in the microwave analysis of these molecules.

References

1. Krainov E P, Prokofeva N I & Sverdlov L M, *Optics Spectrosc.*, 16 (1964), 309.
2. Claassen H H, *J. chem. Phys.*, 18 (1950), 543.
3. Lord R C & Nakagava I, *J. chem. Phys.*, 39 (1963), 2951.
4. Venkateswarlu K & Bhamambal P, *Indian J. pure appl. Phys.*, 6 (1968), 530.
5. Bhamambal P, *Vibrations of polyatomic molecules and some studies in solvent effect* Ph D thesis, Kerala University, 1968.
6. Kivelson D & Wilson (Jr) E B, *J. chem. Phys.*, 20 (1952), 1575; 21 (1953), 1220.
7. Cyvin S J, Cyvin B N & Hagen G, *Z. Naturf.*, 23a (1968), 1649.
8. Fujiyama J & Shimanouchi T, *Spectrochim. Acta*, 20 (1964), 829.
9. Simanouti J, *J. chem. Phys.*, 17 (1949), 848.
10. Venkateswarlu K, Mariam S & Mariamma P, Mathew, *Proc. Indian Acad. Sci.*, 62 (1965), 159.
11. Ramasamy R & Srinivasacharya K G, *Curr. Sci.*, 47 (1978), 658.

Molecular Constants of Acetylenes Part-I Centrifugal Distortion Constants & Thermodynamic Functions of Ge H_3CCH & Ge D_3CCH

K Sabapathy, R Ramasamy & K Venkateswarlu

Department of Physics, P S G Autonomous College of Arts & Science, Coimbatore 641 014

Received 3 *December* 1978

The centrifugal distortion constants of germylacetylene and deuterated germylacetylene have been calculated for the first time using the potential energy constants and following the method suggested by Wilson and Kivelson and Cyvin *et al.* The thermodynamic functions of these molecules have also been evaluated for the ideal gaseous state at one atmospheric pressure for 12 temperatures ranging from 100 to 1000 K assuming an anharmonic and rigid rotor model of the molecule.

By analogy with methyl and silyl acetylenes, it is expected that germylacetylene would be a prolate symmetric top belonging to C_{3v} point group consisting of $5a_1+5e$ species. All the ten fundamentals are infrared and Raman active. The normal coordinate analysis of these two molecules has been carried out by Rao and Rai[1] and Venkateswarlu *et al.*[2] and some of the molecular constants have been evaluated. However, no attempt has so far been made to evaluate the centrifugal distortion constants of these molecules. In the present investigation, these constants have been calculated for the first time using the force constants evaluated on the basis of general valence force field. These constants may be useful to the investigators of the microwave spectra of these molecules.

The thermodynamic functions were calculated using the observed frequencies by Rao and Rai.[1] In the present investigation, the observed frequencies are corrected for the anharmonicity and the corrected frequencies are used to calculate the thermodynamic properties of these molecules.

Centrifugal distortion constants—The rotation distortion constants have been computed for these molecules for the first time using the general valence force field[2] and using the method given by Kivelson and Wilson and Cyvin *et al.*[3,4]

The centrifugal distortion constants $\tau_{\alpha\beta\gamma\delta}$ are related to the quantities $t_{\alpha\beta\gamma\delta}$ by the equation

$$t_{\alpha\beta\gamma\delta} = -2\ I^e_{\alpha\alpha}\ I^e_{\beta\beta}\ I^e_{\gamma\gamma}\ I^e_{\delta\delta}\ \tau_{\alpha\beta\gamma\delta}$$

where $\alpha,\beta,\gamma,\delta = x,y$ or z and I^e_{xx}, I^e_{yy}, I^e_{zz} are the principal moments of inertia at equilibrium. The quantities $t_{\alpha\beta\gamma\delta}$ are given by the matrix relation,

$$t = T_S^t\ \theta\ T_S$$

where T_S is a matrix consisting of the six columns $T_{xx,s}$, $T_{yy,s}$, $T_{zz,s}$, $T_{xy,s}$, $T_{yz,s}$ and $T_{zx,s}$ and are defined as,

$$T_{\alpha\alpha,s} = 2\ Bi^{\alpha\alpha}\ R^e$$

$$\tau_{\alpha\beta,s} = -\ Bi^{\alpha\beta}\ R^e$$

where B is the symmetry coordinate transformation matrix, R^e is a column vector composed of the equilibrium position vector components of the atoms and $i^{\alpha\alpha}$ and $i^{\alpha\beta}$ consist of N matrices, one for each atom along the main diagonal. T_S^t is the transpose of T_S. θ is given by the matrix relation

$$\theta = G^{-1}\ F^{-1}\ G^{-1}$$

The centrifugal stretching coefficients D_J, D_K, D_{JK}, R_5, R_6 and δ_J are the linear combination of the τ_s. These coefficients have been determined using the expressions given by Kivelson and Wilson.[3]

Results and discussion—The data necessary for the calculation of the centrifugal distortion constants have been taken from Ref. 2. The non-vanishing elements of the centrifugal distortion constants are presented in Table 1. The molecules being symmetric top rotors, the elements τ_{xxxx} and τ_{yyyy} are found to be equal. The rotational distortion constants are found to be, in general, small. This may be due to the fact that the major stretching force constants of these molecules are fairly high, which make the molecular bonds relatively rigid. No microwave analysis of these molecules has so far been made and hence it has not been possible to the authors to compare the calculated values with the observed ones. These results would be of much use in the microwave analysis of these molecules.

Table 1 — Centrifugal Distortion Constants in kHz

$\tau_{\alpha\beta\gamma\delta}$	GeH_3CCH	GeD_3CCH
τ_{xxxx}	−0·20368	−0·20921
τ_{xxyy}	−0·20473	−0·20702
τ_{xxzz}	−3·11224	−2·89760
τ_{xxzx}	−0·00112	−0·00502
τ_{yyyy}	−0·20725	−0·21014
τ_{yyzz}	−1·94971	−1·88142
τ_{yyzx}	−0·00662	−0·01419
τ_{zzzz}	−7965·04	−1845·85
τ_{zzzx}	−47·0839	−22·1074
τ_{xyxy}	−0·000009	−0·00003
τ_{xyyz}	−0·00033	−0·00057
τ_{yzyz}	−0·02823	−0·02636
τ_{zxzx}	−4·24162	−3·91726

Table 2—Centrifugal Stretching Coefficients in kHz

Coefficient	GeH_3CCH	GeD_2CCH
D_J	0·05132	0·05225
D_K	1987·909	458·347
D_{JK}	3·2984	3·0621
R_5	−0·5995	−0·5499
R_6	−0·00002	−0·00008
δ_J	−0·00022	−0·00006

Table 3 — Thermodynamic Functions of GeH_3CCH in cal deg^{-1} $mole^{-1}$

Temp., K	Heat content H	Free energy F	Entropy S	Heat capacity C_p
100	8·24	45·61	53·86	8·97
200	9·17	51·59	60·76	11·36
273·2	10·02	54·42	64·44	13·31
298·15	10·32	55·45	65·77	13·91
300	10·34	55·53	65·87	13·95
400	11·51	58·67	70·18	15·94
500	12·88	61·60	74·48	17·86
600	13·48	63·72	67·20	18·75
700	14·31	66·08	80·40	19.85
800	15·06	68·21	83·27	20·80
900	15·75	69·65	85·40	21·63
1000	16·37	71·30	87·67	22·36

Table 4 — Thermodynamic Functions of GeD_3CCH in cal deg^{-1} $mole^{-1}$

Temp., K	Heat content H	Free energy F	Entropy S	Heat capacity C_p
100	8·30	46·44	54·74	9·18
200	9·51	52·53	62·05	12·41
273·2	10·60	55·66	66·26	14·02
298·15	10·96	56·60	67·56	15·27
300	10·99	56·66	67·65	15·32
400	12·34	60·01	72·35	17·35
500	13·50	62·88	76·39	18·94
600	14·52	65·48	80·00	20·20
700	15·41	68·56	83·97	21·22
800	16·19	69·88	86·06	22·07
900	16·88	71·79	88·68	22·79
1000	17·52	73·66	91·18	23·40

The centrifugal stretching coefficients are given in Table 2. These are linear combinations of the τ elements. Since the molecules are symmetric top rotors, the coefficients R_6 and δ_J are vanishingly small.

The thermodynamic functions of GeH_3CCH and GeD_3CCH are presented in Tables 3 and 4 respectively.

References

1. Rao D U R A & Rai D K, *Curr. Sci.*, **37** (1968), 41.
2. Venkateswarlu K, Malathy Devi V & Natarajan A, *Proc. Indian Acad. Sci.*, **70** (1969), 126.
3. Kivelson D & Wilson (Jr) E B, *J. chem. Phys.*, **20** (1952), 1575; **21** (1953), 1220.
4. Cyvin S J, Cyvin B N & Hagen G, *Z. Naturf.*, **230** (1968), 1649.

Centrifugal Distortion Constants & Thermodynamic Functions of C_3H_6, C_3D_6 & C_3F_6

T A Karuppannan, R Ramasamy & K Venkateswarlu

Department of Physics, P S G Autonomous College of Arts & Science, Coimbatore 641 014

Received 21 *February* 1979

The centrifugal distortion constants and thermodynamic functions of cyclopropane, cyclopropane-d_6 and hexafluorocyclopropane, have been evaluated, for the first time, using spectroscopic data. The results have been discussed in relation to the structure and molecular weight.

Cyclopropane is a molecule of considerable interest as it is an important member of the series, cyclopropane-ethylene oxide-cyclobutene and cyclobutane. Recently, a number of workers[1-3] have studied the vibrational spectra of cyclopropane and its deuterated analogue. The normal coordinate analysis of these molecules has been carried out by Gunthard *et al.*[2] Cyvin[4] has obtained the potential constants and parallel mean-square amplitudes of cyclopropane. Venkataswarlu and Bhamambal[5] reported the generalized mean-square amplitudes of vibration and the complete set of Coriolis coupling constants for cyclopropane and cyclopropane-d_6.

The electron diffraction studies[6,7] of cyclopropane support the D_{3h} symmetry, which is also generally accepted in spectroscopic analysis. The fundamental frequencies are distributed into various species as

$$3a_1' + a_2' + 4e' + a_1'' + 2a_2'' + 3e''$$

The study of hexaflurocyclopropane seems to be very interesting, as it is one of the simplest derivatives of cyclopropane, from the standpoint of symmetry. Hexafluorocyclopropane is assumed to have the same symmetry D_{3h} as cyclopropane. Ito[8] and Miller and Hartman[9] made a more comprehensive study of this molecule. Venkateswarlu and Rudra Warrier[10] carried out the normal coordinate analysis

to obtain force constants, mean square amplitudes of vibration and Coriolis coupling constants.

In the present investigation, the centrifugal distortion constants and thermodynamic functions of cyclopropane, cyclopropane-d_6 and hexafluorocyclopropane are evaluated, for the first time, using the force constants obtained on the basis of general valence force field. The values of the centrifugal distortion constants can be used for the microwave spectral analysis of these molecules. The determination of the thermodynamic properties for a molecule has great practical importance since it is often difficult and sometimes impossible to measure these quantities experimentally.

Centrifugal distortion constants—The bonds between the atoms in a molecule are not rigid. As the molecule rotates, the interatomic distances increase with velocity of rotation, giving rise to centrifugal distortion. The centrifugal distortion constants $\tau_{\alpha\beta\gamma\delta}$ are related to the quantities $t_{\alpha\beta\gamma\delta}$ by the equation[11]

$$t_{\alpha\beta\gamma\delta} = -2\, I^e_{\alpha\alpha}\; I^e_{\beta\beta}\, I^e_{\gamma\gamma}\, I^e_{\delta\delta}\, \tau_{\alpha\beta\gamma\delta}$$

Here Is are the principal moments of inertia in equilibrium; $t_{\alpha\beta\gamma\delta}$ are given in terms of partial derivatives of the inertia tensor.

Recently, Cyvin *et al.*[12] have given an easier method for the evaluation of the centrifugal distortion constants by introducing a new matrix T_s, consisting of six columns $T_{xx,s}$, $T_{yy,s}$, $T_{zz,s}$, $T_{xy,s}$, $T_{yz,s}$ and $T_{zx,s}$. The column vectors $T_{\alpha\alpha,s}$ and $T_{\alpha\beta,s}$ are given as

$$T_{\alpha\alpha,s} = 2\, Bi^{\alpha\alpha}\, R^e$$

$$T_{\alpha\beta,s} = -\, Bi^{\alpha\beta}\, R^e$$

where B is the symmetry coordinate transformation matrix, R^e is a column vector composed of the equilibrium vector components of the atoms ($3N$ elements) and $i^{\alpha\alpha}$ and $i^{\alpha\beta}$ consist of N, 3×3 matrices, one for each atom along the main diagonal.

In terms of the T_s matrix, the t-matrix is given by

$$t = T_s'\, 0\, T_s$$

where,

$$\theta = G^{-1}\, F^{-1}\, G^{-1}$$

The centrifugal stretching coefficients D_J, D_K, D_{JK}, R_5, R_6 and δ_J are the linear combinations of $\tau_{\alpha\beta\gamma\delta}$ elements.

Thermodynamic functions—The Thermodynamic functions viz., heat content, free-energy, entropy and heat capacity for cyclopropane, cyclopropane-d_6 and hexafluorocyclopropane have been calculated, for twelve temperatures ranging from 100 to 1000 K, for

Table 1—$t_{\alpha\beta\gamma\delta}$ Elements of C_3H_6, C_3D_6 and C_3F_6 (Values amu^2 Å^3 m dyne^{-1})

$t_{\alpha\beta\gamma\delta}$	C_3H_6	C_3D_6	C_3F_6
t_{xxxx}	121·4243	402·3392	2385·273
t_{yyyy}	138·9087	527·9165	2867·032
t_{zzzz}	236·7320	1067·366	12696·13
t_{xyxy}	70·9459	151·1956	572·0435
t_{yzyz}	15·7557	38·7922	4734·960
t_{zxzx}	14·4566	37·6484	2031·938
t_{xxyy}	−1·4899	197·5671	1669 390
t_{xxzz}	110·7776	528·4415	2217·034
t_{yyzz}	128·4083	643·9997	3459·633

Table 2 – $\tau_{\alpha\beta\gamma\delta}$ Elements of C_3H_6, C_3D_6 and C_3F_6 (All values in kHz)

$\tau_{\alpha\beta\gamma\delta}$	C_3H_6	C_3D_6	C_3F_6
τ_{xxxx}	−35·3572	−32·7491	−0·0652
τ_{xxyy}	0·6912	−22·2978	−0·0449
τ_{xxzz}	−14·7020	−22·0427	−0·0623
τ_{xxxy}	0·1225	0·1204	0·0004
τ_{xxyz}	−0·0267	−0·0010	0·0003
τ_{xxzx}	−0·0242	0·0046	0·0003
τ_{yyyy}	−102·6785	−82·6136	−0·0757
τ_{yyzs}	−27·1524	−37·2472	−0·0955
τ_{yyxy}	−0·2518	−0·2154	−0·0006
τ_{yyyz}	−0·0426	−0·0013	0·0003
τ_{yyzx}	−0·1297	−0·0791	−0·0001
τ_{zzzz}	−14·3198	−22·8161	−0·3660
τ_{zzxy}	−0·1279	−0·1414	−0·0012
τ_{zzyx}	0	0	0
τ_{zzzx}	0·0034	0·0033	0·0001
τ_{xyxy}	−32·9145	−17·0642	−0·0154
τ_{xyyz}	−0·8994	−0·6473	−0·0121
τ_{xyzx}	0·2370	0·1531	0·0045
τ_{yzyz}	−3·3316	−2·2436	−0·1307
τ_{yzzx}	−0·0539	0·0302	0·0061
τ_{zxzx}	−1·9186	−1·5704	−0·0570

Table 3—Centrifugal Stretching Coefficients of C_3H_6, C_3D_6 and C_3F_6 (all values in kHz)

Coefficients	C_3H_6	C_3D_6	C_3F_6
D_J	5·8159	6·7832	0·0515
D_K	6·7472	2·8965	−0·0377
D_{JK}	13·1065	10·9737	0·0052
R_5	−1·3002	−0·6078	0·0082
R_6	−0·1969	−0·0812	−0·0012
δ_J	1·3148	0·6208	−0·0188

Table 4—Thermodynamic Functions of C_3H_6, C_3D_6 and C_3F_6 (Values in $cal^{-1}\ deg^{-1}\ mole^{-1}$)

Temp. K	Heat content	Free energy	Entropy	Heat capacity
		C_3H_6		
100	7·95	38·63	46·58	7·96
200	8·15	44·17	52·32	9·22
273·2	8·79	46·80	55·59	12·03
298·2	9·11	47·58	56·69	13·15
300	9·11	47·63	56·74	13·19
400	10·73	51·95	62·68	15·42
500	12·64	53·08	65·72	22·22
600	14·53	55·55	70·08	25·66
700	16·34	57·93	74·27	28·52
800	17·93	60·14	78·07	30·80
900	19·55	62·44	81·99	32·92
1000	20·98	64·57	85·55	34·71
		C_3D_6		
100	7·96	40·06	48·02	8·10
200	8 66	45·72	54·38	11·36
273·2	9·83	48·53	58·36	15 35
298·2	10·48	49·49	59·97	17·10
300	10·51	49·55	60·06	17·19
400	12·29	52 89	65·78	22·58
500	15·32	56·02	71·34	26·48
600	17·50	59·02	76·52	30·31
700	19·55	61·87	81·42	33·12
800	21·38	64·55	85·93	35·44
900	22·42	67·33	89·75	37·45
1000	24·60	69·76	94·36	39·00
		C_3F_6		
100	8·87	48·47	57·34	11·54
200	12·25	55·59	67·84	19·47
273·2	14·97	59·83	74·80	24·00
298·2	15·66	61·15	76·81	25·37
300	15·72	61·25	76·97	25·44
400	18·74	65·92	84·66	30·01
500	21·38	70·69	92·07	33·47
600	23·60	74·74	98·34	36·04
700	25·53	78·56	104·09	37·98
800	27·18	82·09	109·27	39·43
900	28·59	85·27	113·86	40·32
1000	29·70	88·14	117·84	40·54

ideal gaseous state at 1 atm pressure. The frequencies corrected for anharmonicity[4] have been used in the case of C_3D_6 and C_3H_6.

Results and discussion—The force constants and the molecular parameters used in these investigations have been taken from Refs. 4, 5 and 11. The *t* matrix elements and the centrifugal distortion constants of C_3H_6, C_3D_6 and C_3F_6 are presented in Tables 1 and 2 respectively. As per the theory developed by Cyvin *et al.*[12] for the evaluation of rotational distortion constants, the force constants and the moments of inertia of the molecule are the two important factorswhich govern the rotation of the molecule. The centrifugal distortion constants vary inversely with the first power of the force constants and the fourth power of the moments of inertia. The lower values of the moments of inertia for the molecules C_3H_6 and C_3D_6 account for the larger values of their centrifugal distortion constants, whereas comparatively larger value of the moment of inertia of the molecule C_3F_6 results in lower values for its centrifugal distortion constants.

The centrifugal stretching coefficients for the molecules C_3H_6, C_3D_6 and C_3F_6 are presented in Table 3. It is observed that the value of D_J is positive, for all the three molecules, which indicates that the centrifugal forces about any given axis will always tend to increase the moment of inertia about that axis which in turn decreases the effective rotational constant. The values of D_J, D_K and D_{JK} for the above three molecules are found to be in the decreasing order, indicating that they are sensitive to mass, varying inversely with the mass of the molecule. Since these molecules are asymmetric rotors, all the six centrifugal distortion coefficients exist.

Since no experimental values of the rotational constants of these molecules are available in the literature, it has not been possible to compare the calculated values with the experimental ones. However, as the force fields used in these evaluations fairly reproduce the observed vibrational frequencies, the present values of the centrifugal distortion constants may be considered to be sufficiently accurate.

The calculated values of the thermodynamic properties for the molecules C_3H_6, C_3D_6 and C_3F_6 are given in Table 4. At any given temperature, these values are found to be larger for molecules of greater mass.

References

1. Baker A W & Lord R C, *J. chem. Phys.*, 23 (1955), 1636.
2. Gunthard H H, Lord R C & McCubbin (Jr) T K, *J. chem. Phys.*, 25 (1956), 768.

3. Mathai P M, Shepherd G G & Welsh H L, *Can. J. Phys.*, 34 (1956), 1448.
4. Cyvin S J, *Spectrochim. Acta*, 16 (1960), 1022; 1421.
5. Venkateswarlu K & Bhamambal P, *Z. Naturf.*, 22b (1967), 945.
6. Skencke P N, Thesis, Technical University, Trondheim, Norway, 1960.
7. Bastiansen O, Fritsch F N & Hedberg K, *Acta Crystallogr.*, 17 (1964), 538.
8. Ito M, *Spectrochim. Acta*, 22 (1966), 1581.
9. Miller F A & Kenneth O, Hartman, *Spectrochim. Acta*, 23 (1967), 1609.
10. Venkateswarlu K & Rudra Warrier M K, *Indian J. pure appl. Phys.*, 11 (1973), 319.
11. Kivelson D & Wilson (Jr) E B, *J. chem. Phys.*, 20 (1952), 1575; 21 (1953), 1220.
12. Cyvin S J, Cyvin B N & Hagen G, *Z. Naturf.*, 23a (1968), 1649.

Microwave Conductivity & Relaxation Time of Polar Liquids

S K Ghosh, A K Ghosh & S Acharyya

Department of Physics, University College, Raiganj
West Dinajpur (W B)

Received 26 *August* 1978; *accepted* 20 *March* 1980

The hf conductivity K' of five polar liquids in benzene have been estimated for different weight fractions ω_j of polar solute under the application of 3·2 cm wavelength electric field. A simple formula in order to evaluate the exact value of τ_s the relaxation time of polar solutes in solution has been arrived at from Smyth's relation for K' for polar-nonpolar liquid mixture, to have further information regarding the structure of molecules. Values of τ_s calculated by this method are in close agreement with those reported in literature indicating the applicability of this simple method based on purely mathematical logic.

The relaxation time τ_s of polar solute in solvent can be computed by various methods—Gopala Krishna's[1] concentration variation method in the microwave region and the graphical method[2] in rf region, but both these methods invite a slight personal judgement to locate the exactness of the value of τ within a certain range. Recently in the process of derivation of the dipole moment μ of polar liquids in solvent from the rf conductivity, Ghosh *et al.*[3] observed that τ plays a very significant role in yielding the proper value of μ, which at once prompted us to devise a procedure to evaluate τ_s from the hf conductivity data based on sound mathematical foundation.

According to Murphy and Morgan,[4] the hf conductivity is a complex quantity given by $K=K'+jK''$ where K' is the real part of the conductivity :

$$K' = \frac{\omega\epsilon''}{4\pi} \qquad \ldots (1)$$

and K'' the imaginary part, ω the high frequency of the applied field and ϵ'' the dielectric loss.

In view of the scanty experimental data we have chosen the ϵ'' values of measured following Gopala Krishna's method for five polar liquids in benzene in the microwave region and calculated the values of K' as shown in Fig. 1. The very nature of the curves suggests that the hf K' can be represented by a fitted formula

$$K' = \alpha + \beta\omega_j + \gamma\omega_j^2 \qquad \ldots (2)$$

where ω_j is the weight fraction of the polar solute, α, β, γ are the arbitrary constants depending upon the nature of the respective solution of polar-nonpolar liquid mixture.

Now from Eq. (2)

$$\left(\frac{dk'}{d\omega_j}\right)_{\omega_j \to 0} = \beta \qquad \ldots (3)$$

The hf conductivity of solution of N_j number of solute molecules per cc $\left(N_j = \frac{Nd_{ij}}{M_j}\omega_j \right)$ is given by Ghosh *et al.*[3] as

$$K' = \frac{\mu^2 N d_{ij}}{3 M_j kT} \cdot \frac{(\epsilon_{ij}+2)^2}{9} \left(\frac{\omega^2\tau}{1+\omega^2\tau^2}\right)\omega_j = \frac{\mu^2 N d_{ij} F_{i\,j\omega}}{3 M_j kT} \left(\frac{\omega\tau}{1+\omega^2\tau^2}\right)\omega_j \qquad \ldots (4)$$

where N is the Avogadro's number; d_{ij}, density of solution; M_j, molecular weight of the solute; T=temperature in K; μ, dipole moment; ω, microwave frequency;

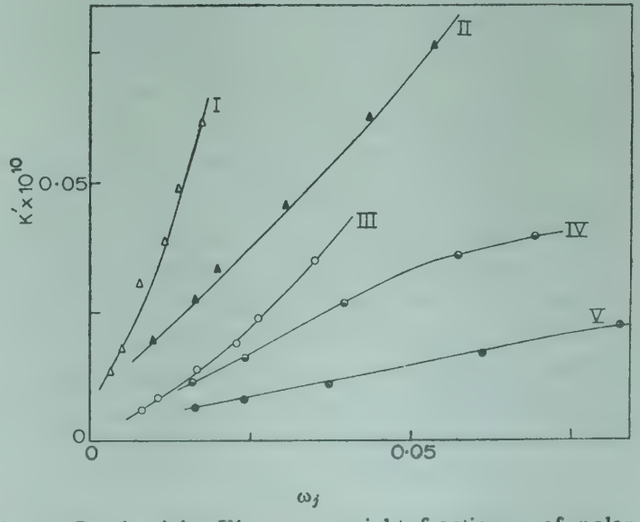

Fig. 1—Conductivity K' versus weight fraction ω_j of polar liquids in benzene at 28°C [I, nitrobenzene; II, ethyl benzoate; III, Methylacetate; IV,ben zophenone and V, acetone]

k, Boltzmann's constant and F_{ij} local field $(\epsilon_{ij}+2)^2/9$ where ϵ_{ij} is the dielectric constant of solution. On differentiation with respect to ω_j and under the conditions $\omega_j \to 0$, $d_{ij} \to d_i$ and $F_{ij} \to F_i$, Eq. (4) becomes

$$\left(\frac{d\,k'}{d\,\omega_j}\right)_{\omega_j \to 0} = \frac{\mu^2\, N\, d_i\, F_j}{3\, M_j\, kT}\,\omega\left(\frac{\omega\,\tau_s}{1+\omega^2\,\tau_s^2}\right)$$

$$= R\,\omega\left(\frac{\omega\,\tau_s}{1+\omega^2\tau_s^2}\right) \qquad \ldots (5)$$

where $R = \dfrac{\mu^2\, N d_i\, F_i}{3\, M_j\, kT}$

Now from Eqs. (3) and (5) we can write:

$$\frac{\omega\,\tau_s}{1+\omega^2\,\tau^2} = \frac{\beta}{R\omega}\; b \text{ (say)} \qquad \ldots (6)$$

which is a quadratic equation in $\omega\tau_s$, the solutions being

$$\omega\,\tau_s = \frac{1 \pm \sqrt{1-4\,b^2}}{2\,b} \qquad \ldots (7)$$

usually giving the two real or imaginary values of τ_s at a single frequency ω.

A linear least square fitting was made on the available experimental data of the following systems (i) nitrobenzene (ii) ethyl benzoate (iii) methyl acetate (iv) benzophenon and (v) acetone, dissolved in benzene at 28°C, to evaluate β by using Cramer's rule in Eq. (2) for K'. Hence the value of b was determined in each case and presented in Table 1 along with the τ_s values and the reported ones according to Gopala Krishna's method and others. Eq. (7) gives two real values of τ_s, the lower values of which agree with the reported ones while the other is large. Sometimes the value of $\omega\tau_s$ comes out to be imaginary as seen in the system ethyl benzoate and benzophenon in benzene. Thus to get a unique value of τ_s in all cases, Eq. (6) has been converted into a linear one by considering $\omega\tau_s = \tan\theta$, where θ is any arbirary value given by $\theta = \frac{1}{2}\sin^{-1} 2b$, so that $\omega\tau_s = \tan(\frac{1}{2}\sin^{-1} 2b)$. The values of τ_s thus calculated are also shown in Table 1.

The accurate value of τ_s of the polar solute is of much importance as it throws much light on the structure of the molecule concerned. The molecular diameter of the polar solute can be computed from the kinetic relation $a_0 = (3\,M_j/4\pi\,N\rho)^{1/3}$, where M_j is the molecular weight, ρ the density of the liquid and a_0 the molecular radius. But according to Smyth[5] the molecular radius a_s involved in the relaxation phenomenon is that along the axis in which the molecular dipoles lie; by assuming the dipolar molecule to be a sphere of radius a_s moving in a continuous viscous fluid possessing a coefficient of internal friction η, we obtained $\tau_s = 4\pi\eta a_s^3/kT$. Though this relation between τ_s and η is not an accurate one,[6] still we have calculated a_s for five polar solutes from the τ_s values determined by us and shown in Table 1 for comparison.

Table 1—Calculated Values of b and τ_s for Different Systems at 28°C

System	b	$\tau_s \times 10^{12}$ From: Eq. (7)	$\omega\,\tau_s = \tan(\frac{1}{2}\sin^{-1} 2\,b)$	Gopala Krishna's method	Others	$a_s \times 10^8$ [calc. from τ_s]	$a_0 \times 10^8$ [calc. from kinetic theory]	Ratio of a_s and a_0
Nitrobenzene	0·4901	13·80, 20·78	13·8	12·3	11·6 to 13·0	1·9871	3·4425	0·57784
Ethyl Benzoate	0·8046	imaginary	8·54	11·8	12·0 to 17·6	1·6950	3·8538	0·43984
Methyl Acetate	0·1260	2·17, 132·60	2·17	2·2	2·5 to 3·1	1·0735	3·1671	0·33894
Benzophenone	0·5508	imaginary	18·78	18·3	17·4 to 22·0	2·2042	4·0405	0·54550
Acetone	0·0856	1·46, 197·00	1·46	2·2	2·5 to 3·13	0·9405	3·0874	0·30463

For the system under consideration a_s/a_0 are found to lie between 0·3 to 0·6 (Table 1) showing that the molecular radius of the solute under the application of 3·2 cm wavelength electric field is always less than vapour kinetic value, while in case of vapours, according to Maryott and Kryder,[7] the molecular radius is always greater. The reason behind this observed result is, however, not known but may be attributed to the weak collisions among fluid molecules when placed in the microwave electric field. Thus the microwave conductivity still offers an advantageous tool to estimate the molecular radius along the axis of the dipole and thereby shows that a part, and not the whole, of the molecule is rotating under the influence of the microwave field.

References

1. Gopala Krishna K V, *Trans. Faraday Soc.*, **53** (1957), 767.
2. Sen S N & Ghosh R, *Indian J. pure appl. Phys.*, **10** (1972), 701.

3. Ghosh A K & Acharyya S, *Indian J. pure appl. Phys.*, **15** (1977), 667.

4. Murphy F J & Morgan S O, *Bell Syst. tech. J.*, **18** (1939), 502.

5. Smyth C P, *Dielectric behaviour and structure* (McGraw Hill, New York), 1955.

6. Debye P, *Polar molecules*, (Chemical Catalog Co., New York), 1929.

7. Marryot A A & Kryder S J, *J. chem. Phys.*, **31** (1959), 617.

Substituent Group Effects on NQR Frequency of Br in Certain Bromomethane Derivatives

C V L Narasimha Rao & D Premaswarup

Department of Physics, Nagarjuna University
Nagarjunanagar 522 510

Received 26 *November* 1979

The empirical additive relationship for the NQR frequencies of substituted bromomethanes has been used to evaluate the m_i parameters of the substituent groups. A comparison of the m_i values so obtained with similar substituent parameters for chloromethanes and chloro- and bromobenzenes is used to conclude that : (1) the shift in frequencies due to substituent groups is additive only to a first approximation, and when there are two or more substituent groups their interactions are also to be considered, and (2) the shift in frequency depends on the nature of the substituent group, on the nature of the resonating nucleus and its resonant frequency in a monosubstituted compound, and the distance and the linkage between the substituent group and the resonating nucleus.

As early as 1952 it was realized that the shifts of the NQR frequencies of substituted chlorobenzenes from the NQR frequency of chlorobenzene are additive functions of the substituent groups, to a first order of approximation. While Bray and Barnes[1] suggested that the shifts due to different substituents are proportional to their Hammett σ parameters,[2] Beidenkapp and Weiss[3] introduced empirical parameters k_i, which are not strictly proportional to σ_i. In their notation, the frequency of a substituted chlorobenzene compound is given by

$$\nu = \nu_0 + \sum_i k_i \qquad \ldots (1)$$

A similar relation for substituted bromobenzenes was tested with satisfactory results by Rangacharyulu and Premaswarup[4]; while Ramanamurti *et al.*[5] tested a similar relation for the chloromethanes. As an extension of this work, the relation is tested for bromomethanes in the present study.

NQR frequencies are available for 12 bromomethanes in literature.[6–8] The twelve compounds involve 6 substituent groups. The experimental frequencies observed at 77 K are used to calculate the values of the parameters m_i in relation (1) corresponding to bromomethane, i.e.

$$\nu = \nu_0 + \sum_i m_i \qquad \ldots (2)$$

where ν is the NQR frequency of the bromine nucleus in the compound, ν_0 the NQR frequency of the bromomethane and m_i parameters characteristic of the substituents and the summation is over all substituent groups. All the experimental frequencies refer to the ^{79}Br nucleus. In a few cases where frequencies are available for the ^{81}Br only, the corresponding frequencies for ^{79}Br are obtained by multiplying the ^{81}Br frequencies by the factor 1·19707 which represents the ratio of the quadrupole moments of the two nuclei.[9] Whenever there is a splitting of the NQR line due to crystal field effects, the arithmetical mean of all the close-lying frequencies is taken as the NQR frequency. The calculated values of m_i (indicated as $m_{i\ \mathrm{bromo}}$) are given in Table 1, where they are compared with similar values in chloromethanes ($m_{i\ \mathrm{chloro}}$), chlorobenzenes ($k_{i\ \mathrm{chloro}}$) and bromobenzenes ($k_{i\ \mathrm{bromo}}$). In Table 2 experimentally observed frequencies of the bromomethanes are compared with those calculated from

Table 1—Calculated m_i Values in Chloro- and Bromomethanes and Benzenes

Substituent	$m_i$bromo	$m_i$chloro (Ref.5)	$k_i$bromo (Ref. 4)			$k_i$chloro (Ref. 8)			$\frac{m_i\text{bromo}}{m_i\text{chloro}}$	$\frac{k_i^{\text{ortho}}\text{bromo}}{k_i^{\text{ortho}}\text{chloro}}$	$\frac{k_i^{\text{ortho}}\text{bromo}}{m_i\text{bromo}}$	$\frac{k_i^{\text{ortho}}\text{chloro}}{m_i\text{chloro}}$
			ortho	*meta*	*para*	*ortho*	*meta*	*para*				
Br	17·046	2·103	11·58	5·11	2·37	0·975	0·449	0·312	8·1056	11·8769	0·6793	0·4636
COOH	21·377	1·958	10·60	2·79	0·83	1·704	0·377	0·409	10·9178	6·2207	0·4959	0·8703
CH_3	−9·142	−0·865	−2·53	−2·64	—	−0·392	−0·207	−0·004	10·5688	6·4541	0·2767	0·4532
NO_2	31·679	3·216	26·52	13·19	4·71	2·096	1·069	0·607	9·8504	12·6527	0·8371	0·6517
F	11·042	1·139	—	—	—	1·603	0·548	0·413	9·6945	—	—	1·4074
COBr	−24·903	—	—	—	—	—	—	—	—	—	—	—

Table 2 — Observed and Calculated NQR Frequencies

Compound	Substituent	$\Sigma_i m_i$	$\nu_{obs.}$	$\nu_{calc.}$	$\Delta\nu$ (μ obs. $-\mu$calc.)
		value	MHz	MHz	MHz
Br. CH_3	—	0	264·508	—	—
Br. CH_2. Br	Br	17·046	281·554	—	—
Br. CH_2. COOH	COOH	21·377	285·885	—	—
Br· CH_2. COBR.	COBr	−24·903	239·605	—	—
Br. CH. Br_2.	Br_2	34·092	300·529	298·600	1·929
Br. CH. CH_3.-	CH_3+	12·235	276·743	—	—
COOH	COOH				
Br. C. F_3	F_3	33·128	301·976	297·636	4·340
Br. C. Br_3	Br_3	51·138	320·814	315·646	5·168
Br.C. $(NO_2)_3$	$(NO_2)_3$	95·037	359·394	359·545	0·151
Br.C. Br. F_2	Br+F_2	39·13	303·639	—	—
Br. C. Br. $(NO_2)_2$	Br+ $(NO_2)_2$	80·404	344·913	—	—
Br. C. F. Br_2	F+Br_2	45·134	310·616	309·642	0·974

Eq. (2) above. Such a comparison is omitted in those cases where the observed frequencies are used to calculate the m_i values.

Table 2 indicates a rather large disagreement between calculated and observed frequencies. By far, the largest deviations occur in the case of the compounds where all the 4 hydrogen atoms are replaced by substituent groups. In general, the comparison indicates that the purely additive relationship is only very approximate. For a more accurate relationship one will have to consider the interactions of the substituents among themselves which necessitates the availability of frequencies for a very large number of compounds. In the present case, with frequencies available for only a very limited number of compounds this is not possible.

A second comparison that can be made is the relative m_i and k_i values for the same substituent in chloro and bromo compounds of methanes and benzenes. All these values as well as some ratios are given in Table 1. In general, one finds that the effect of the substituent is greater in methanes than in benzenes. This is presumably due to the shorter distance between the bromine nucleus and the substituent group in methanes than in benzenes. The gradation of the k_i values for the same group in *ortho*, *meta* and *para* positions in the benzene ring also arises from the same cause. That the distance between the groups is not the only factor but is only one of the factors affecting the interactions is evident from the widely varying ratios of k_i to m_i for different substituents. The ratio of the m_i values in bromomethanes to that in chloromethanes is nearly equal for all the groups and is of the same order of magnitude as the ratio of ν_0 for bromo- and chloromethanes (7·783). However, similar ratios for the benzene ring substituents are more widely varying among themselves. This may be due to the fact that in chloro- or bromobenzenes the resonating nucleus and the substituent group are separated through two or more carbon atoms, while in the methane compounds they are linked only through one carbon atom and are also at a comparatively much shorter distance. Correspondingly, the effect of distance is proportionately larger in the methane compounds and hence they show a more constant ratio while in the benzene compounds the distance effect is smaller, the shift in the frequency due to other effects is larger and hence the ratios are more widely varying.

One of the authors (CVLNR) is thankful to the Nagarjuna University authorities, for the award of a research fellowship, making this work possible.

References

1. Bray P J & Barnes RG, *J. chem. Phys.*, 22 (1954), 2023.
2. Hammett L P, *Physical organic chemistry* (Mc-Graw Hill, New York), 1940.
3. Biedenkapp D & Weiss A, *J. chem. Phys.*, 49 (1968), 3933.
4. Rangacharyulu M & Premaswarup D, *Indian J. pure appl. Phys.*, 13 (1975), 302.
5. Ramanamurti D V, Venkatacharyulu P & Premaswarup D, *J. Org. Magn. Resonance*, 12 (1979), 655.
6. Segel S L & Barnes R G, *Catalog of nuclear quadrupole interactions and resonance frequencies in solids*, 1965.
7. Biryukov I P, Vorenkov M G & Safin I A, *Tables of NQR frequencies*, Israel Programme for Scientific Translations, 1969.
8. Ramanamurti D V, ^{35}Cl *NQR Investigations in certain molecular crystals*, Ph D thesis, Andhra University, Waltair, 1976.
9. Townes C H & Schawlow A L, *Microwave spectroscopy* (Mc-Graw Hill, New York), 1955.

Acoustic Behaviour of Electrolytic Solutions in Alcohols

SHEO PRAKASH, S SINGH, A PRAKASH, S K SINGH & A KUMAR

Chemistry Department, Allahabad University, Allahabad

Received 5 *February* 1979; *revised received* 21 *March* 1979

Ultrasonic velocity v and density measurements have been used to calculate isentropic compressibility (β_s), intermolecular free length (L_f), specific acoustic impedance (Z), molar sound velocity (R), apparent molal compressibility (ϕ_k), and solvation number (S_n) of solutions of zinc nitrate and lanthanum nitrate in methanol and ethanol. In each case, v increases and β_s and L_f decrease with the increase in

molar concentration of solutions. As usual, ϕ_k has been found to be negative in both the cases. S_n too varies with the change in concentration of the solutions but there is no regular trend. The results have been interpreted in terms of modern concepts regarding acoustic properties of solutions.

The compressibility of dilute aqueous solutions of electrolytes decreases with concentration indicating a strong interaction of the dissolved ions with the water molecules. Much work has been done on ultrasonic studies in aqueous solutions. The non-aqueous solutions of electrolytes have drawn the attention of some workers.[1-5] In this note, we are reporting the findings of a study of ultrasonic velocity, isentropic compressibility, intermolecular free length, molar sound velocity, specific acoustic impedance, apparent molal compressibility and solvation number of lanthanum and zinc nitrates in methanol and ethanol.

Zinc nitrate and lanthanum nitrate used for preparation of salt solutions in methanol and ethanol were of BCPW grade. They were fused cooled in vacuum desiccator and lumps of the fused salts were powdered and reheated in glass vial up to 105°C in the case of zinc nitrate, and up to 150°C in the case of lanthanum nitrate. The process was repeated till the weight becomes constant and then the salt was stored in a vacuum desiccator for further use. Methanol (BCPW grade) and ethanol from BDH (analaR grade) were further purified by standard methods; their densities agreed with those of literature values. The solutions were prepared by dissolving the accurately known weight of the salt in liquid and kept for some time. The densities were determined pyknometrically with an accuracy of 1 in 10^4. A continuous wave interferometric technique was employed for the measurement of the ultrasonic velocity at 2 MHz. The results of the experiments have been presented in Tables 1-3.

For any homogeneous non-dissipative fluid system, the velocity v of a compressional acoustic wave is related to the density ρ and the isentropic compressibility β_s by the equation

$$v = (\rho\, \beta_s)^{-1/2} \qquad \ldots(1)$$

Table 1—Ultrasonic Velocity and Other Related Parameters for $La(NO_3)_3$

Conc. (moles/1)	Velocity (m/sec)	Density (g/ml)	$\beta_s \times 10^{12}$ (cm^2 $dyne^{-1}$)	L_f (Å)	Solvation number (S_n)	Molar sound velocity (R)	$Z \times 10^{-5}$ (c g s units)	$\phi_k \times 10^9$ (cm^2 $dyne^{-1}$)
in methanol (32°C) $\beta_{s,0} = 107{\cdot}45 \times 10^{-12}$ cm^2 $dyne^{-1}$								
0·0224	1093	0·7876	106·28	0·6525	12·06	422·50	0·861	−54·27
0·0285	1094	0·7893	105·85	0·6512	12·96	422·66	0·863	−56·39
0·0353	1094	0·7913	105·59	0·6504	12·10	422·93	0·866	−51·18
0 0432	1095	0·7934	105·11	0·6489	12·34	422·94	0·869	−51·12
0·0541	1098	0·7972	104·04	0·6456	14·34	423·01	0·875	−61·33
0·0820	1100	0·8013	103·13	0·6428	12·26	424·85	0·881	−45·11
0·1040	1104	0·8077	101·58	0·6379	12·81	425·92	0·892	−47·91
0·1280	1106	0·8132	100·52	0·6346	12·27	426·93	0·899	−44·75
0·1600	1108	0·8216	99·14	0·6302	11·78	427·61	0·910	−42·63
0·2000	1113	0·8395	96·15	0·6206	12·81	424·97	0·934	−52·39
in ethanol (32°C) $\beta_{s,0} = 100{\cdot}50 \times 10^{-12}$ cm^2 $dyne^{-1}$								
0·0224	1131	0·7855	99·52	0·6314	7·53	615·87	0·888	−47·81
0·0285	1132	0·7879	99·04	0·6299	8·75	615·48	0·892	−58·52
0·0353	1133	0·7924	98·31	0·6276	10·53	613·68	0·898	−77·67
0·0432	1134	0·7932	98·04	0·6267	9·63	614·97	0·899	−65·99
0·0541	1134	0·7969	97·58	0·6252	9·11	614·48	0·904	−63·04
0·0820	1136	0·8017	96·65	0·6223	8·30	616·69	0·911	−51·53
0·1040	1139	0·8066	95·56	0·6182	8·00	618·55	0·919	−48·63
0·1280	1140	0·8133	94·61	0·6157	7·74	618·65	0·927	−47·53
0·1600	1142	0·8229	93·18	0·6110	7·69	618·38	0·939	−48·16
0·2000	1143	0·8329	91·89	0·6067	7·24	619·25	0·952	−44·89

Table 2—Ultrasonic Velocity and Other Related Parameters for $Zn(NO_3)_2$

Conc. (moles/l)	Velocity (m/sec)	Density (g/ml)	$\beta_s \times 10^{12}$ (cm^2 $dyne^{-1}$)	L_f (Å)	Solvation number (S_n)	Molar sound velocity (R)	$Z \times 10^{-5}$ (c g s units)	$\phi_k \times 10^9$ (cm^2 $dyne^{-1}$)
in methanol (32°C) $\beta_{s,0} = 106{\cdot}30 \times 10^{-12}$ cm^2 $dyne^{-1}$								
0·0224	1101	0·7847	105·12	0·6490	11·18	424·10	0·864	−47·22
0·0285	1102	0·7855	104·83	0·6481	12·00	424·50	0·866	−44·18
0·0353	1103	0·7873	104·40	0·6467	12·45	424·76	0·868	−47·75
0·0435	1104	0·7893	103·90	0·6452	12·80	424·91	0·871	−50·87
0·0541	1105	0·7904	103·62	0·6443	11·41	425·19	0·873	−41·58
0·0820	1108	0·7920	102·84	0·6419	9·89	427·65	0·877	−29·79
0·1040	1108	0·7950	102·45	0·6406	8·47	428·73	0·881	−22·90
0·1280	1113	0·7991	101·02	0·6362	9·45	429·84	0·889	−28·00
0·1600	1114	0·8038	100·24	0·6337	8·69	431·00	0·895	−24·66
0·2000	1121	0·8096	98·29	0·6275	9·18	433·19	0·908	−26·80
in ethanol (32°C) $\beta_{s,0} = 100{\cdot}50 \times 10^{-12}$ cm^2 $dyne^{-1}$								
0·0224	1133	0·7829	99·50	0·6314	8·38	616·65	0·887	−42·63
0·0285	1135	0·7849	98·89	0·6294	10·20	616·59	0·891	−57·46
0·0353	1136	0·7857	98·62	0·6286	9·52	617·22	0·892	−54·34
0·0435	1138	0·7876	98·04	0·6267	9·99	617·33	0·896	−54·49
0·0541	1139	0·7896	97·62	0·6254	9·27	617·63	0·899	−49·58
0·0820	1139	0·7919	97·33	0·6245	6·85	619·81	0·902	−30·62
0·1040	1140	0·7943	96·87	0·6230	6·03	821·94	0·905	−23·70
0·1280	1143	0·7980	95·92	0·6199	6·14	623·41	0·912	−24·49
0·1600	1144	0·8020	95·27	0·6178	5·60	624·90	0·917	−20·60
0·2000	1150	0·8068	93·72	0·6128	5·78	628·20	0·928	−21·09

Table 3—Values of ϕ_k^0 and the Constants A and B of Bachem's Relation

System	A	B	ϕ_k^0
$La(NO_3)_3$ in methanol	−58·50	20·63	−51·00
$La(NO_3)_3$ in ethanol	−56·50	26·84	−63·00
$Zn(NO_3)_2$ in methanol	−43·88	14·25	−40·50
$Zn(NO_3)_2$ in ethanol	−41·50	16·77	−32·75

Thus the variation of velocity (v) with concentration C in an electrolytic solution depends on the concentration derivatives of ρ and β_s as follows:

$$\frac{dv}{dC} = -\frac{v}{2}\left(\frac{1}{\rho}\frac{d\rho}{dC} + \frac{1}{\beta_s}\frac{d\beta_s}{dC}\right) \qquad ...(2)$$

The quantity $d\rho/dC$ is always positive while $d\beta_s/dC$ appears to be negative for ionic solutions as in the present case. Since these factors have opposite signs, the velocity may either increase or decrease with concentration.

The isentropic compressibility of solutions is found to obey Bachem's relation $\beta_s = \beta_{s,0} + AC + BC^{3/2}$, where $\beta_{s,0}$ is the compressibility of solvents, C is the molar concentration, A and B are constants. The values of A and B have been determined with the help of the graph and are given in Table 3. As usual, the values of A are negative.

Intermolecular free length is given by $K\sqrt{\beta_s}$, where K is a temperature-dependent constant.[6] The compressibility decreases with concentration and hence free length also decreases with increase in concentration (Tables 1 and 2). Specific acoustic impedance has been found to increase with increasing concentration.

If n_1 moles of the solute of molecular weight M_1 has been dissolved in n_2 moles of solvent of molecular weight M_2, the molar sound velocity R of the solution is given by

$$R = \left(\frac{\bar{M}}{\rho}\right)v^{1/3} \qquad ...(3)$$

where $\bar{M} = \sum \frac{M_i n_i}{n_i}$ and ρ is the density of the solution.

INSTRUCTIONS TO CONTRIBUTORS

Manuscripts should be typewritten in double space and on *only one side* of good quality paper; the original and *one carbon copy are to be submitted.*

Papers must be written in clear and concise English. Good attention to spelling and grammar should be given. Long introductions should be avoided. Standard international nomenclature should be followed in giving names of chemical compounds. Standard abbreviations for units of measurement should be used in the text, tables and illustrations. The abbreviations should be used without fullstops.

Title—The title should be neither too brief/general nor unnecessarily long. It should reflect the content of the paper so as to derive the maximum advantage in indexing and information retrieval. A short title for use as running title should also be supplied. If a paper forms part of a series, a subtitle indicating the aspects of the work covered in the paper should be provided.

Abstract—The abstract should indicate the scope of the work and the principal findings of the paper. It should not exceed 3% of the length of the paper and, barring exceptional cases, it should not exceed 200 words. The abstract should be prepared in such a form that abstracting periodicals can use it without modification.

Data—Only such primary data as are essential for understanding the discussion and the main conclusions emerging from the study should be included. All such secondary data as are of interest to a specific category of readership may, if necessary, be deposited in the editorial office (or retained by the authors) for supply on demand. A footnote to this effect may be inserted at a suitable place in the paper.

Mathematical portions—Special attention should be given to the mathematical portions of the paper. Equations must be well separated from the text and written clearly with good separation between the successive lines. The usual norms of breaking long mathematical expressions may be adhered to. Equations should be numbered consecutively in Arabic numerals with the number in parentheses near the right hand margin. Superscripts and subscripts should be clearly indicated in pencil by V and Λ sign respectively. Capital and small letters, particularly of the same letter when both occur, as well as letters or symbols likely to be confused one for the other, should be clearly distinguished. Special characters (e.g. Greek, script, vector, tensor, matrix, etc.) required must be indicated by marginal notes. Letters and symbols which should appear in bold face must be clearly indicated. To simplify typesetting: (i) long and complicated mathematical expressions which are frequently repeated should be replaced with single letter/symbol, without clashing with the others used in the paper; (ii) the "exp" form of complex exponential functions should be used; and (iii) to simplify fractions, the solidus (/) is to be used and fractional exponents are to be used instead of root signs, e.g.

write $\left(4\omega_{pl} K_{3\lambda}^2 \Big/ \tilde{\omega}\ K_D^2\right)^{1/2}$ and *not* $\sqrt{4\,\frac{\omega_{pl} K_{3\lambda}^2}{\tilde{\omega}\, K_D^2}}$

write $\exp\{-j\omega_0 (t_1 - t_2)/2\}$ and *not* $e^{-j\omega_0 (t_1 - t_2)/2}$

Tables—Tables should be typed *on separate sheets* of paper without any text matter on the page. They should be numbered consecutively in Arabic numerals and should bear brief titles. *Column headings should be brief.* Units of measurements should be abbreviated and placed below the headings. Nil results should be indicated and distinguished clearly from absence of data. Graphs as well as tables, both representing the same set of data, must be strictly avoided. Inclusion of structural formulae inside the tables should be avoided as far as possible. Tables should be referred to in the text by numbers and not by terms like 'above', 'below', 'preceding' or 'following'.

Illustrations—All illustrations should be numbered consecutively in Arabic numerals. Captions and legends to the figures should be self-explanatory and should be typed on a separate sheet of paper and attached at the end of the manuscript. Line drawings should be made with Indian ink on white drawing paper (perferably Bristol board), cellophane sheet or tracing cloth. In addition to the originals, a set of blue-prints or photostat copies should be sent. For satisfactory reproduction, the graphs and line drawings should be drawn to approximately twice the printed size.

The lettering should be uniform, perferably in stencil, so as to be *not less than 2 mm after reduction* widthwise to 3″ or 6″ as required. The size of geometrical shapes (used to distinguish different graphs), dot, lines, etc. should be sufficiently large to permit the necessary reduction without loss of detail. In the case of *photographs*, prints *must be on glossy paper and contrasty*. If an illustration is taken from another publication, reference to the source should be given and prior permission secured. Illustrations should be protected by thick cardboard packing against creases, folds and broken corners during transit. Illustrations should be referred to in the text by numbers and not by terms like 'above', 'below', 'preceding' or 'following,.

Infrared, ultraviolet, NMR and other spectra, DTA curves, etc. should be included only if they pertain to new compounds and/or are essential to the discussion; otherwise only significant numerical data should be included in the text.

References—The list of references should be prepared strictly in accordance with the style followed

in the Journal. In the text, references to literatures should be numbered consecutively, in the order of their first occurence, and should be indicated by superscripts at the relevant places; as far as possible the placement of references on numerals of other symbols should be avoided; in such cases the reference may be given in parentheses in running text, e.g. "this yielded for n a value of 2·3 (Ref. 5)". Full bibliographic details for all the references mentioned in the text should be listed in serial order at the end of the paper.

In citing references to research papers, names and initials of authors should be followed, in order, by the title of the periodical in the abbreviated form (underlined), the volume number (two lines underneath), the year within circular brackets and the page reference [e.g. Venkatesh, H G & Guha Sarkar, G, *Indian J. pure appl. Phys.*, **12** (1974), 502]. For names of periodicals, the standard abbreviations listed in the *World list of scientific periodicals* edited by P Brown & G B Stratton (Butterworths & Co. Ltd, London), 4th Edition, 1963-65, should be used. If the reference is to an article published without any authorship in a periodical, the title of the article takes the place of the author in the citation [e.g. The content, influence and value of scientific conference papers and proceedings. *Unesco Bull. Libr.*, **16** (1952), 113-26.]. If a paper has been accepted for publication, the names of the authors and the journals should be given followed by the words "in press" within circular brackets [e.g. Sastry, B. A. & Sastry, G. S., *Physica*, (in press).].

In the list of references, unpublished work, accepted papers in press and personal communications should be clearly distinguished.

Even if a reference contains more than two authors, the names of all the authors with their respective initials should be given. The abbreviations *et al.*, *idem* and *ibid* should be avoided.

Reference to a book should include details in the following order: names and initials of authors, the title of the book (underlined), name of publisher and place of publication within circular brackets and year [e.g. Herzberg, G, *Spectra of diatomic molecules* (D Van Nostand & Co. Inc., New Jersey), 2nd Edn, 1950, 31.]. If the reference is to the work of an author published in a book by a different author or edited by a different person, the fact that it is cited from the source book should be clearly indicated [e.g. Garlick, G F J, cited in *Encyclopedia of Physics*, Vol. 26—*Light and matter* II, edited by S Flugge (Springer Verlag, Berlin), 1958, 1.].

Proceedings of conferences and symposia should be treated in the same manner as books. Reference to a paper presented at a conference, the proceedings of which are not published, should include, in the following order, names and initials of authors, title of the paper (underlined), name of the conference, place where the conference was held and date (Deekshitulu, B L, *Design and fabrication of drum scanner for picture processing*, paper presented in the Symposuim on Applied Optics, Indian Institute of Science, Bangalore, 28-30 Nov. 1974).

Reference to a thesis should include the name of the author, title of the thesis (underlined), university or institution to which it was submitted and year of submission (e.g. Chandrasekaran, K S., *Studies on crystal structure and absolute configuration of crystals*, Ph. D. thesis, Madras University, 1956).

Reference to a patent should include names of patentees, country of origin (underlined) and patent number, the organization to which the patent has been assigned within circular brackets, data of acceptance of the patent and reference to an abstracting periodical where available [Trepagnier, J H, *US Pat.* 2,463,219 (to E I du Pont de Nemours & Co.), 1 March 1949, *Chem. Abstr.*, 43 (1949), 7258.].

Abbreviations and symbols—Abbreviations used should conform to the style of the journals. The following prefixes to units of measurements may be used for expressing submultiples and multiples.

Submultiples	*Abbreviation*	*Multiples*	*Abbreviation*
Deci- ($=10^{-1}$)	deci	deca- ($=10^{1}$)	deca-
centi- ($=10^{-2}$)	c	hecto- (10^{2})	hecto
milli- (10^{-3})	m	kilo- ($=10^{3}$)	k
micro- ($=10^{-6}$)	μ	mega- ($=10^{6}$)	M
nano- ($=10^{-9}$)	n	giga- ($=10^{9}$)	G
pico- ($=10^{-12}$)	p	tera- ($=10^{12}$)	T
femto- ($=10^{-15}$)	f		
atto- ($=10^{-18}$)	at		

Frequently repeating combinations of words, e.g. electric field gradient (EFG), junction field effect transistor (JFET), stimulated Raman emission (SRE), should be abbreviated subsequently, indicating the abbreviated form in parentheses, as shown, at the place of their first occurrence.

Nomenclature—Where too many symbols are used in the text, a section entitled "Nomenclature", explaining the significance of the various symbols, may be given and placed just above the Acknowledgement section.

Acknowledgement—Acknowledgements should not be exuberant and must be made only to real assistance rendered in connection with the work reported in the paper.

Appendixes—Appendixes, typed on separate sheets, should be numbered consecutively, in Arabic numerals, in the order of their occurence in the text, and should be placed at the very end of the paper.

Printed and Published by Shri D S Sastry, Publications & Information Directorate, Council of Scientific & Industrial Research, New Delhi, at the Leipzig Press, D-62 South Extension Part I, New Delhi 110 049, India

Regd. D-(C)-540